A STUDY OF STATE OF HEALTH ESTIMATION METHODS FOR LI-ION BATTERIES

by

Hassan Shabbir

BS, Lahore University of Management Sciences, 2014

A THESIS SUBMITTED IN PARTIAL FULFILLMENT OF

THE REQUIREMENTS FOR THE DEGREE OF

MASTER OF APPLIED SCIENCE

in

THE FACULTY OF GRADUATE AND POSTDOCTORAL STUDIES

(Electrical and Computer Engineering)

THE UNIVERSITY OF BRITISH COLUMBIA

(Vancouver)

April, 2016

© Hassan Shabbir, 2016

Abstract

Currently, battery management systems are battery chargers, commonly comprised of power electronic circuits, which lack the ability to accurately estimate the state of health of a battery. Since, batteries have a limited lifetime, repeated charge and discharge cycles quickly deteriorate the electrical properties of the battery. With the reduced capacity and several other changes in the state of health of a battery, the electronic device might malfunction. This research is aimed to provide on device upgrade for all battery management systems and battery chargers to include battery health monitoring ability. For the evaluation of state of health of batteries, two approaches are considered in parallel, Electrochemical Impedance Spectroscopy (EIS) and profiling through charge and discharge curves.

For EIS, the initial focus of this research is to design and validate the hardware that can perform EIS scans over a desired range of frequencies. Based on the footprints of scan, a state of health classification algorithm is proposed which categorizes batteries according to the set threshold. The main contribution of this project to existing EIS technology is the eradication of the need of battery modeling and parameter estimation from Nyquist plot to find the state of health of a battery. Tests are performed on hardware prototype to validate the designed algorithm that shows State of Health estimation accuracy of almost 90%.

Another method considered for State of Health estimation is profiling through charge and discharge curves of the Li Ion batteries. Raw profiling data is examined to decipher the correlation between shape of charge and discharge curves and state of health. From the charging

profile of the battery, constant charge current duration parameter is identified to possess promising potential to provide information about state of health of a battery. The behavior of the parameter is investigated in detail with repeated laboratory tests on almost 200 samples gathered from five different battery vendors. This technique showed above 90% classification accuracy.

Finally a comparison is drawn between the EIS technology and charge curve profiling method with respective advantages and disadvantages to emphasize the suitability of each technique for different field applications.

Preface

The text of the thesis is original and unpublished work of the author, Hassan Shabbir. The work is done in collaboration with Cadex Electronics Inc. and for publication purposes a written approval is required from both sources. Some sensitive details of the work are kept confidential and not included in the thesis, under Non-Disclosure Agreement of the industrial partner.

Table of Contents

Abstract ..... **ii**

Preface ..... **iv**

Table of Contents ..... **v**

List of Tables ..... **viii**

List of Figures ..... **ix**

List of Abbreviations ..... **xiii**

Acknowledgements ..... **xiv**

Chapter 1: Introduction **15**

1.1 Importance of Li ion batteries 15

1.2 Li ion cell design and chemistry 17

1.3 Thesis outline and objective 18

Chapter 2: Literature Review **20**

2.1 Background research 20

Chapter 3: Electrochemical Impedance Spectroscopy (EIS) **22**

3.1 Electrochemical impedance spectroscopy 22

3.2 Review of selected publications 29

3.3 Parameters to be considered for EIS method 32

3.3.1 Steady state condition 32

3.3.2 State of Charge (SoC) 33

3.3.3 State of Health (SoH) algorithm 33

Chapter 4: Test Plan and Experimental Setup For EIS **34**

4.1 Batteries selected for study 34
4.2 Test plan and experimental setup for SoC factor 35
4.3 Experimental results and analysis for SoC factor 37
4.4 Test plan and experimental setup for non-steady state analysis 39
4.5 Experimental results and analysis for non-steady state analysis 42
4.6 Data analysis for SoH algorithm 47
Chapter 5: Health Check Charger Prototype 56
5.1 Hardware setup 56
5.2 Software 58
5.3 User interface 60
5.4 Nyquist plots using the HCC hardware 61
5.5 SoH algorithm implementation and validation 62
5.5.1 SoH algorithm implementation 62
5.5.2 SoH algorithm validation 63
5.6 Cost estimate and economic analysis 69
Chapter 6: Charge and Discharge Curve Profiling 70
6.1 Background research 70
6.2 Proposed strategy 75
6.3 Data acquisition and analysis 76
6.4 Charge vs. discharge capacity analysis 80
6.5 Comparison across different battery models 85
Chapter 7: Results and Conclusions 88
7.1 Results and accomplishments of EIS technique 88

7.2 Results and accomplishments of charge profiling method 92

7.3 Comparison of EIS with charge/discharge profiling 94

7.4 Future work 95

Bibliography 96

Appendix A 98

List of Tables

Table 3-1 Accelerated cycling aging conditions [9] 29

Table 4-1 Characteristics of the batteries used in study 34

Table 4-2 Batteries selected for SoC analysis..... 35

Table 4-3 Batteries selected for non-steady state analysis..... 39

Table 4-4 Test plan details after each charge cycle 39

Table 5-1 Cost breakdown of the HCC hardware..... 69

Table 6-1 Type of battery Models used for data acquisition and analysis..... 75

List of Figures

Figure 1.1. Energy density comparison 15

Figure 1.2. Comparison of Li ion and lead acid Battery 16

Figure 1.3. Health Check Charger desirable features 19

Figure 3.1. I-V profile of the electrochemical cell 23

Figure 3.2. Typical nyquist plot for a lead acid battery 25

Figure 3.3. Warburg impedance formula and response 27

Figure 3.4. Change of impedance characteristic during battery's life: TC1 (Left), TC2 (Center) and TC3 (Right) [9] 29

Figure 3.5. Blocked diagram of intelligent integrated charger [10] 31

Figure 4.1. Settings for EIS scan 36

Figure 4.2. Impact of SoC on EIS scans 37

Figure 4.3. Dirt and residue on battery terminal 38

Figure 4.4. EIS scan with poor terminal connection 38

Figure 4.5. Nyquist plot after 30 seconds of rest for test 3 42

Figure 4.6. Nyquist plot after 2.5 minutes rest for test 3 43

Figure 4.7. Nyquist plot after 10.5 minutes rest for test 3 43

Figure 4.8. All EIS scans for non-steady state analysis 44

Figure 4.9. OCV gradient for battery 2 45

Figure 4.10. OCV recording after tests for battery 2 (90% SoH) 46

Figure 4.11. OCV recording after tests for battery 4 (02% SoH) 46

Figure 4.12. Points of interest in Nyquist Plot 48

Figure 4.13. Raw data vs smooth data using moving point average algorithm 49

Figure 4.14. All EIS scans with marked points of interests 49
Figure 4.15. Zero-crossing point evaluation 50
Figure 4.16. Minimum Point (X value) evaluation 50
Figure 4.17. Maximum point (Y value) evaluation 51
Figure 4.18. Maximum point (X value) evaluation 51
Figure 4.19. Zero crossing point error bar 52
Figure 4.20. Maximum point Y values error bar 53
Figure 4.21. Maximum point X values error bar 53
Figure 4.22. Minimum point X values error bar 54
Figure 4.23. Piece wise linear model for SoH vs Function output 55
Figure 5.1. Hardware implementation with LCD display 56
Figure 5.2. Potentiostatic block diagram 57
Figure 5.3. EIS test circuit block diagram 58
Figure 5.4. Impedance spectrum acquisition diagram 59
Figure 5.5. User interface with LCD display 60
Figure 5.6. HCC nyquist plot comparison with VMP2 61
Figure 5.7. SoH algorithm result display on LCD 62
Figure 5.8. Nyquist graph display on LCD 62
Figure 5.9. SoH algorithm validation tests 63
Figure 5.10. SoH algorithm validation with varying SoC 64
Figure 5.11. SoH Vs SoC readings for algorithm validation 64
Figure 5.12. HCC comparison with VMP2 battery 1: SoH 64% 65
Figure 5.13. HCC comparison with VMP2 battery 2: SoH 90% 66

Figure 5.14. HCC comparison with VMP2 battery 3: SoH 30% 66
Figure 5.15. HCC comparison with VMP2 battery 4: SoH 12% 67
Figure 5.16. HCC comparison with VMP2 battery 5: SoH 02% 67
Figure 5.17. Comparison of EIS scans 68
Figure 6.1. Charge profile variation with number of cycles 71
Figure 6.2. Charge profile characteristics for a battery [14] 71
Figure 6.3. Number of cycles Vs battery capacity 72
Figure 6.4. Number of cycles Vs battery resistance 72
Figure 6.5. Number of cycles Vs constant charge current time 73
Figure 6.6. Number of cycles Vs constant voltage charging time 73
Figure 6.7. Charge current characteristics of Samsung Galaxy S4 batteries 77
Figure 6.8. Overlap of single charging current cycle for Samsung Galaxy S4 batteries 77
Figure 6.9. Samsung Galaxy Note 1 charge current profiles 78
Figure 6.10. Overlap of single charging current cycle for Samsung Galaxy Note 1 batteries 78
Figure 6.11. Samsung Galaxy S3 charge current profiles 79
Figure 6.12. Overlap of single charging current cycle for Samsung Galaxy S3 batteries 79
Figure 6.13. List of battery models used for the study 80
Figure 6.14. Comparison of measured capacity for Samsung Note 1 during charge and discharge operation 81
Figure 6.15. Comparison of measured capacity for Samsung Galaxy S3 during charge and discharge operation 82
Figure 6.16. Comparison of measured capacity for Li Air Canada during charge and discharge operation 82

Figure 6.17. Comparison of measured capacity for Samsung Galaxy S4 during charge and discharge operation without temperature compensation..... 83
Figure 6.18. Comparison of measured capacity for Samsung Galaxy S4 during charge and discharge operation with temperature compensation..... 84
Figure 6.19. Battery models with varying charge voltage threshold and capacities..... 85
Figure 6.20. Current profile comparison of different battery models..... 86
Figure 6.21. Voltage profile comparison of different battery models 87
Figure 7.1. State of Health algorithm average error analysis 88
Figure 7.2. SoH algorithm evaluation with varying SoC..... 89
Figure 7.3. EIS scans of batteries after 30 seconds of rest time 90
Figure 7.4. EIS scans after 10.5 minutes of the rest time 90
Figure 7.5. OVC gradient for Battery 2 91
Figure 7.6. Relation between SoH of the batteries and normalized constant current duration..... 92
Figure 7.7. Percentage of overall test time saved Vs. SoH of the batteries 93
Figure 7.8. Comparison of EIS technique with charge curve profiling 94

List of Abbreviations

Li Ion	Lithium Ion
HCC	Health Check Charger
EIS	Electrochemical Impedance Spectroscopy
AC	Alternating Current
DC	Direct Current
SoH	State of Health
SoC	State of Charge
BMS	Battery Management System
EMI	Electromagnetic Interference
DoD	Depth of Discharge
PCB	Printed Circuit Board
PWM	Pulse Width Modulation
OCV	Open Circuit Voltage
V	Volts
A	Amperes
BMS	Battery Management System
Hz	Hertz
EoL	End of Life
BoL	Beginning of Life

Acknowledgements

First and foremost, I would like to thank Almighty Allah for giving me strength and courage to carry out this task.

Secondly, I would like to thank my parents and family for being always there for me. Whenever, I needed someone, they showed up with their kind support to encourage and motivate me, in all spheres of life, throughout my life. I can just not simply thank them enough for everything they did for me, for all their efforts and sacrifices.

Third, I would like to take this opportunity to present my sincere gratitude to my academic supervisor Dr. William Dunford and coop supervisor Dr. Tina Shoa for their endless support and guidance to carry out research on this project. Their dedication, resourcefulness and overwhelming support were key factors in the completion of this project. With their keen supervision, timely advice and meticulous scrutiny, I have been able to glide through the experimental stage of the project, which otherwise, would have been a daunting task to accomplish.

Next, I would like to acknowledge the contribution of the close circle of my friends. Mr. Asad Rana, Mr. Ahsen Khan, Mr. Edmundo Gonzalez, Mr. Moksh Mata, Mr. Parampal Singh and Miss Maheen for making this journey exciting and fun for me.

Chapter 1: Introduction

1.1 Importance of Li ion batteries

Li ion batteries have emerged as the backbone of rechargeable energy store. In 2013, the number of Li ion cells sold for electronic devices were reported to be around five billion [1] with exponential rise expected in the sales for coming years. The increased focus on Li ion batteries emerges from its ability to offer substantial power density and fast charge/discharge capability. The comparison of energy density of Li Ion technology is shown in figure 1.1 [1].

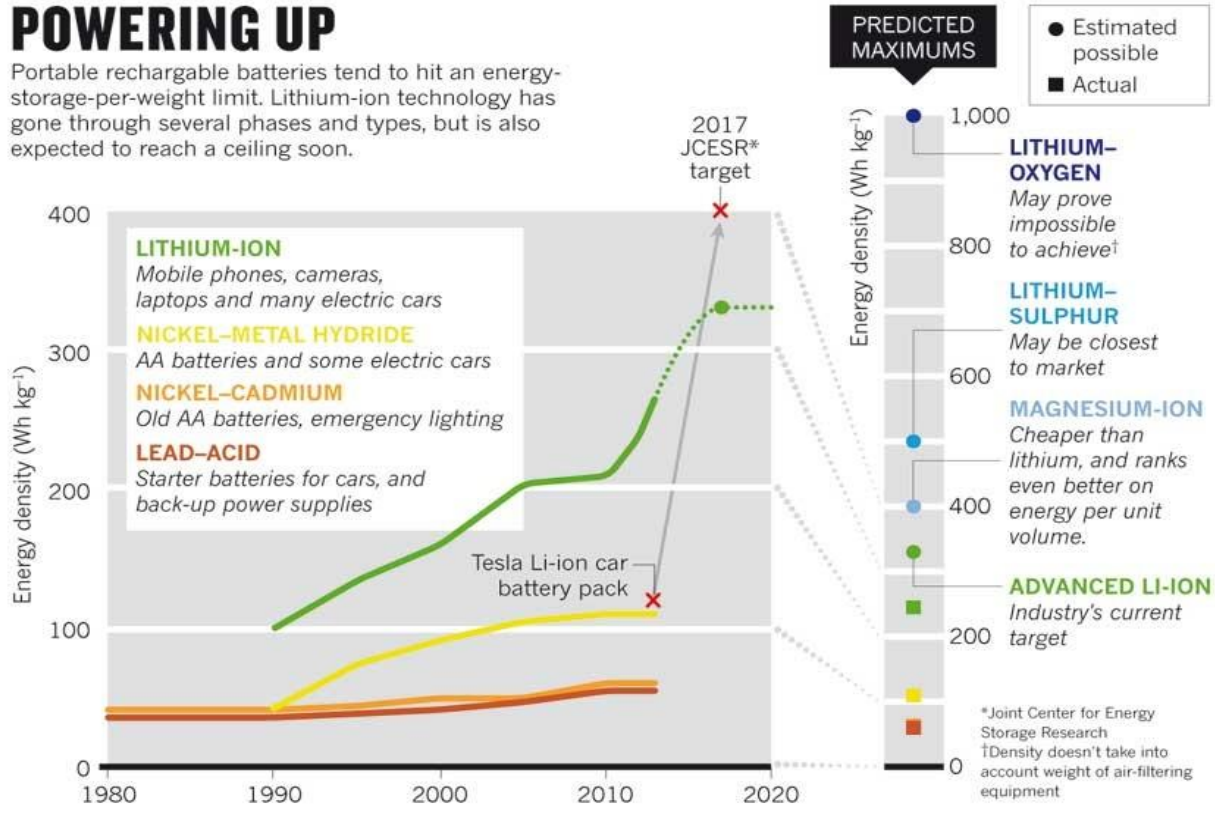

Figure 1.1. Energy density comparison

The present performance of Li ion technology in terms of energy density show significant advantage over other technologies such as Lead-Acid and Nickel based batteries, and has shown potential to undergo significant improvements. Therefore, this technology has lately caught the attention of researchers throughout the world.

Li Ion cells are compact in size, pose high specific energy and require no maintenance once installed. The cells are designed to exhibit deep cycle performance, i.e. designed to function normally when completely discharged and charged again. Several chemical configurations exist for lithium-ion batteries, but generally Li ion batteries can be separated into two groups: lithium iron phosphate (LFP, LiFePO4) and metal oxides (NCM, NCA, Cobalt, Manganese). A cell level comparison of Li ion technology with other technologies is presented in figure 1.2 [2].

	Flooded lead acid	VRLA lead acid	Lithium-ion (LiNCM)
Energy Density (Wh/L)	80	100	250
Specific Energy (Wh/kg)	30	40	150
Regular Maintenance	Yes	No	No
Initial Cost ($/kWh)	65	120	600[1]
Cycle Life	1,200 @ 50%	1,000 @ 50% DoD	1,900 @ 80% DoD
Typical state of charge window	50%	50%	80%
Temperature sensitivity	Degrades significantly above 25°C	Degrades significantly above 25°C	Degrades significantly above 45°C
Efficiency	100% @20-hr rate 80% @4-hr rate 60% @1-hr rate	100% @20-hr rate 80% @4-hr rate 60% @1-hr rate	100% @20-hr rate 99% @4-hr rate 92% @1-hr rate
Voltage increments	2 V	2 V	3.7 V

Figure 1.2. Comparison of Li ion and lead acid Battery

Due to superior energy density, lifetime and efficiency Li ion technology has become the future of portable electronic devices. With the elevated importance in the electronic world, the need of deciphering the operational characteristics and parameters of this technology has also become pertinent. This provides the motivation for this project to investigate, explore and analyze the characteristics of Li Ion batteries to design appropriate battery management systems for smooth and safe operation of power-hungry portable electronic devices.

1.2 Li ion cell design and chemistry

A Li Ion cell comprises two electrodes separated by a separator. The positive terminal is called the cathode and is made up of Li-metal oxide and negative terminal is called anode, usually made from carbon (graphite). Similar to other battery types, the Li ion battery exploits a reversible chemical reaction to perform its operation. The chemical charge is stored in the battery when the battery is charged, while process of discharge involves extraction of stored chemical energy into electrical energy. Following are the typical chemical reactions going on inside a Li ion battery at the respective terminals.

Positive: $LiXXO_2 \underset{\text{Discharging}}{\overset{\text{Charging}}{\rightleftharpoons}} Li_{1-x}XXO_2 + Li^+ + xe^-$

Negative: $C + xLi^+ + xe^- \underset{\text{Discharging}}{\overset{\text{Charging}}{\rightleftharpoons}} Li_xC$

Overall: $LiXXO_2 + C \underset{\text{Discharging}}{\overset{\text{Charging}}{\rightleftharpoons}} Li_xC + Li_{1-x}XXO_2$

Where XX = several combinations of Cobalt and Manganese

Irrespective of the precise chemical composition of the Li ion batteries, the following general qualities make Li ion batteries distinctive from other type of batteries:

1) *Light weight among other rechargeable batteries*
2) *Fast charge/discharge ability and deep cycle operation*
3) *Very low self-discharge rate (about 1.5% per month)*
4) *High open circuit voltage at the terminals*

1.3 Thesis outline and objective

The condition of Li ion batteries deteriorates as they age through repeated charge and discharge cycles. In order to ensure optimal use of these electronic devices, it is vital to know how much remaining capacity of the battery is remaining which primarily corresponds to amount of energy storing capability of the battery. The remaining capacity of the battery is termed as State of Health (SoH) of a battery and can be calculated as:

$$SoH\ (t)\ in\ \% = \frac{C_{max}}{C_{rated}} * 100$$

Where

$$C_{max} = C_{rated} - C_{unavialable}(t)$$

The SoH of a battery decreases along with time as some part of the overall capacity of the battery becomes unavailable due to change in internal resistance, dielectric properties and mobility of electrolyte of the battery.

Although there are several devices available in the market, which can decipher the SoH of a battery by performing different tests, these products have some serious drawbacks for large-scale application. The main shortcomings of these devices range from cost ineffectiveness to practical infeasibility, from strict restrictions on battery operating conditions to an intricate technical user interface. Therefore, the demand for a sophisticated, cost effective, general health check charger that can analyze, determine and classify the SoH of a battery with minimal restrictions on the operating conditions of the battery is growing in electronic industry.

The aim of this study is to extend on the existing battery health diagnosing technologies to develop a state of the art health check charger. The distinctive features of Health Check Charger

(HCC) will be to provide instantaneous SoH information to the user about the health of the battery with minimal restrictions on the preoperational conditions of the battery. The goal is to estimate the health of the battery with the accuracy of 10% of margin of error.

But before moving on to the technical details of test strategy and implementation technique, it is critical to set the desirable features and goals for the end product. Since HCC is consumer end product, it is vital to include some desirable features that are listed as follows:

Figure 1.3. Health Check Charger desirable features

The combination of the all these features will result in an intelligent product that can serve as an efficient battery health monitoring solution. Therefore, the goal of this thesis is to come up with a hardware prototype for a device that comprises of all these features. The scientific proof of concept and related technical details of the device technology are discussed in later chapters.

Chapter 2: Literature Review

2.1 Background research

In order to characterize the batteries, several types of methods have been devised which can be segregated into destructible and non-destructible categories [3]. Although destructive methods give precise information about the chemical properties of battery, they are rarely employed because they are impractical, largely because when a battery is tested through this method, it can no longer be reused. Popular non-destructive methods that are in practice to determine the state of health of a battery are series impedance measurement, voltammetry and electrochemical impedance spectroscopy.

The Ampere Hour (Ah) counting method is one of the most commonly used methods to determine the state of charge and capacity of the battery [4]. The method involves completely discharging of the battery and counting the coulombs provided by the battery to the load. The drawbacks of this method are that the method is time consuming and involves complete charge and discharge of battery, which might not be pragmatic in certain applications. The method also fails to distinguish between different battery aging mechanisms and provides an overall integral result. Another issue associated with this technique is the error accumulated while performing the integral over current, since the process of charging and discharging is not unity efficient (some of the energy is dissipated as heat across the series resistance of the battery).

Another commonly used method for state of health determination of a battery is impedance measurement at single frequency or at a range of frequencies. This method provides information about the electrolyte conductivity that deteriorates as battery ages and can be used to differentiate

different type of batteries. However, this method provides limited information, as certain mechanisms show their effect in a specific frequency range i.e. at usually low frequencies [5].

Electrochemical Impedance spectroscopy has been verified on the laboratory scale as a promising method to determine a range of aging effects in batteries [6]. The method is quick and provides instant results. The frequency range of the interest usually comprises of 10KHz to 0.1mHz and therefore the testing of the battery only takes few minutes. However, with the existing approach, the results of this method are largely affected by variation in battery model used to calculate the parameters. The process of optimizing the parameters obtained from the Nyquist plot requires intensive processing and good initial estimate, which might not be possible sometimes. In addition to this the battery is required to be in a steady state condition before a test could be performed, the details of this limitation are explored in detail in chapter 3. These restrictions limit the application of this technique. However, this method is inherently cost effective, fast and reliable.

Similarly, work has been done to find state of health of a battery using other methods such as profiling voltage across terminals during discharge [7]. Charge and discharge curves of the batteries show the impact of the aging effects and also provide vital information regarding battery capacity. This approach requires precisely calibrated instruments for voltage profile logging and requires the battery monitoring system to track the history of charge and discharge profiles of the battery. The method is reliable and has potential to accurately classify the state of health of a battery irrespective of the preoperational conditions, but industrial application is limited by model specific solution.

Chapter 3: Electrochemical Impedance Spectroscopy (EIS)

3.1 Electrochemical impedance spectroscopy

Electrochemical Impedance Spectroscopy (EIS) is a recent solid-state technique used to decipher dielectric and electric properties of materials. The technique is also sometimes referred as AC impedance spectroscopy due to the nature of the test. It is a non-destructive method to find the electrochemical properties of the batteries that provide quantitative information about individual components and properties of the battery. Batteries show non-linear relation between current and voltage, however, this method is only applicable to linear systems.

The figure 3.1 shows how an electrochemical cell has a non-linear I-V relation. Therefore, in order to find the frequency response, a small excitation signal is applied such that the overall non-linear I-V curve shows pseudo linearity. In this small linear region, the non-linear properties of a battery can be approximated as pseudo linear I-V curve. The linearity assumption is only valid if the small signal AC excitation at the terminal of the cells is less than 10mV for single cell Li Ion Battery.

The linearity condition basically implies that if

$$\alpha x_1(\omega) = \alpha y_1(\omega)$$

And

$$\beta x_2(\omega) = \beta y_2(\omega)$$

Then,

$$\alpha x_1(\omega) + \beta x_2(\omega) = \alpha y_1(\omega) + \beta y_2(\omega)$$

Such that the overall response in time domain is sum of the individual input signals (principle of superposition). If signal is not small enough, the system shows non-linear I-V characteristics and the steady state condition is not fulfilled resulting in issues related to drift, a phenomena that will be discussed, in detail, later in this chapter. However, in steady state condition, the frequency of the small ac signal can be varied and the response of current can be logged to find complex impedance. Figure 3.1 shows Electrochemical cell with small AC excitation.

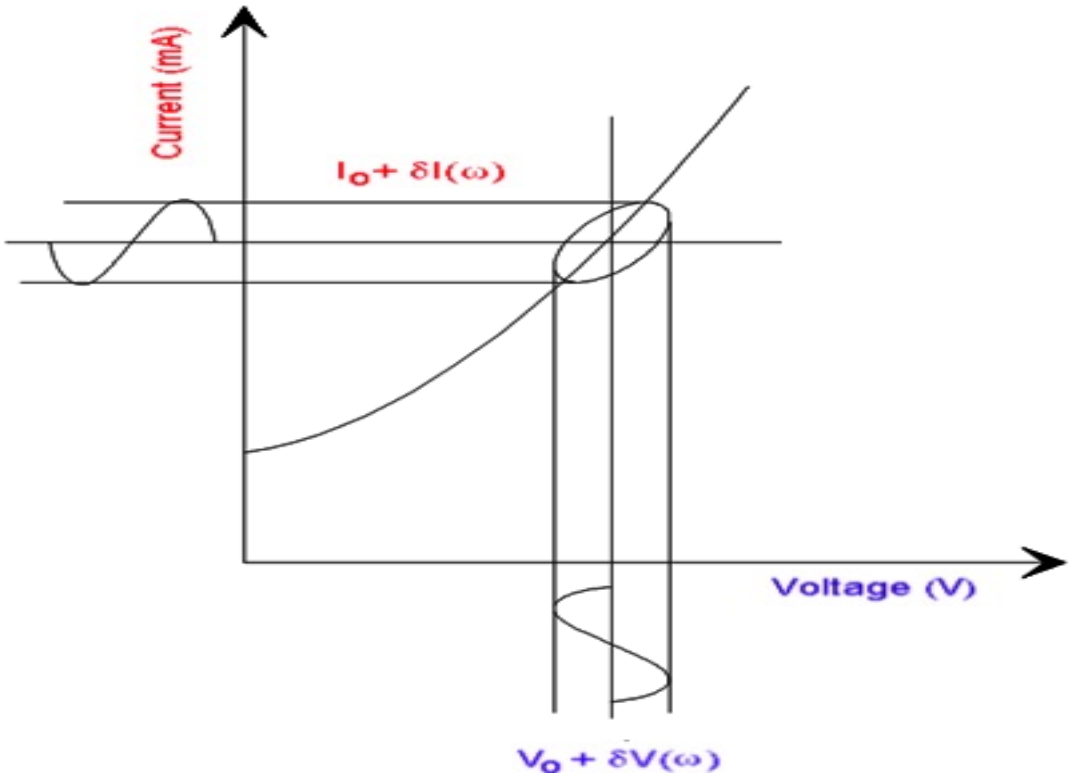

Figure 3.1. I-V profile of the electrochemical cell

Initially, the voltage of a potentiostat circuit V_t is made to match the open circuit voltage (OCV) across the terminals of the battery such that there is no current flowing through a battery. Then a small ac perturbation is applied $\delta V(j\omega t)$ on the top of the constant voltage V_0 ◦ but the amplitude of the perturbation is kept small such that pseudo linear assumption is valid.

$$V_t(j\omega t) = V_0 + \delta V\ (j\omega t)$$

The current response $\delta I(j\omega t - j\varphi)$, of the battery is recorded and the test cycle is repeated for perturbation signals comprising of different frequencies.

$$I_t(j\omega t) \;=\; \delta I\,(j\omega t - j\varphi)$$

The angular frequency of the signal expressed in radians per seconds is associated with frequency in Hz by the following relation.

$$\omega = 2\pi f$$

Using the small signal voltage perturbation $\delta V\,(j\omega t)$ and current response$\delta I\,(j\omega t - j\varphi)$, the complex impedance Z (ω) is calculated.

$$\mathrm{Z}\,(\omega) = \frac{\delta V exp(j\omega t)}{\delta I exp(j\omega t - j\varphi)}$$

$$= Z_{\circ} exp(j\varphi)$$

Using Euler's relationship to expand the exponential term to get real and imaginary component of the complex impedance.

$$\exp\,(\mathrm{j}\varphi) = \cos(\varphi) + \mathrm{j}\sin(\varphi)$$

$$\mathrm{Z}\,(\omega) = Z_{\circ}(\cos(\varphi) + jsin(\varphi))$$

The impedance is recorded at several excitation frequencies of interest such that a spectrum of impedances is captured for analysis. The impedance is a complex number with a real and imaginary part and usually a Nyquist plot is constructed with real impedance on the x-axis and negative of imaginary impedance on the y-axis to plot the results. The Nyquist plot shows how impedance of the system varies as a function of frequency and is used to study the electrochemical properties of the cells as shown in figure 3.2 [8].

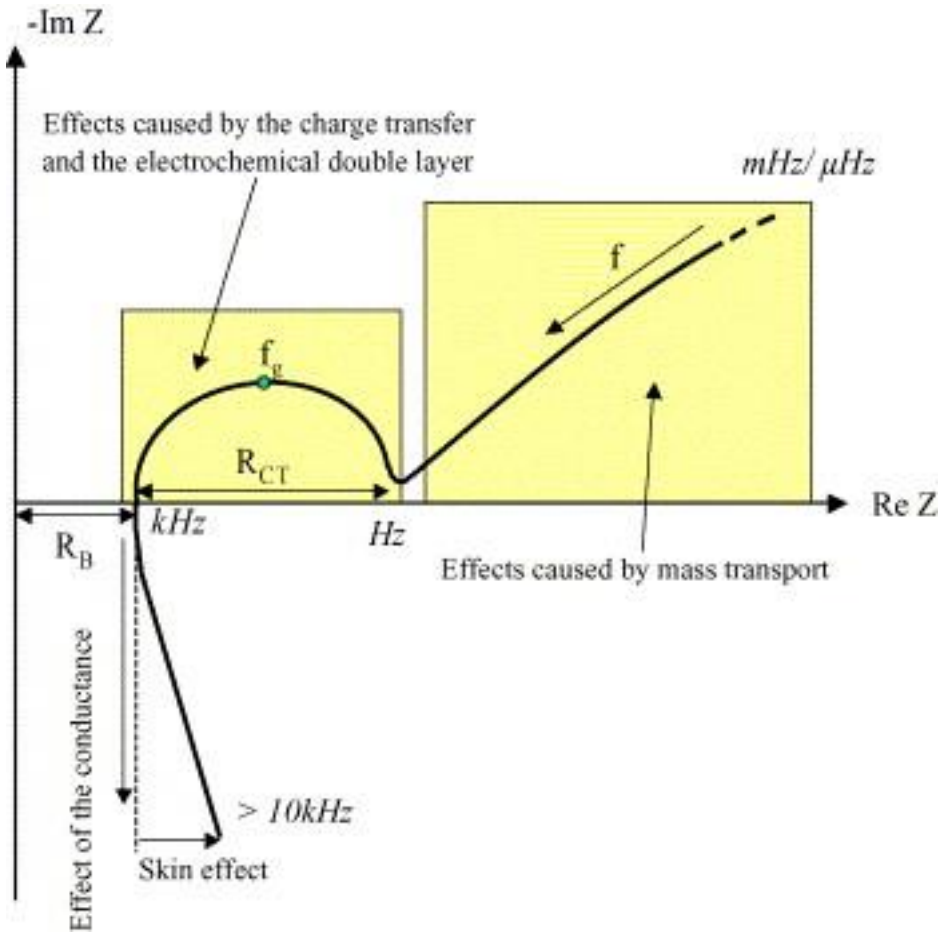

Figure 3.2. Typical nyquist plot for a lead acid battery

The mathematical expression for the double layer capacitance and charge transfer resistance shown in the Nyquist plot is presented here. This region of the Nyquist plot is important because they electrochemical properties determine the overall available storage capacity of the battery.

Later in the coming chapter, this region of the EIS scan will be used to design a SoH estimation algorithm. To start off with, the expression of electrolyte resistance for a bounded area with cross-sectional area A, length L is:

$$R = \rho \frac{L}{A}$$

Where ρ is the solution's resistivity. Normally the reciprocal of the resistivity is used which is called the conductivity κ, therefore the relation becomes

$$R = \frac{L}{A} . \frac{1}{\kappa}$$

Using faraday's law, for an electrochemical cell, the charge transfer relation that relates current and potential of an electrochemical cell is give as follows:

$$i = i_{\circ} \left(\left(\frac{C_{\circ}}{C_{\circ}^{*}} exp\left(\frac{\alpha n F \eta}{RT} \right) \right) - \left(\frac{C_R}{C_{\circ R}^{*}} exp\left(\frac{-(1-\alpha) n F \eta}{RT} \right) \right) \right)$$

Where, $i_{\circ}$ is exchange current density, $C_{\circ}$ is concentration of oxidant at the electrode surface, $C_{\circ}^{*}$ is concentration of oxidant in bulk, C_R is concentration of reductant at the electrode surface, $C_{\circ R}^{*}$ is the concentration of the reductant in bulk, F is faraday constant, R is gas constant, T is temperature, α is the reaction order, n is number of electrons involved and η is the over potential. Under the condition of $C_{\circ} = C_{\circ}^{*}$ and $C_R = C_{\circ R}^{*}$, the above charge transfer equation reduces to the Butler-Volmer equation:

$$i = i_{\circ} \left(\left(exp\left(\frac{\alpha n F \eta}{RT} \right) \right) - \left(exp\left(\frac{-(1-\alpha) n F \eta}{RT} \right) \right) \right)$$

Using the small over-potential approximation, the exponential term reduces down to a linear relation and we can write the expression for the charge transfer resistance R_{ct} as,

$$R_{ct} = \frac{RT}{nFi_o}$$

Other important characteristic that relates the electrochemical property of the battery to the shape of the Nyquist plot is double layer capacitance C_{dl}. The value of double layer capacitance depends on the electrode potential, temperature, ionic concentration, electrode roughness and impurity concentration. Usually, the value for C_{dl} is around 20-60 μF/cm^2.

Since the process involves diffusion of charges and ions, this process can also induce an impedance term, also referred to as the Warburg Impedance. This impedance comes into effect at very low frequencies and normally results in a 45 degree slanted line on Nyquist plot. The Warburg -Impedance equation is

$$Z_\omega = \sigma\,(\omega)^{-0.5}\,(1 - j)$$

Where $\sigma(\omega)$ represents frequency dependent Warburg coefficient, ω is the angular frequency. Therefore, combining together the electrical components presented to model the electrochemical processes of a cell, we get Randles cell model that represent reaction kinetics and charge transfer processes. The model is presented in figure 3.4 along with Nyquist diagram of the model:

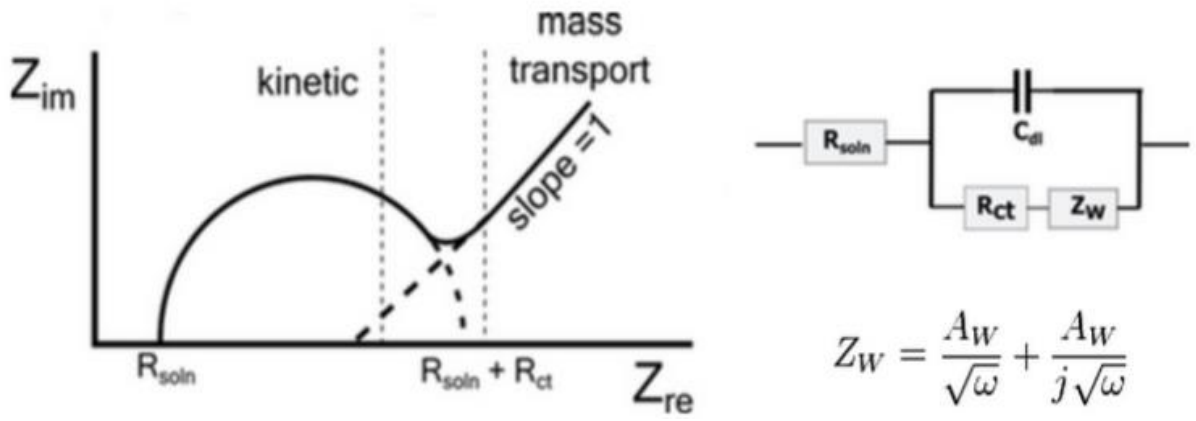

Figure 3.3. Warburg impedance formula and response

However, in order to model the non-ideality of the cell's model, a constant phase element is used rather than an ideal capacitor for double layer capacitance. The impedance relation for this constant phase element is given as follows:

$$Z_{CPE} = \frac{1}{Q(j\omega)^{\alpha}}$$

Where Q is the bulk capacitance, ω is the angular frequency and α is the non-ideality coefficient that can range from 0 to 1. For an ideal capacitor, α will have value of 1.

The following relations can be used to model the electrochemical properties of the cell and the respective regions are shown in fig. 3.3.These properties define the overall state of condition of an electrochemical cell and therefore, an EIS scan essentially carries important information about the chemical properties and configuration of the electrochemical cell.

In the upcoming chapters, EIS scans will be analyzed such that an estimate of the state of health of the battery can be obtained without using the equivalent circuit model and optimization technique for optimization method. A major advantage of using EIS technique for testing a battery is that the EIS technique is time efficient. The test is comprised of a very small duration of time as compared to other methods used to categorize batteries such as Ah counting. Other advantages are that the test by nature is non-destructive and does not require the battery to be discharged. However, in order to perform the EIS test, the battery is expected to be in a certain state. The factors that can have an impact on EIS method are identified and discussed later in this chapter in section 3.3.

3.2 Review of selected publications

Work has been done previously on SoH estimation of the battery using EIS technique as proposed in [9]. In this study, batteries were repeatedly charged and discharged using different SoC intervals as shown in table 3-1 for the artificial aging. An impedance spectrum was recorded from the Beginning of Life of batteries (fresh batteries) to End of Life (after accelerated aging). The Nyquist plots were used for comparison as batteries get aged with the aging conditions quoted in table 3-1. A key point to note herein figure 3.4 is that the Nyquist plot shifts towards the right side along the real axis as the battery ages (regardless of the cycling conditions of the battery as shown in the table). This result is experimentally verified and endorsed with the experimental results of the EIS scans presented in the Chapter 4.

Test case name	Cycle depth	SOC interval	Temperature	C-rate/ Current
TC 1	10 %	45% - 55%	50 °C	4 C-rate (10A)
TC 2	35 %	32.5% - 67.5%		
TC 3	60 %	20 % - 80%		

Table 3-1 Accelerated cycling aging conditions [9]

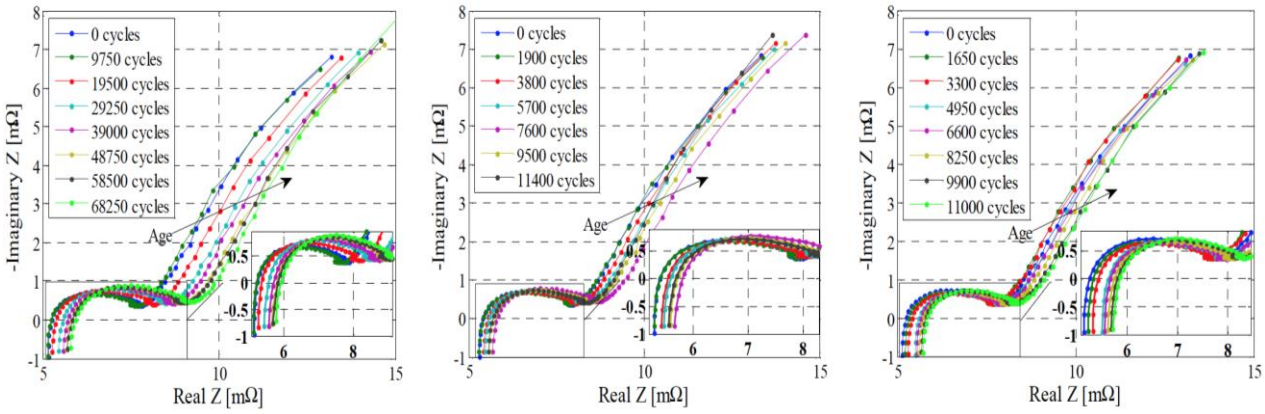

Figure 3.4. Change of impedance characteristic during battery's life: TC1 (Left), TC2 (Center) and TC3 (Right) [9]

(25℃ 50% SoC) for cells aged under Table 3-1 conditions

However, there are some shortcomings of the results presented in study [9]. The batteries were always tested while they were in steady state i.e. the batteries were resting for sufficient time such that all transients due to charge/discharge process had settled down. This condition might not be always applicable in real world scenario. If HCC has to operate and charge the battery, it is imperative to know the minimum possible time battery needs to be in rest before a test could be performed. This limitation holds vital significance because time is of essence, as user cannot wait for long period before the batteries could be used in critical applications. This thesis addresses this issue in detail in the later sections.

Besides this, another limitation of the study was that the batteries were artificially aged using repeated cycles with same SoC span as shown in table 3-1. This artificial aging mechanism can impact some parts of the Nyquist plot more than the other parts. Batteries aged in real world application might show different behavior since the C-rate during charge and discharge process is not always similar, neither depth of discharge is identical for each cycle. This accelerated aging strategy might not cover the full breadth of change incurring in batteries operating in real world, hence, these shortcomings reduce the overall authenticity of this study.

Similarly, EIS technique is suggested for SoH evaluation of batteries as proposed in [10]. The study recommends using intelligent integrated charger to perform EIS scan on a battery and the block diagram of the schematic of intelligent integrated charger circuit is shown in figure 3.5. However, according to the results presented in the paper, this approach poses strict restrictions on the state of condition of the battery as EIS scans were performed on the battery only when they were completely charged, a condition, which is very unlikely to be fulfilled in real world

application as battery might be sitting at any SoC. The authors once again assumed a steady state condition when OCV of the battery is not changing after charging, without stating how much time the user have to wait before an EIS scan can be performed. Therefore, this solution needs in depth analysis, as the proposed solution is insufficient to cater contingencies of the real world.

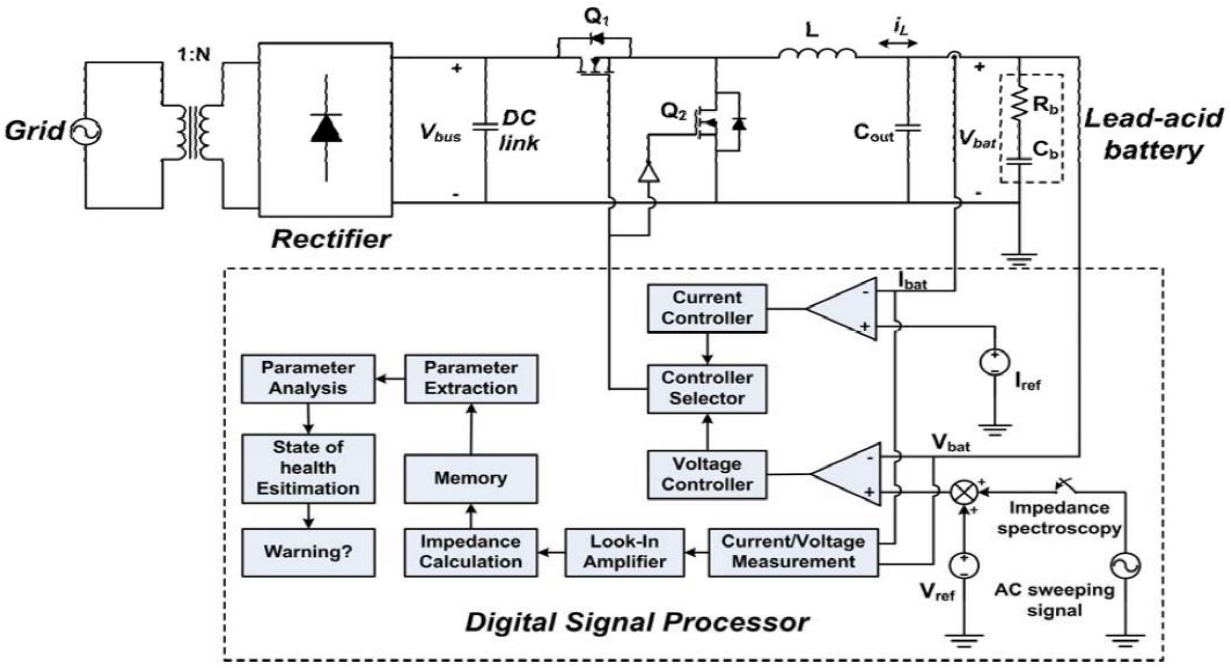

Figure 3.5. Blocked diagram of intelligent integrated charger [10]

Both studies [9] and [10] used equivalent battery circuit for modeling purpose and parameter estimation to optimize the values of electrical components to match the Nyquist plot obtained by the EIS test. The reliability of using optimization techniques for parameter evaluation is debatable as the results of optimization method can vary largely even if Nyquist plots look similar. It is also essential to provide good initial estimate to the algorithm to begin with such that number of iterations required for the convergence are minimal. Parameter estimation using the optimization method is time-consuming, computation intensive and can result in misleading results. Nevertheless, there will be a need of a function to relate SoH to the modeling parameters.

3.3 Parameters to be considered for EIS method

Although using EIS technique has proved to be a promising method to categorize batteries with different electrical characteristics and dielectric properties in a laboratory setting, the industrial application of this method requires in depth analysis of parameters that affects this technique. This limitation largely stems from the restrictions on the preoperational conditions of the battery that are not always met in an industrial environment as discussed in section 3.2. The factors that will be addressed in this thesis that can impact the EIS method are listed below:

3.3.1 Steady state condition

Conventionally, before the EIS test is performed on the battery, the OCV of the battery is supposed to be constant which indicates that the battery has been resting for a while. This is primarily because when a battery is charged or discharged, the process of pumping in and removal of the charge disturbs the reversible chemical reactions going on in the battery. When the battery is removed from charge/discharge process, it takes a while before the OCV settles down. Conventionally, the battery is maintained to be in rest state for a long period to reach the desirable steady state. However, in real world application, time is of essence as the user cannot wait indefinitely for the battery to rest before a test could be performed especially in critical usage such as medical and warfare applications.

Therefore, it is important to figure out how much time the battery has to be in rest state before an EIS scan could be performed on it. This study explores the regime in time domain where battery will be in quasi steady state such that impact of transient is negligible. As established earlier, the need to explore this limitation is vital for robust design of a consumer end device such as HCC.

3.3.2 State of Charge (SoC)

SoC is basically the measure of amount of charge stored in the battery. The SoC of 100% corresponds to fully charged battery and 0% corresponds to a battery that is completely void of charge. Commonly SoC is also stated to be equivalent of fuel gauge of battery. A battery operating in the field could be at any SoC hence, it is important to come up with a robust SoH algorithm for the health check charger which can perform the operation at all level of SoC. This is critical because a user cannot wait for the battery to be completely charged or discharged before a test could be performed. Therefore, SoC is another parameter that has to be considered while designing health check charger SoH algorithm.

$$SoC\ (t) = \frac{C_{available}(t)}{C_{max}} = SoC_{initial} - \frac{[\int i_{cell}(t)dt + C_{unavailable}(t)]}{C_{max}}$$

3.3.3 State of Health (SoH) algorithm

Once the abovementioned conditions are met and the EIS test is performed successfully to record the impedance data, only a part of the overall task is accomplished. The recorded data needs to be processed before an estimate of the SoH of a battery could be provided. This part of the test makes the health check charger device battery model specific, as model specific reference or thresholds are required to relate impedance data to the overall capacity of the battery. Usually a specific model comprising of basic electrical components is selected to model the battery and the values for the equivalent circuit components are calculated using optimization techniques. Commonly non-linear iterative search methods such as Newton method or Levenberg-Marquardt methods are used for optimization. However, the values of modeled electrical components obtained after optimization can vary largely with a slight deviation in the Nyquist plot. This can pacify the overall accuracy of the device by wrongly categorizing the battery therefore; there is substantial need to devise an efficient SoH determination algorithm.

Chapter 4: Test Plan and Experimental Setup For EIS

4.1 Batteries selected for study

For this extensive study on health check charger, 3.7 nominal voltage, 4.8Ah Li-ion batteries were chosen. A pool of 30 different samples of batteries was available from which every time, suitable numbers of batteries were chosen depending on the type of test. The batteries were accumulated after they served in the field to power up radio sets for a long period of time. The batteries comprised of a wide spectrum of SoH that made contrasts and comparisons in the results very prominent. The batteries were used with a serial adapter, which was used to ensure concrete connection of testing equipment to the battery terminals. Since all the batteries were of the same model and manufacturer, they had same electrical characteristics. The values are quoted from their datasheet in table 4-1:

Nominal Voltage	**3.7 V**
Capacity	**4800 mAh**
Maximum Charge Voltage	**4.2 V**
Minimum Discharge Voltage	**3.0 V**
Charge Cut off point	**0.24 A**
Safe operating temperature	**0 – 40 degree Celsius**

Table 4-1 Characteristics of the batteries used in study

The batteries were labeled with battery index each time the test was performed and the thermal and electrical limits of the battery were not breached. The voltage, current and temperature of the batteries were recorded simultaneously while a test was performed to ensure safe and reliable operation of the samples considered for the test.

4.2 Test plan and experimental setup for SoC factor

In order to find the impact of SoC on the EIS method, a sample set of 14 batteries was selected. The table shows the batteries selected and their true corresponding SoH (capacity) that was measured by coulomb counting the discharge cycle of fully charge battery at C/4 discharge rate, which was then compared to overall rated capacity. A SoH of 100% corresponds to a battery having full capacity available of the rated capacity i.e. 4800mAh, whereas, SoH of 0 % relates to a battery with no capacity left. A SoH of 50% corresponds to 2400mAh of storage capacity.

Battery ID	State of Health in %
Battery 1	63
Battery 2	92
Battery 3	30
Battery 4	65
Battery 5	02
Battery 6	90
Battery 7	89
Battery 8	84
Battery 9	79
Battery 10	76
Battery 11	64
Battery 12	13
Battery 13	86
Battery 14	83

Table 4-2 Batteries selected for SoC analysis

The batteries were completely charged initially and EIS scans were performed for each battery at an interval of discharge of 10% of the overall battery capacity using VMP2 biologic equipment. The discharge test was performed using Cadex c7400 battery analyzer and the battery was allowed to sufficient time such that a steady state condition was reached. The data of the EIS scan was logged in an excel file containing all the frequencies, real and imaginary impedance. All tests were performed at room temperature and pressure. Figure 4.1 shows the settings chosen for the EIS scan.

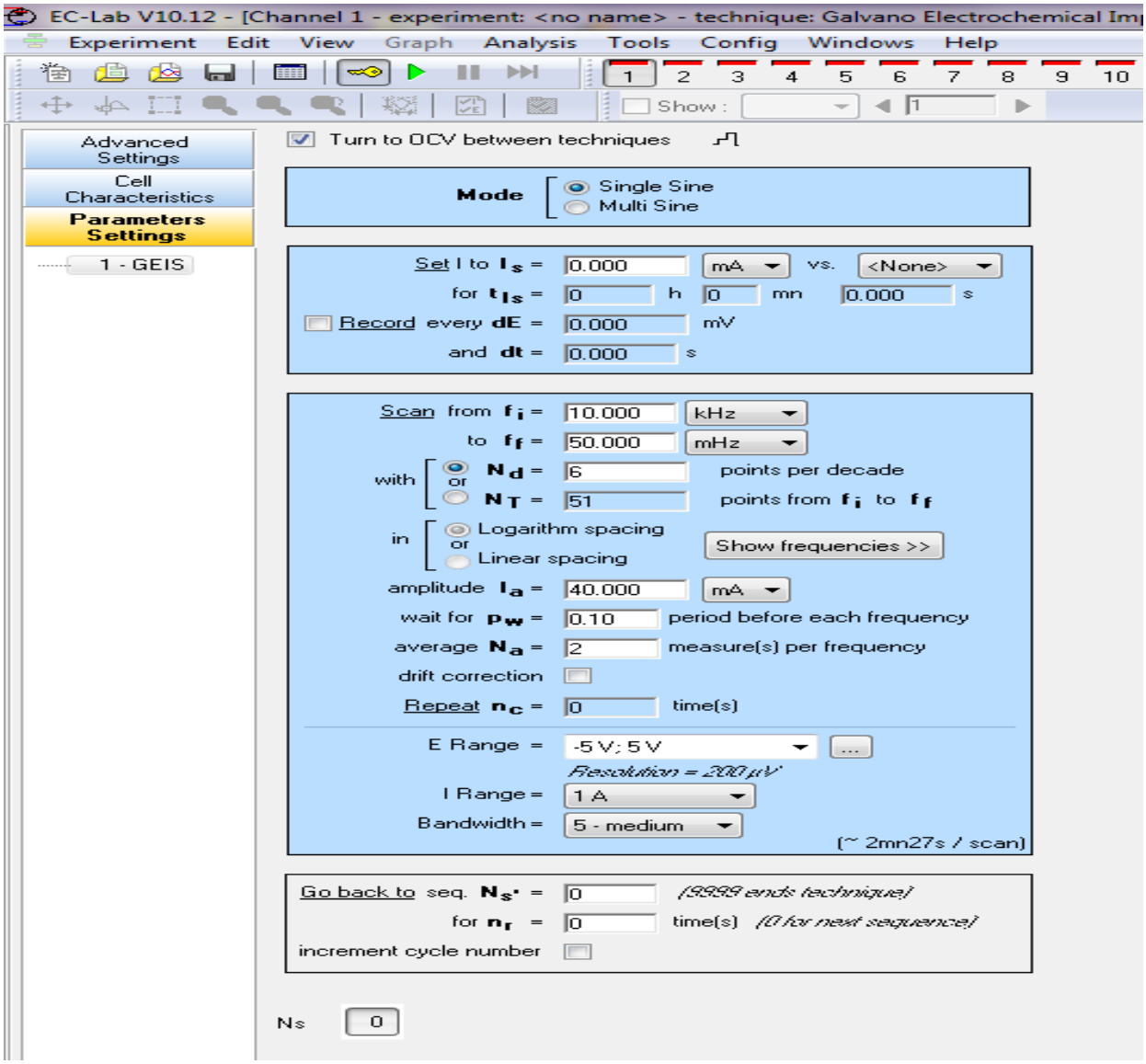

Figure 4.1. Settings for EIS scan

The frequency range of 10 KHz to 50 mHz was selected to perform the EIS scans such that dielectric and electrochemical properties of the battery under observation could be investigated. A two point average over all test frequencies was performed to obtain a smooth scan and amplitude of the current signal was set to 40.0 mA such that pseudo linear assumption is valid and battery behaves as a linear system. Test frequencies were logarithmically spaced over the frequency range with six points per decade to have optimal resolution of the EIS scan.

4.3 Experimental results and analysis for SoC factor

The EIS scans captured for all batteries were exported to Matlab, where the data was processed and plotted for analysis. There was slight variation in the EIS scans recorded for all batteries with no specific pattern observed. The impact of SoC on EIS scans was negligible as compared to the impact due to the solid electrolyte interface, charge transfer capacity and internal resistance of the batteries, since they determine the small signal response of a battery. A comparison of three batteries of different SoH is presented in the Nyquist plot shown in figure 4.2 for all SoC.

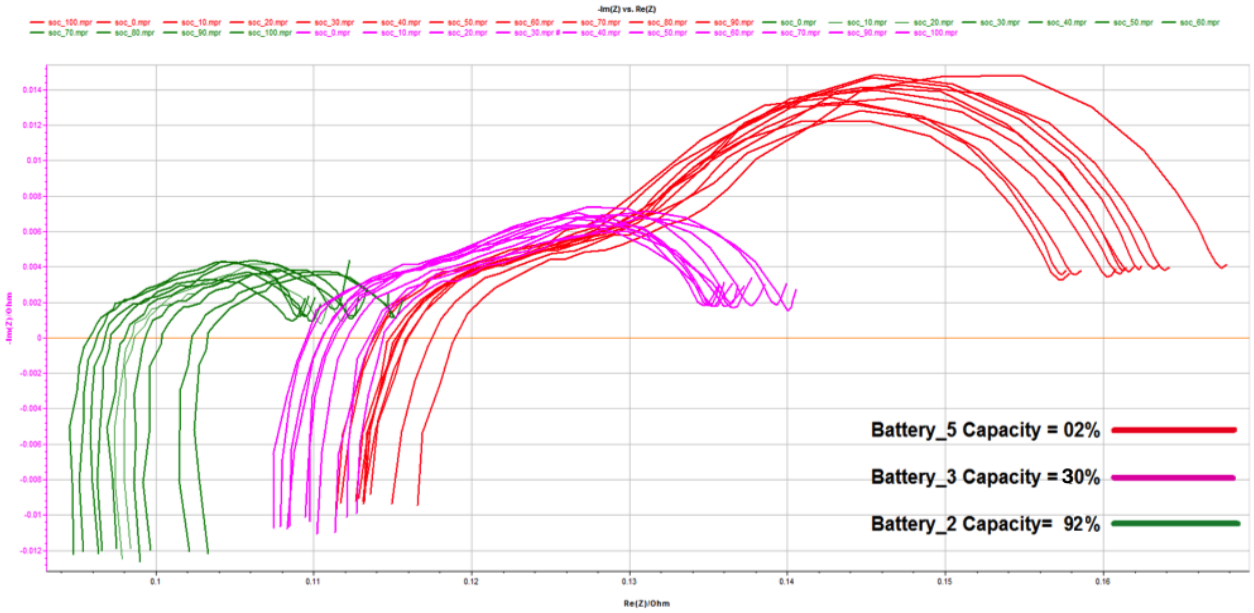

Figure 4.2. Impact of SoC on EIS scans

As shown in the figure, the overall shape of EIS scans remains intact for a specific battery, irrespective of the SoC. The slight variation is due to the change in amount of charge stored and partly due to battery terminal connection. Sometimes, the parasitic resistance of the connections was observed to impact the EIS scans and therefore, it can have result in small deviation, however, overall, the scans remain in close vicinity and adhere to the same profile.

The issue associated with the terminal connection of battery is illustrated in figure 4.3 and 4.4.

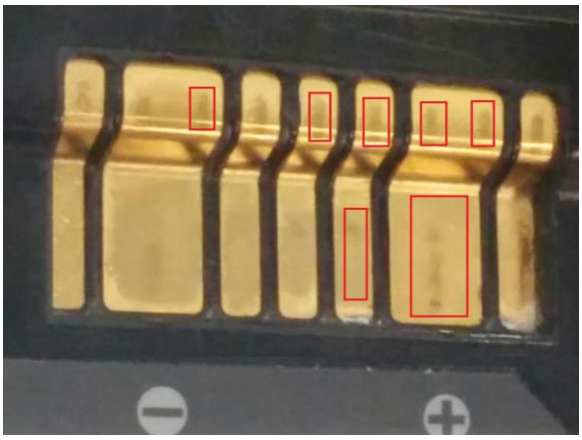

Figure 4.3. Dirt and residue on battery terminal

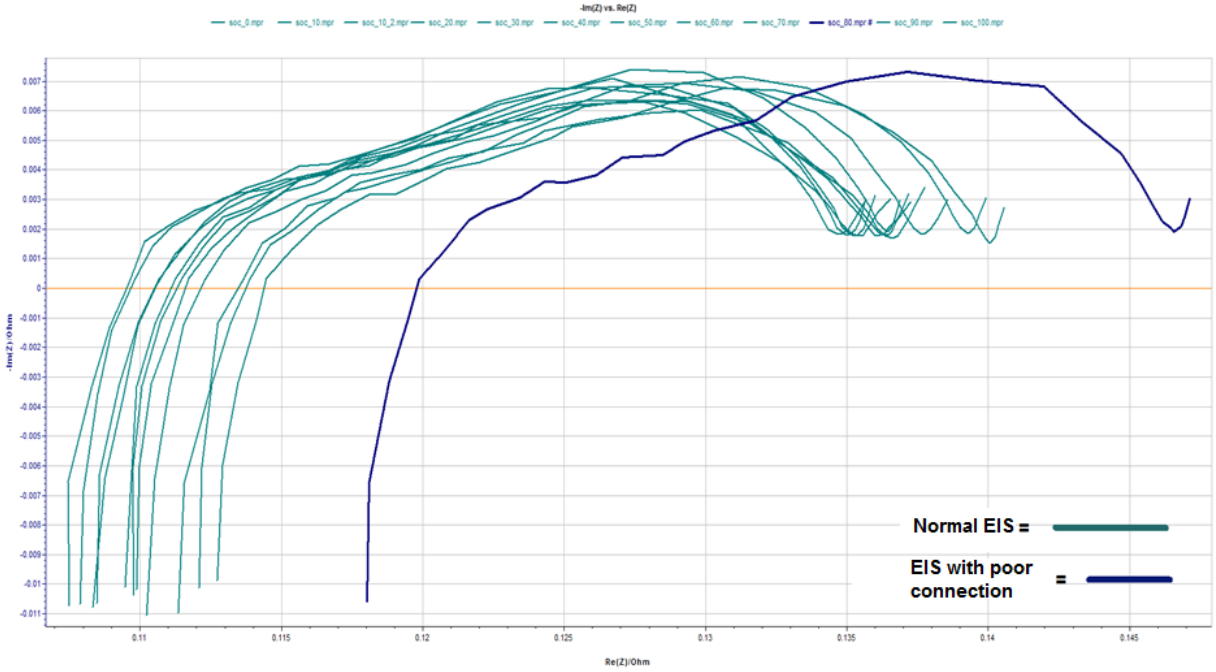

Figure 4.4. EIS scan with poor terminal connection

The impact of poor connection can be observed on the EIS scan with a large shift in the overall real impedance of the battery. This is because the terminal parasitic impedance only adds up to the series resistance, causing the EIS scans to shift towards the right side on a Nyquist plot. The overall shape of the Nyquist plot still remains the same as no change occurs in the dielectric and charge transfer properties of the battery.

4.4 Test plan and experimental setup for non-steady state analysis

As discussed earlier, in real world application, time is of essence as the user cannot wait indefinitely for the battery to rest before a test could be performed especially in critical usage such as medical and warfare applications. It is imperative to know for how long the battery has to stay in the rest condition before an EIS scan could be performed to decipher the SoH condition of the battery. Therefore, a test plan was devised to determine the duration of the rest time.

The batteries selected for this study are shown in table 4-3 and test plan details in table 4-4. Note that the batteries are selected from a pool of 14 batteries and have different battery ID's from the previous test. Four batteries are selected such that we have good overall spread in SoH.

Battery ID	Battery State of Health in %
Battery 1	64
Battery 2	90
Battery 3	30
Battery 4	02

Table 4-3 Batteries selected for non-steady state analysis

EIS Scan Test ID	Time at which test is performed
1	30 seconds
2	2 minutes 30 seconds
3	5 minutes 30 seconds
4	7 minutes 30 seconds
5	10 minutes 30 seconds

Table 4-4 Test plan details after each charge cycle

Once a battery was removed from the charging port after charging, the battery was allowed to rest and during that time OCV was recorded. After 30 seconds of rest time, first EIS scan was performed using VMP2 equipment. The battery was allowed to rest after the scan and OCV was recorded during rest time, before the next EIS scan was performed and so on. The final EIS scan was performed after 10.50 minutes when the battery had almost reached the steady state because the OCV of the battery was not changing afterwards.

Since user can request the EIS scan to be performed at any SoC while the battery is charging, it is important to repeat the analysis at varying SoC. Therefore, three different types of tests were devised to come up with contingency analysis from user's perspective. The difference between these tests was that the charging time was different in each test. The pictorial representation of the tests is shown below:

Test 1: 25% SoC Increment

In this test, the batteries selected for the study was completely discharged at first. Then the batteries were charged at an increment of 25 % of its actual capacity and the series of tests were performed.

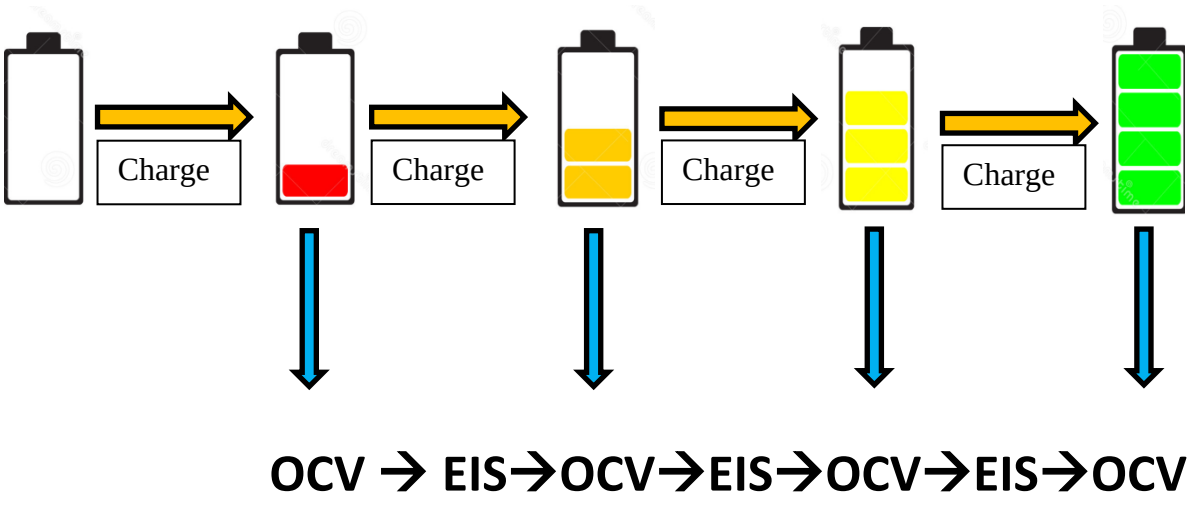

Test 2: 50% SoC Increment

In this test, the batteries were completely discharged first. Then the batteries were charged at an increment of 50 % of its actual capacity and the series of tests were performed.

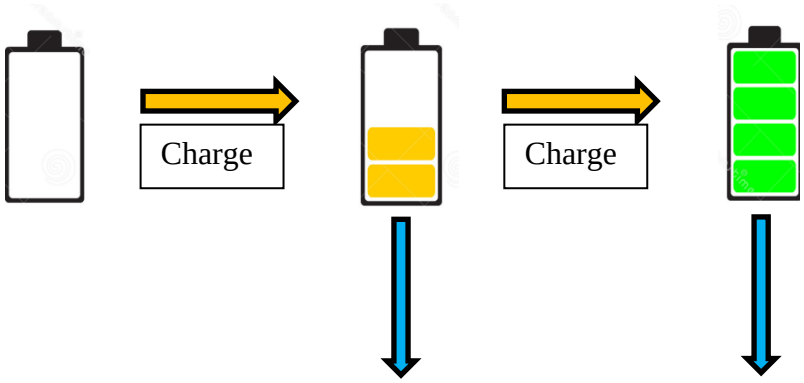

OCV → EIS→OCV→EIS→OCV→EIS→OCV

Test 3: 90% SoC Increment

Again, the batteries were completely discharged at first. Then the batteries were charged at an increment of 90 % of its actual capacity and the series of tests were performed.

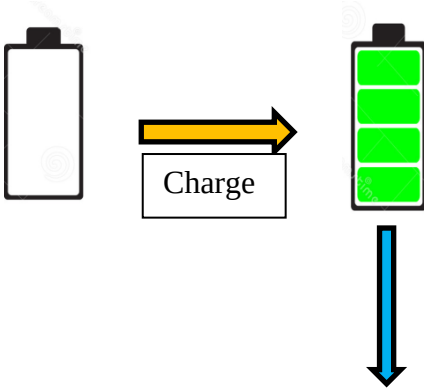

OCV → EIS→OCV→EIS→OCV→EIS→OCV

For the charging purpose, Cadex c8000 battery testing equipment was used. The charging current was selected to be 1200 mA (c-rate= 0.25). C8000 has built in protection to cater for over charging and overcurrent and it also has runtime interface with PC via Cadex battery shop.

4.5 Experimental results and analysis for non-steady state analysis

The data recorded from the experimental setup for non-steady state analysis was imported in Matlab for data processing. Tests performed after 30 seconds of the rest were observed to have kinky and non-smooth Nyquist plot as shown in figure 4.5. The noise in the low frequency region was observed because the voltage at the terminals of the battery was changing with time and therefore the impedance captured at low frequencies was subjected to the drift. This drift was very evident at lowest frequency points. However, the deviation was observed to be smaller in the EIS scans performed at 2.5 minutes as shown in figure 4.6. This is because the voltage at the terminals of the battery was getting stable and the resulting drift effect at low frequencies was smaller. Finally, EIS the scan taken after 10 minutes of the rest was shown to be smooth Nyquist plot, because the steady state condition of the battery was reached. The impact of the drift on the low-end frequencies was no longer there; hence a smooth Nyquist shape was obtained.

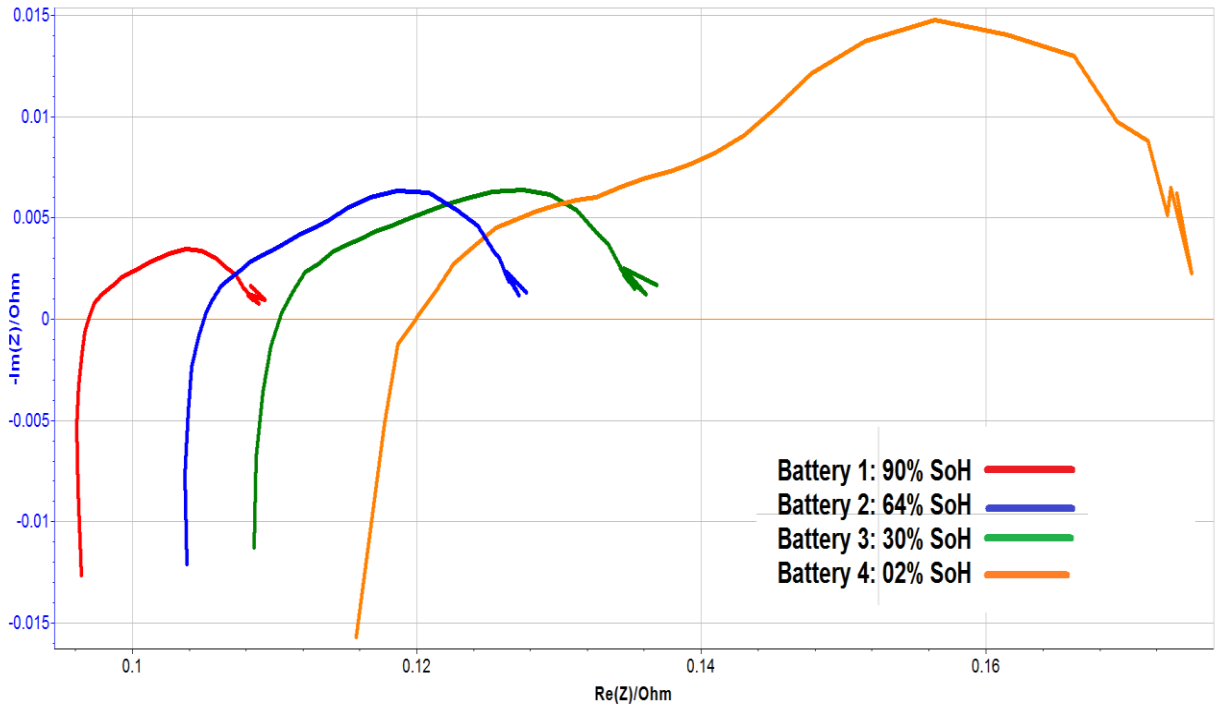

Figure 4.5. Nyquist plot after 30 seconds of rest for test 3

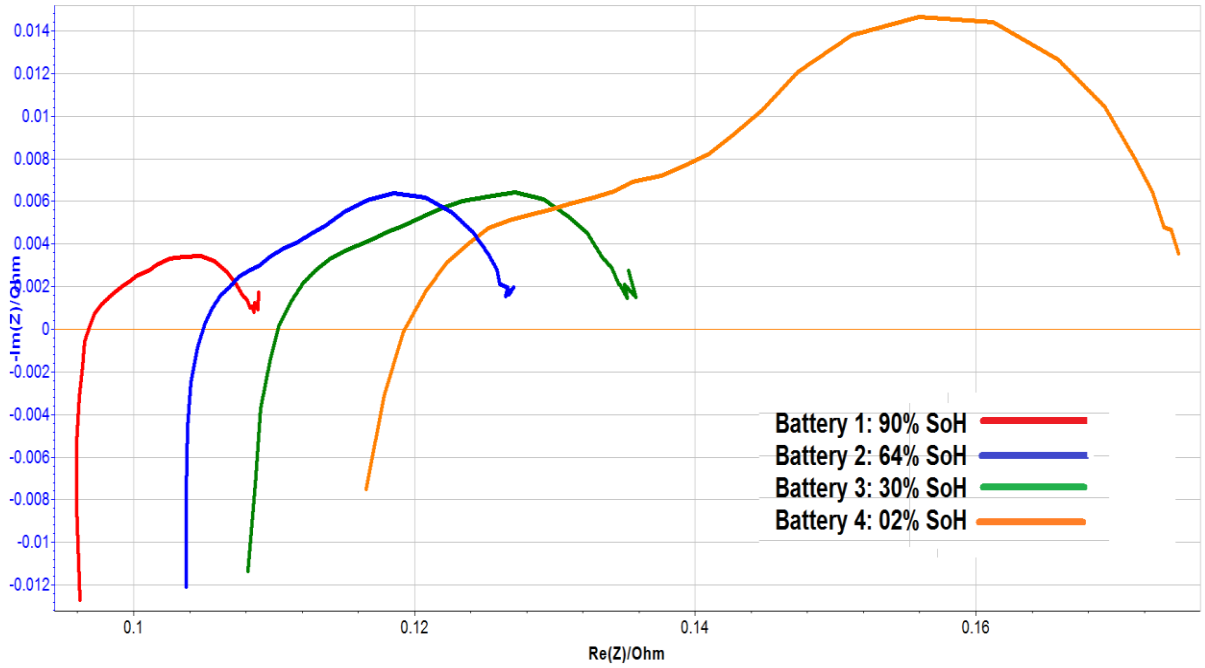

Figure 4.6. Nyquist plot after 2.5 minutes rest for test 3

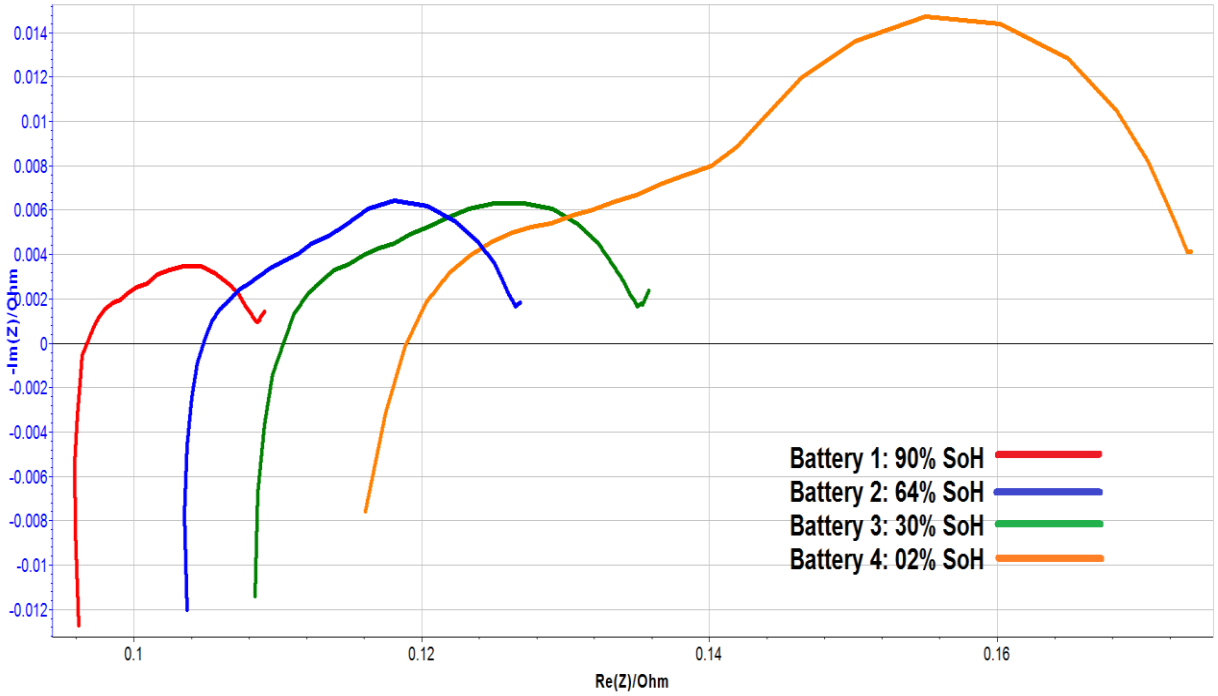

Figure 4.7. Nyquist plot after 10.5 minutes rest for test 3

All Nyquist plots captured for all the tests are shown in figure 4.8. The data was processed to locate the zero crossing and maximum point on the Nyquist plot for SoH algorithm analysis. With slight deviation along the real axis, the overall results came out to be coherent. The data showed that the Nyquist plot for each battery remains in the close proximity and follows similar shape, regardless of the charging status of the battery. This turned out to be a fortunate thing for HCC prototyping as the user can have the opportunity to stop the charging process and run the SoH determination test.

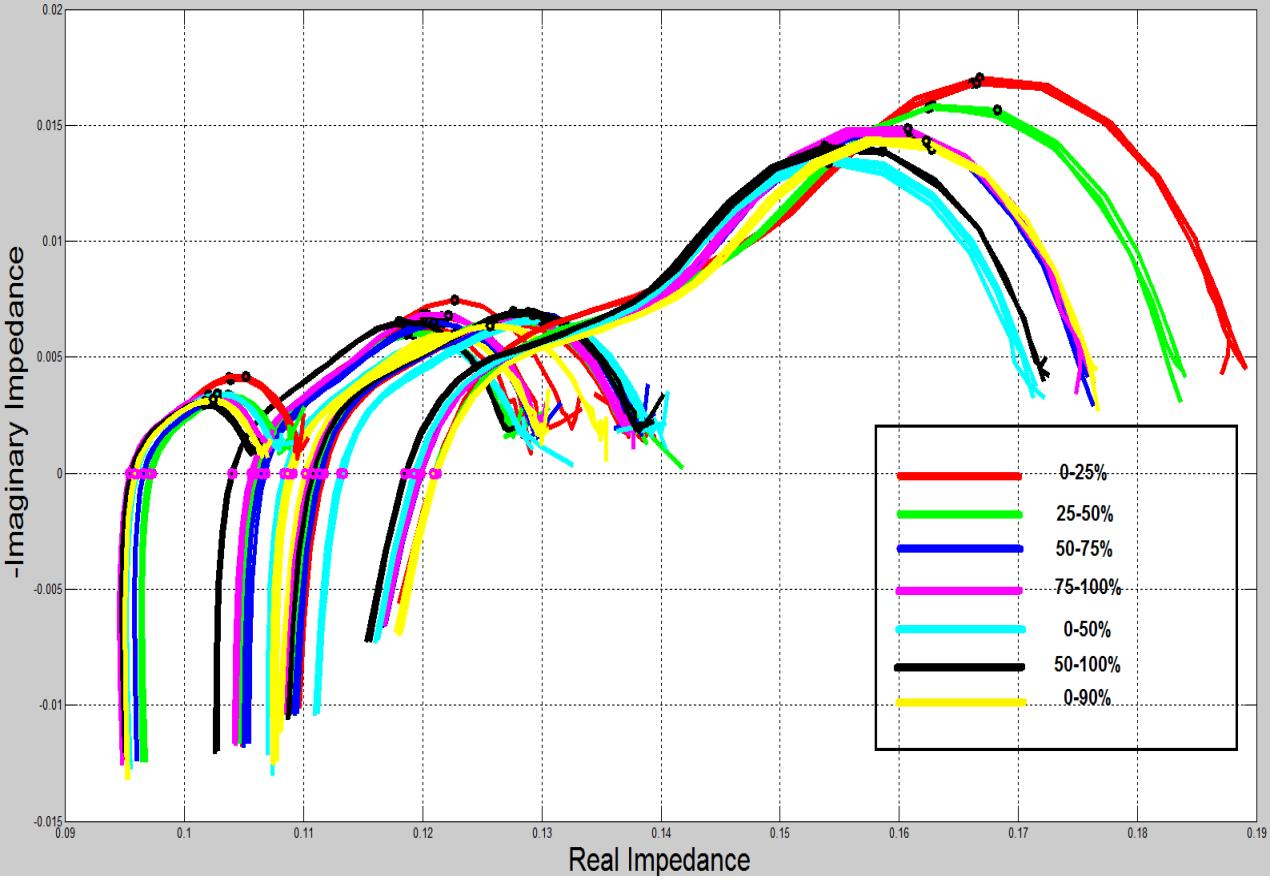

Figure 4.8. All EIS scans for non-steady state analysis

This slight deviation in the Nyquist plots along the real axis is due to the variable parasitic resistance across the battery terminals. This induces small error in SoH estimation that will be discussed in the later sections. However, for overall battery characterization, this impact is

minimal. The only factor of concern is the rest time before the EIS test could be performed which will be addressed in detail in chapter 5 where EIS scans were captured using HCC board. The OCV of the batteries was logged during resting time that showed that the voltage at the terminals of the battery settles down with the passage of time, resulting in suitable condition such that EIS scan could be performed. Figure 4.9 shows the gradient of the OCV for the battery 2.

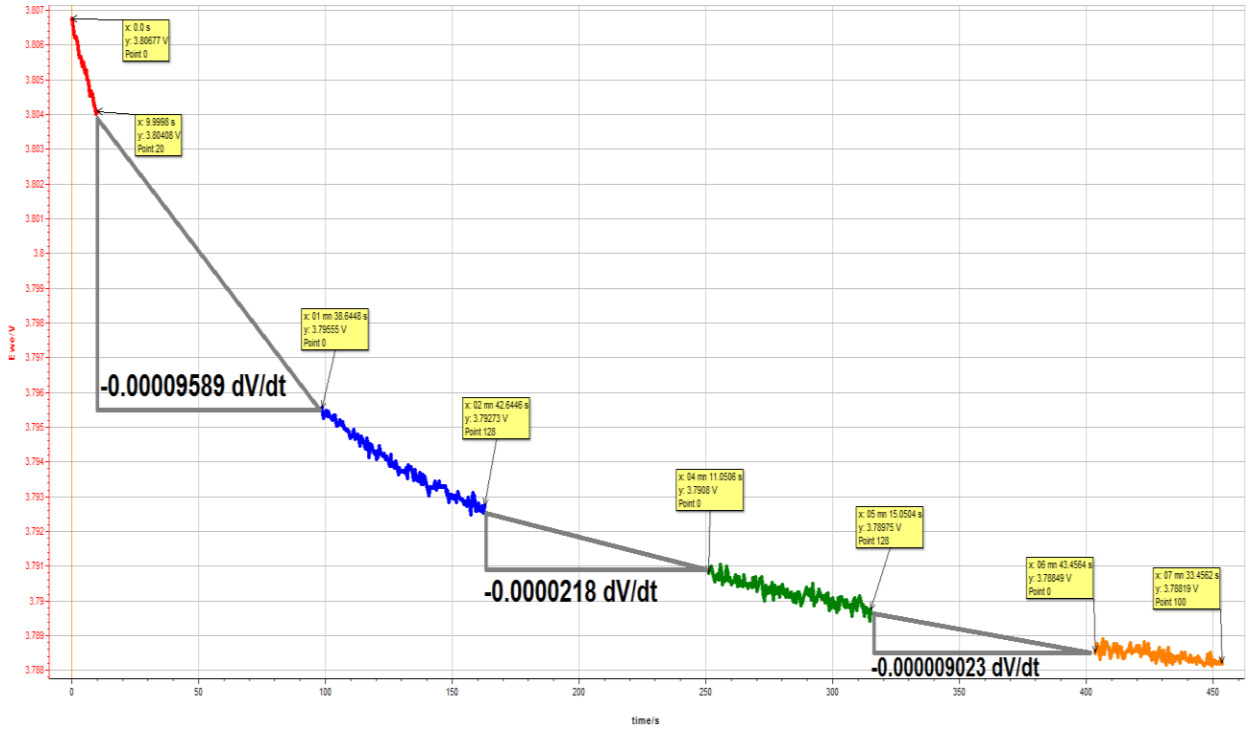

Figure 4.9. OCV gradient for battery 2

This shows that with the passage of time, the transients of the battery die down. After 2 minutes the change in the voltage across the terminals of the battery is not very large, therefore an EIS scan could be captured. However, the best result can only be possible if the battery is in steady state. The tests illustrated that the OCV settles down non-linearly when the battery is allowed to rest at several SoC's and after some time the gradient is small enough to assume quasi steady state condition. Figure 4.10 and 4.11 shows OCV comparison for batteries as test 1, 2 and 3 were performed on them.

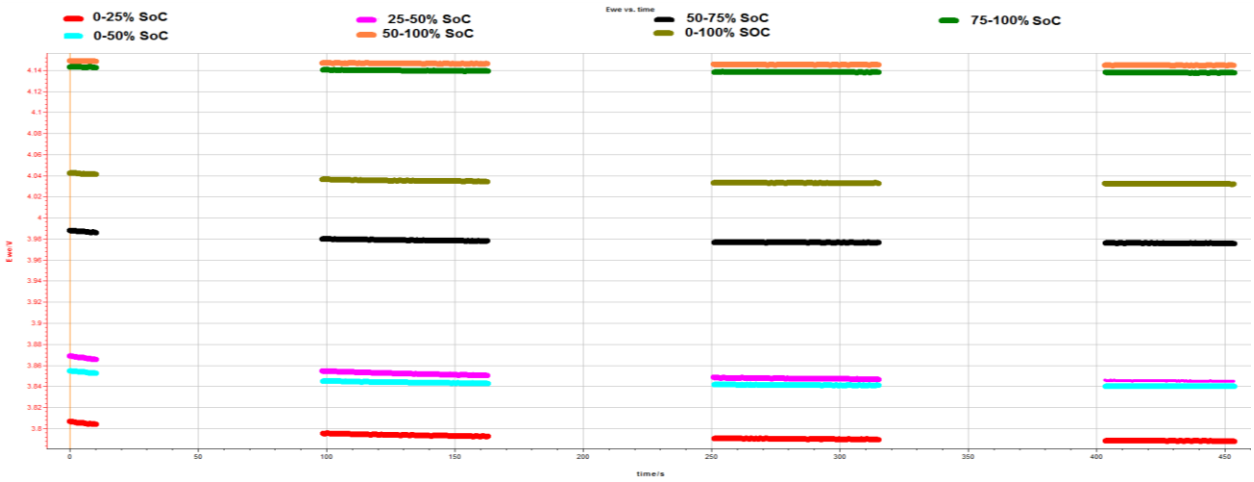

Figure 4.10. OCV recording after tests for battery 2 (90% SoH)

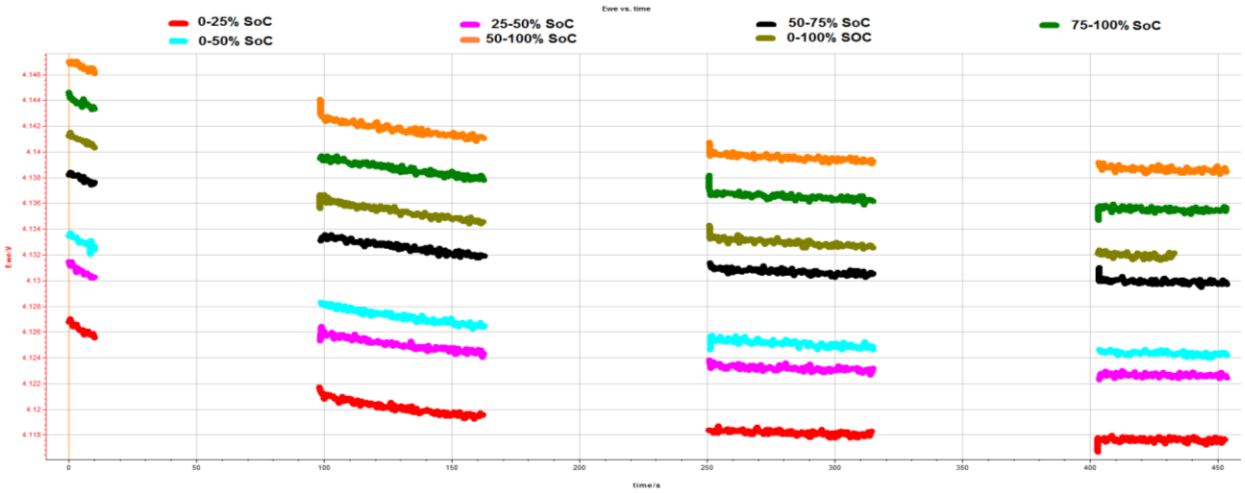

Figure 4.11. OCV recording after tests for battery 4 (02% SoH)

The plots show that the OCV of the battery settles down in the similar way and is not related to the operational condition or SoC of the battery. The time it takes for the battery to reach the steady state condition was found to be constant throughout the tests. This observation hold key significance in determination of waiting time required, that the HCC needs to wait before it performs the EIS scans on the batteries. The independence from the SoC or the charge profile allows a generic algorithm to be designed. This topic will be explored further in detail in section 5, where results recorded from HCC will be processed to decide the suitable resting time before the EIS test could be performed.

4.6 Data analysis for SoH algorithm

After an EIS scan is successfully performed and the desired data is recorded, only part of the job is done. The data itself provides information about the individual characteristics and electrochemical properties of the battery, but in order to relate it to the state of health some operations are required to be performed. The user cannot take raw data and process it on his own to find the SoH of the battery. Therefore, an efficient SoH determination algorithm is has to be designed to give a prompt reply to the user's request in a quantitative way.

As discussed in previous section, the process of battery modeling and parameter evaluation through optimization is one option to estimate the SoH. However, the process is time consuming and requires complex computation. The process requires fast microcontroller chip for computation and it can extend the overall test time depending on number of iterations performed to obtain the final result. This reduces the overall feasibility of the battery modeling and parameter evaluation.

Hence, a new approach is proposed in this thesis, according to which a SoH determination algorithm can be designed directly from the EIS plot. A function can be designed to to relate the characteristics of EIS scan to the overall state of health of a battery. The points of interest chosen to design the SoH algorithm are shown in figure 4.12 and they correspond to different characteristics of the battery's electrochemical properties. The zero crossing point corresponds to series resistance. The maximum x and maximum y values correspond to double layer capacitance, charge transfer resistance and dielectric properties. The minimum x value corresponds to mass

kinetic properties such as diffusion of ions and Warburg impedance. Section 3.1 shows how these properties impact the corresponding regions of EIS scans by equivalent circuit modeling.

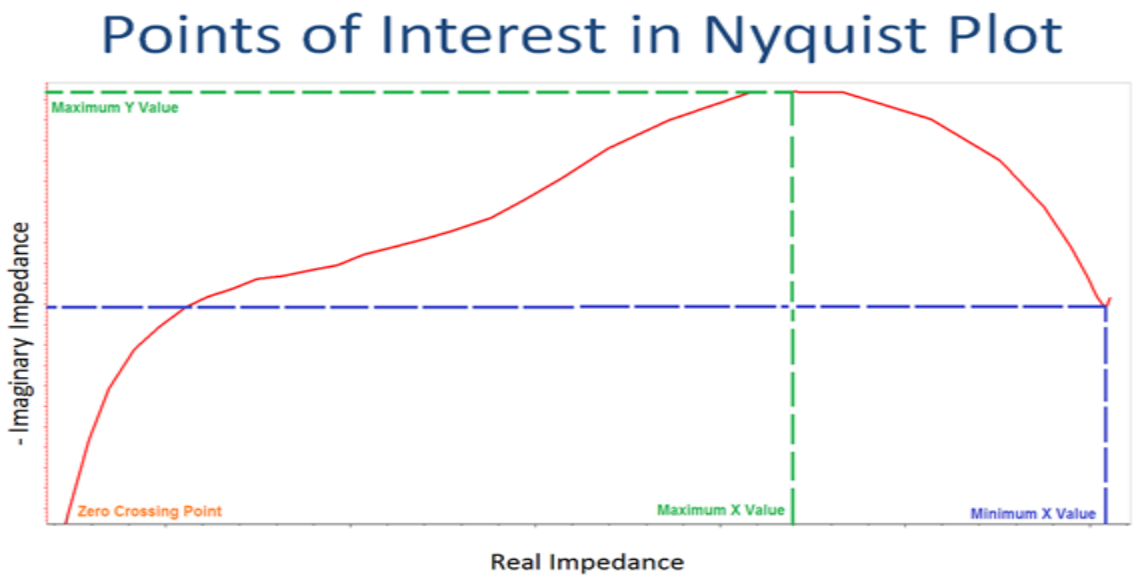

Figure 4.12. Points of interest in Nyquist Plot

All these factors correspond to electrochemical properties that relate to the ageing processes in a battery, as a result, SoH is a function of all of these characteristics. Therefore, a program was written in Matlab that could detect the points of interest in an EIS scans automatically. The zero-crossing point, minimum x-value, maximum x-value, minimum y-value and maximum y-value were recorded for all EIS scans. However, before these points were directly calculated from the EIS scans, the raw data was processed to give a smooth EIS plot. In order to smooth the raw data obtained from the EIS scan, a moving point algorithm was implemented in Matlab.

$$\text{Simple Moving Average (SMA)} = \frac{p_M + p_{M-1} + p_{M-2} + \cdots + p_{M-(n-1)}}{n}$$

$$= \frac{1}{n}\sum_{i=0}^{n-1} p_{M-i}$$

The algorithm was used to smooth down the raw data obtained from the EIS scan such that the impact of noise and time variations in data logging could be minimized. Figure 4.13 shows normal EIS scan plotted along with the data smoothed by the moving point average algorithm.

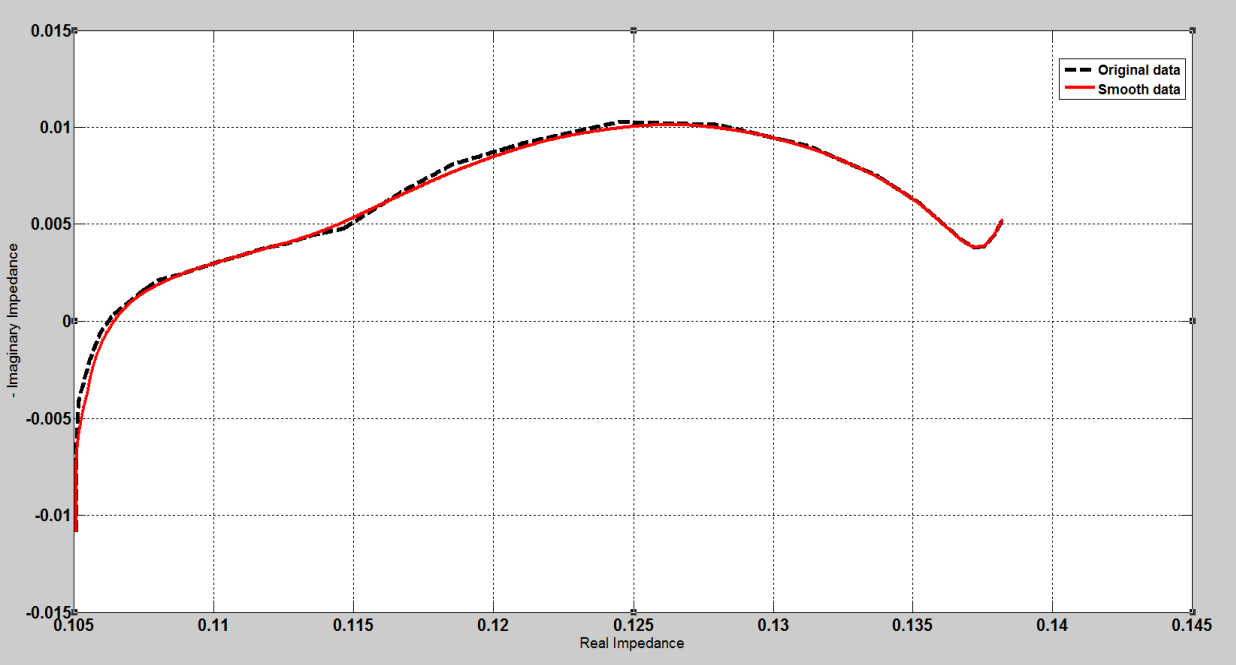

Figure 4.13. Raw data vs smooth data using moving point average algorithm

The algorithm was used to smooth all the EIS scans taken for the batteries for SoC study

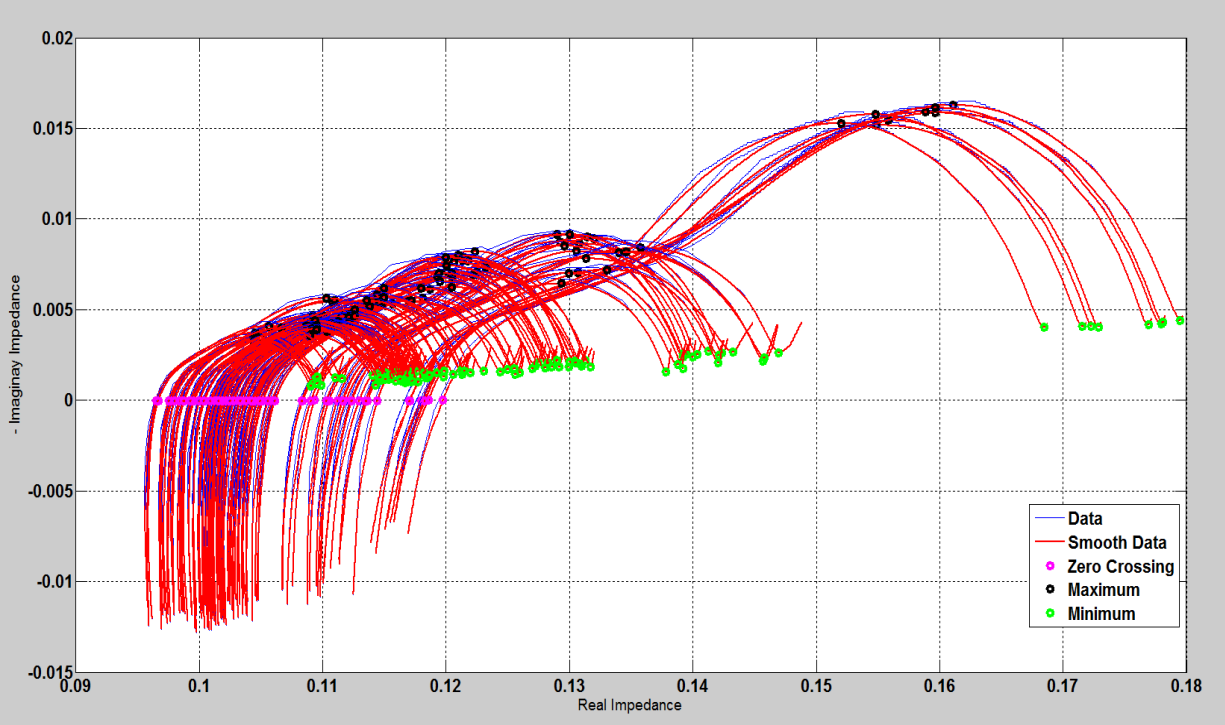

Figure 4.14. All EIS scans with marked points of interests

The points of interests were plotted individually on z-axis with different SoH on y-axis, SoC on x-axis. The bar plots are shown in figure 4.15, 4.16, 4.17 and 4.18.

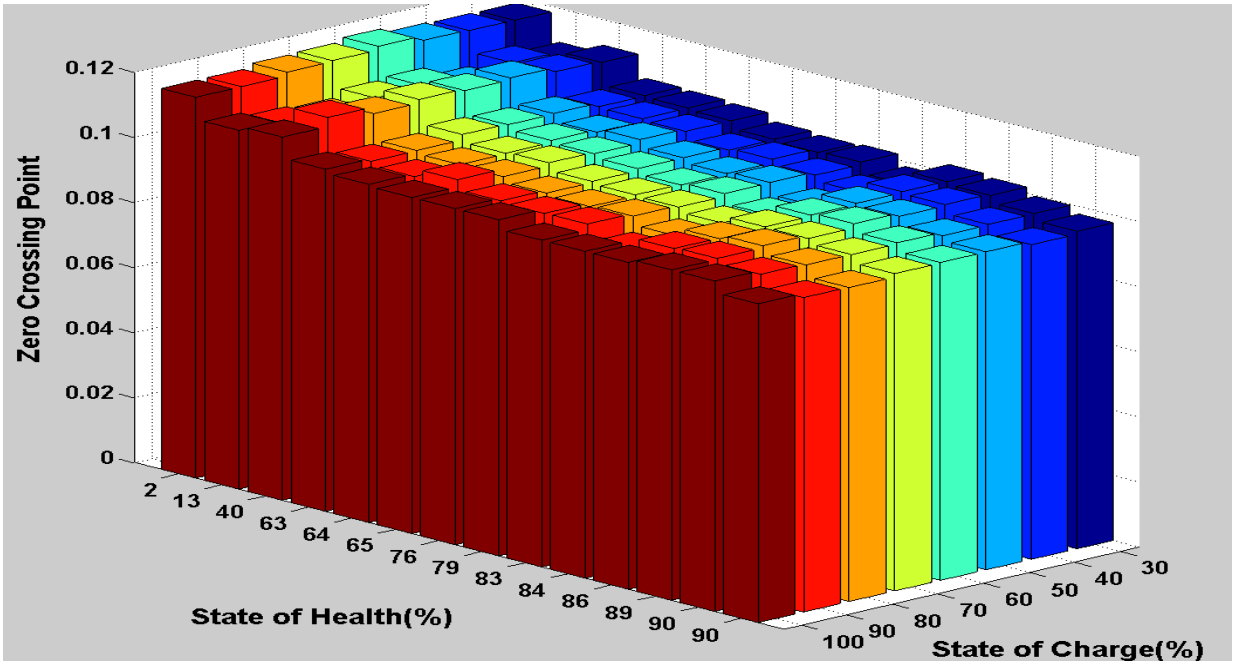

Figure 4.15. Zero-crossing point evaluation

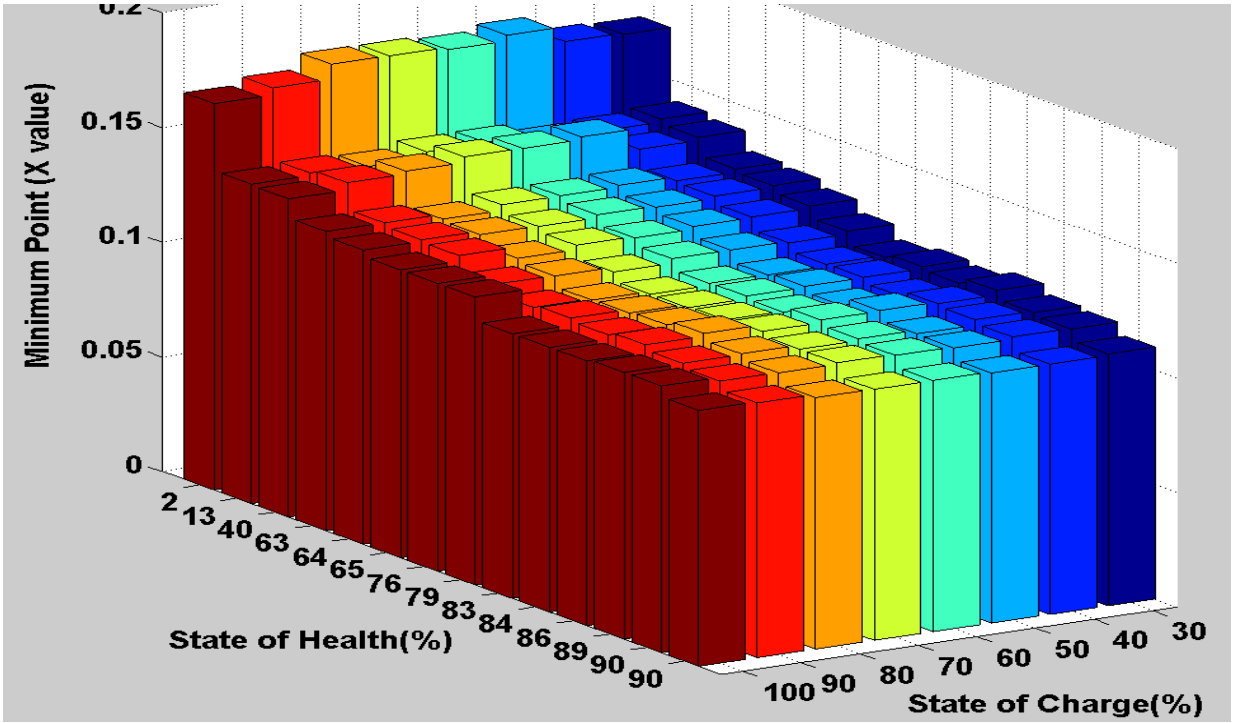

Figure 4.16. Minimum Point (X value) evaluation

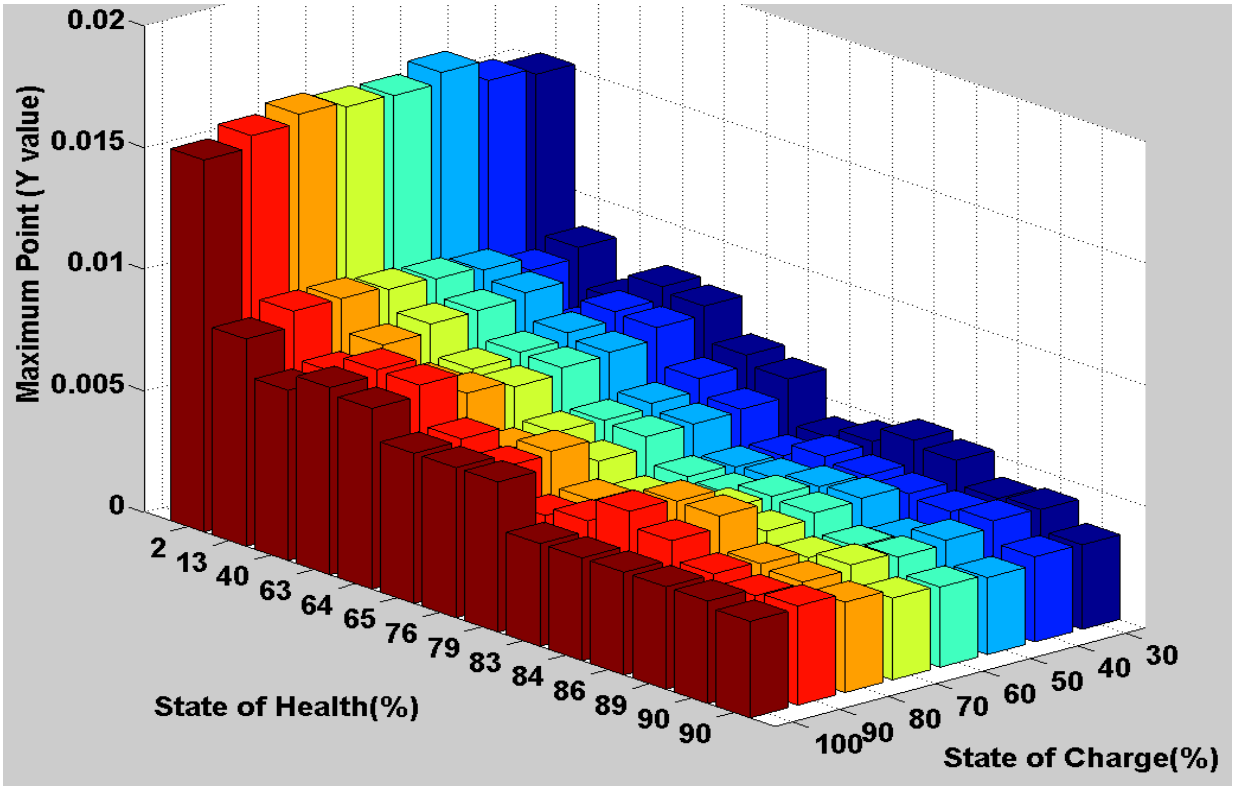

Figure 4.17. Maximum point (Y value) evaluation

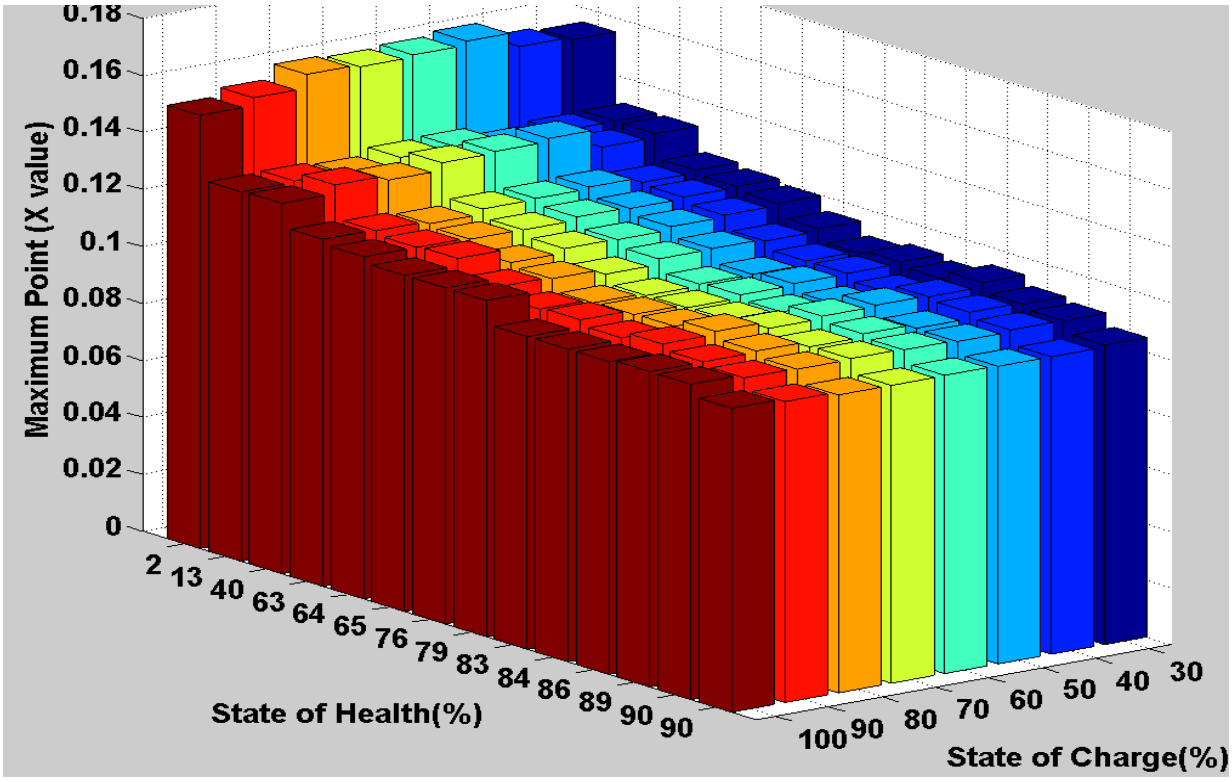

Figure 4.18. Maximum point (X value) evaluation

The data shows that the points of interest chosen for SoH algorithm had strong correlation with the SoH. The impact of SoC on these points is minimal as compared to variation coming from the SoH. However, the low SoC data was removed from analysis, since these batteries were discharged with rated 10% capacity and not actual 10% capacity. Therefore, the results of very low SoC for few batteries came out to be very divergent and non-coherent. In practice, when these batteries will be tested, the batteries will be operating according to their actual capacity so, the algorithm is expected to work fine on low SoC as well. This assumption was put to test in algorithm validation section and results presented in chapter 5 support this hypothesis.

Using these points calculated for all EIS scans, a plot was constructed to estimate the error that can come from SoC. The SoH of batteries were plotted on the y-axis along with individual point of interest on the x-axis. The error bars show the variation in the point of interest that can happen due to the difference in SoC. The results are shown in figure 4.19, 4.20, 4.21 and 4.22.

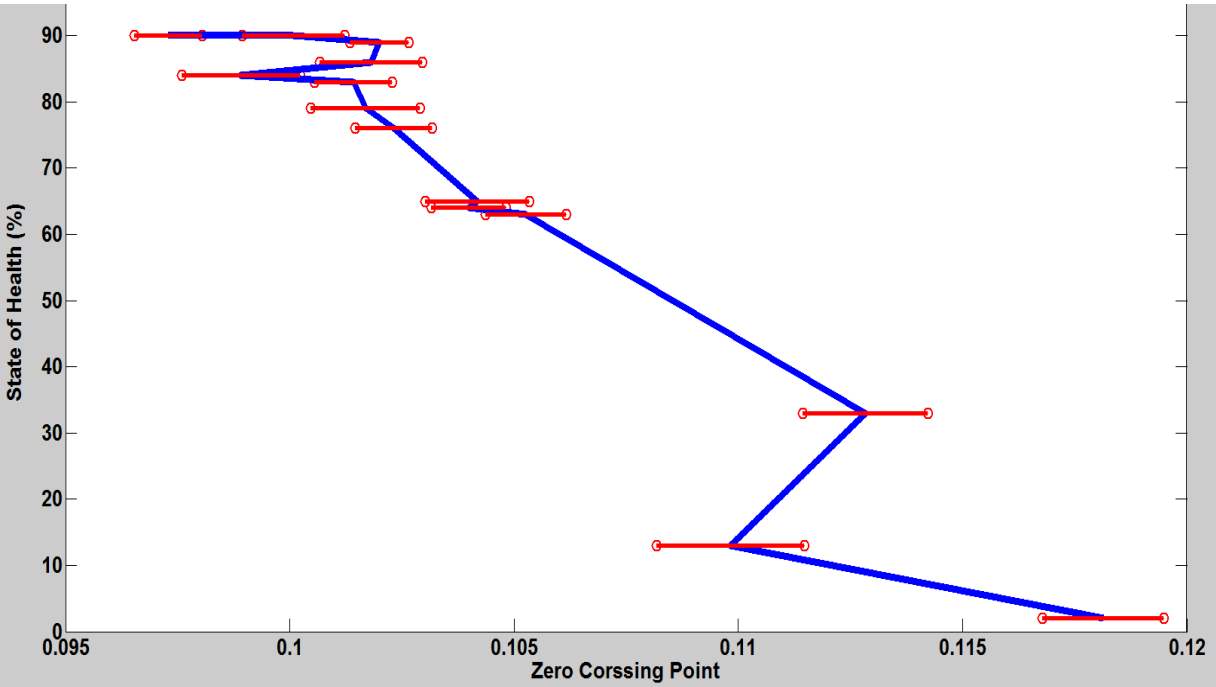

Figure 4.19. Zero crossing point error bar

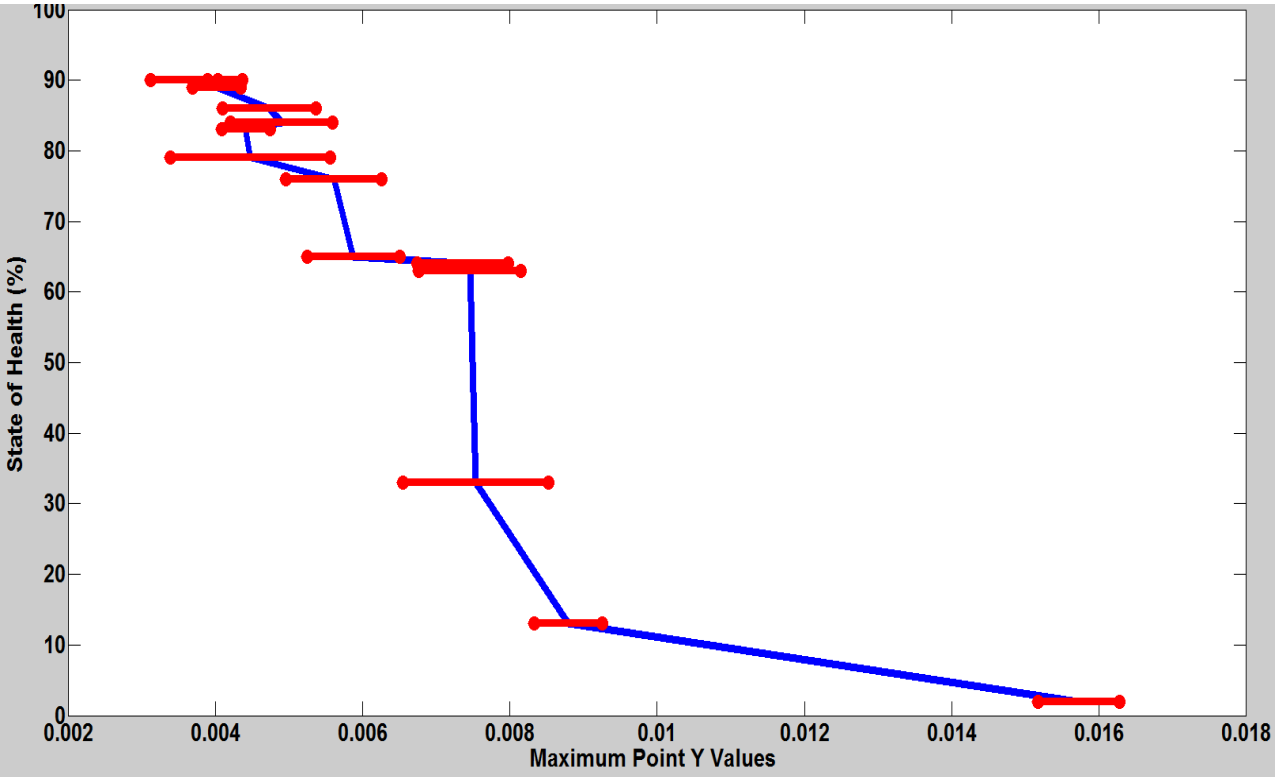

Figure 4.20. Maximum point Y values error bar

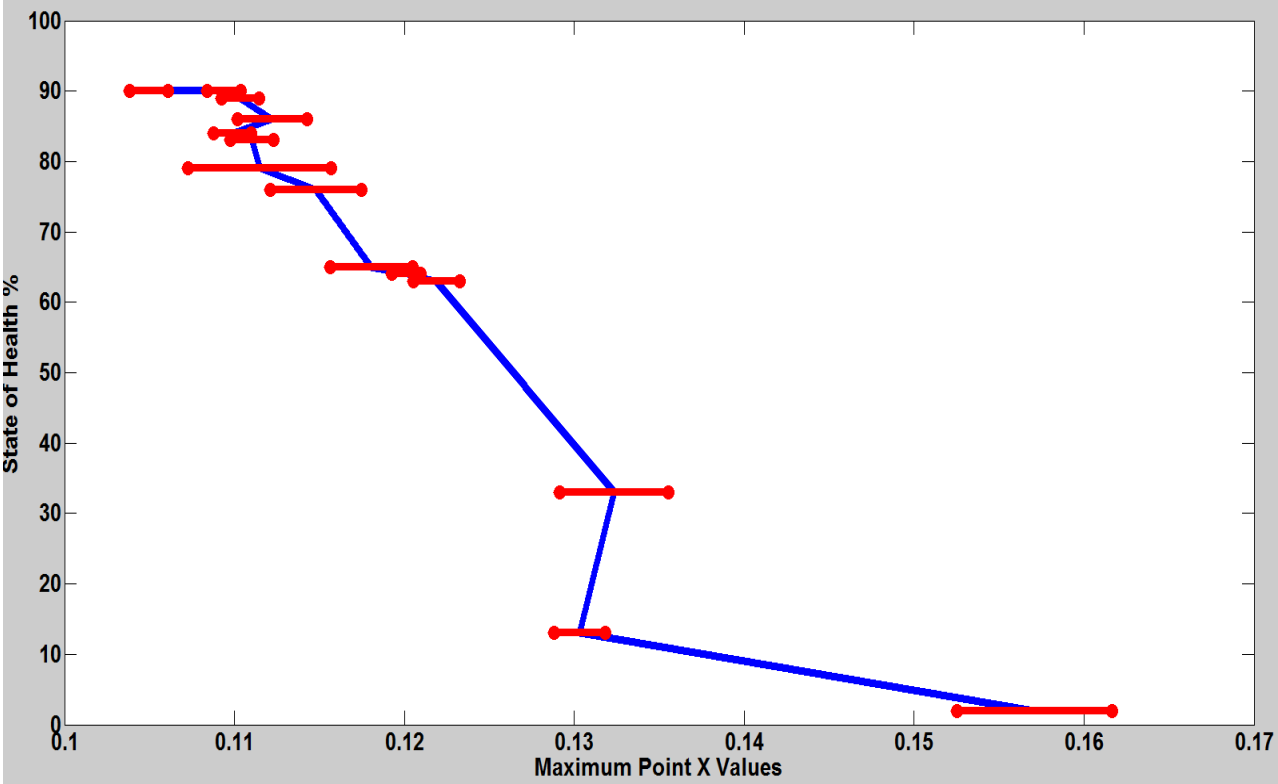

Figure 4.21. Maximum point X values error bar

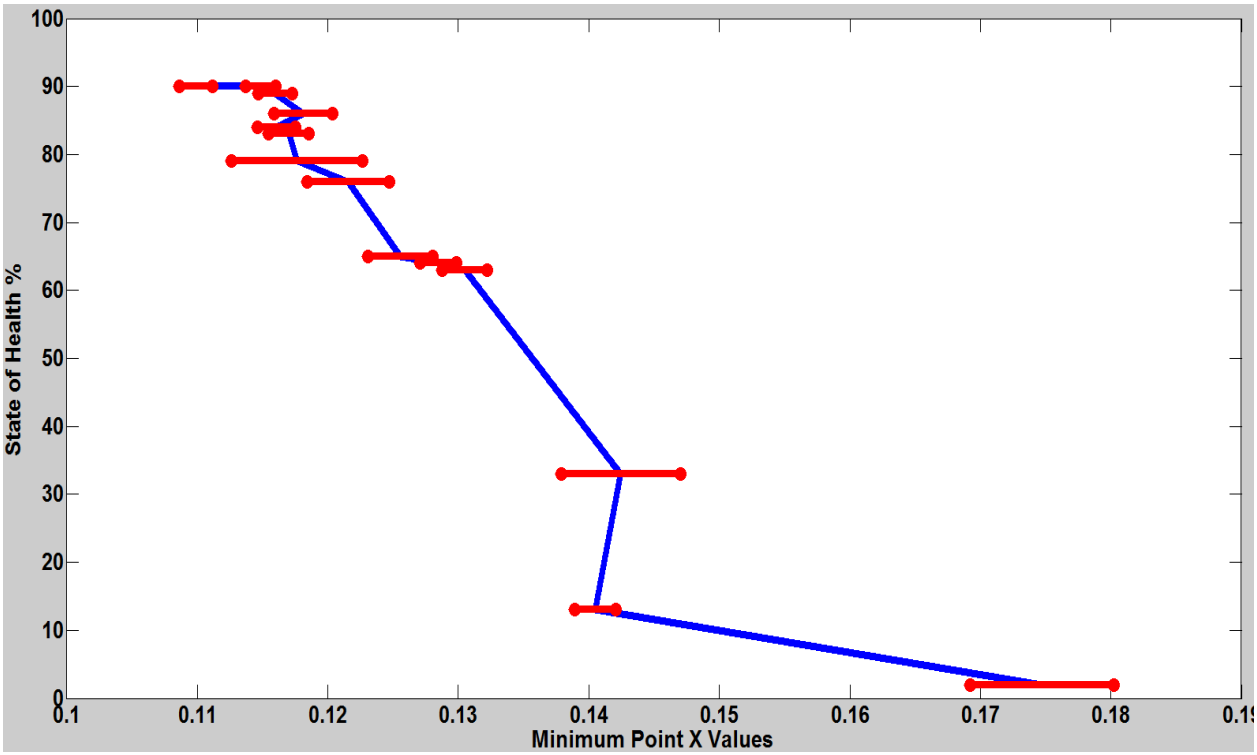

Figure 4.22. Minimum point X values error bar

The error bars on all these graphs indicate a small deviation that is caused by the variation in state of charge. The deviation is small as compared to overall span of values and therefore, the impact of this factor on SoH algorithm function can be eliminated if battery is not completely void of charge.

Now the final SoH algorithm has to be a combination of all these points such that variation in one of these factors contributes partially to the overall SoH of the battery. Based on the variation shown by the points of interest in comparison to the overall SoH, the sensitivity factors were designed. More weight was assigned to the point of interest that showed larger correlation with the SoH. The overall function that relates all these point of interest to single function input value is shown below:

$$Function\ Input = 30*Max_x + 20*Max_y + 40*Min_x + 10*Zero$$

The function input relation to the SoH of the battery is shown in figure 4.23.

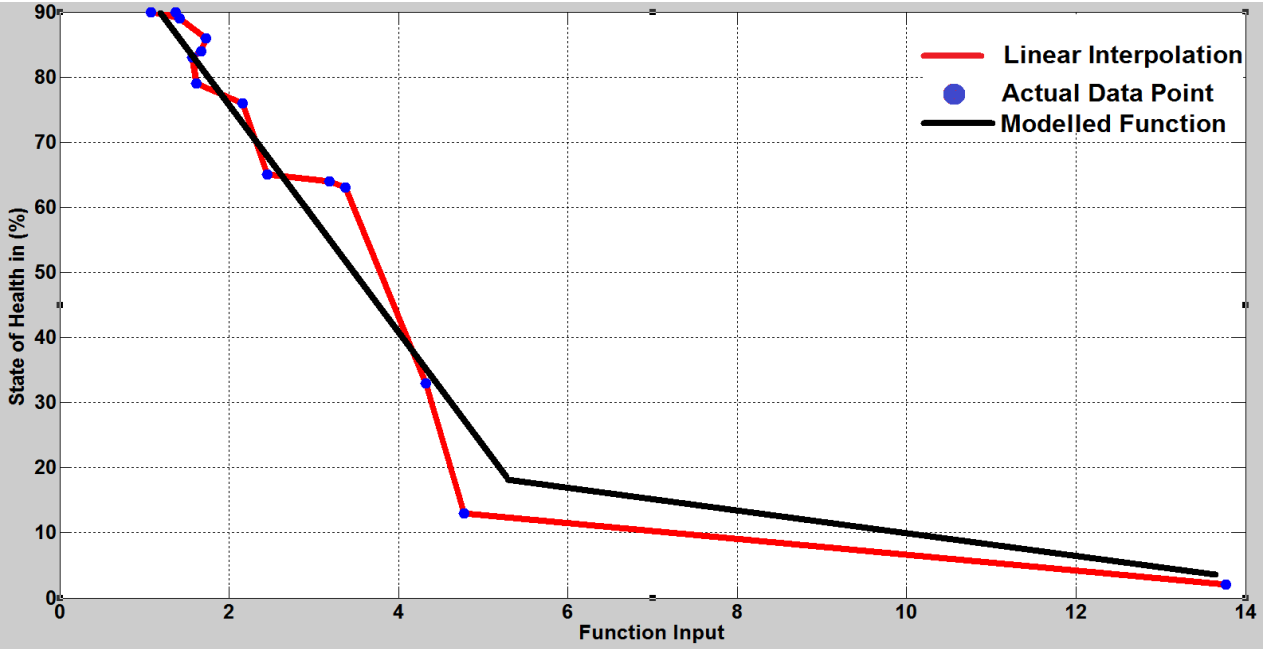

Figure 4.23. Piece wise linear model for SoH vs Function output

Since the function output itself cannot map to the SoH of the battery, another one to one function was required. Therefore, in order to make a suitable fit, a piece wise linear function was proposed such that the function input, *x*, maps to give SoH as a percentage as shown

$$\text{State of Health}(x) = \begin{cases} -16.3 * x + 107.6, & 0 < x < 5.5 \\ -1.77 * x + 27.7 & 5.5 < x < 14.5 \end{cases}$$

So, now the after successfully recording the EIS scan, this algorithm can process the data captured to determine the SoH of the battery. Although this SoH algorithm is designed using 14 batteries as data points, the algorithm accuracy can be improved by increasing battery sample set. The error in batteries having very low SoH is observed partly because their response to EIS scan can vary by large amount. However, the method promises to accurately estimate batteries with high SoH. The algorithm is designed to estimate SoH accurately in a time effective manner.

Chapter 5: Health Check Charger Prototype

5.1 Hardware setup

So far we have discussed EIS as a technique to evaluate the SoH of the battery. However, for product development of HCC, a portable hardware platform was needed that can perform EIS scan on Li Ion batteries. Therefore, for the development of HCC, the existing schematic and circuit provided by Cadex Electronics Inc. was used. A team of students of UBC developed the platform for their capstone project. The schematic was designed to performed EIS scans for 2.7 V to 4.3 V batteries. The hardware comprised two parts: potentiostat circuit and digital signal processor. The potentiostat circuit comprised analog amplifiers and instrumentation amplifier to perform the EIS test. The circuit voltage and current sensors were used to record battery terminal voltage and current using ADC's of DSP chip. The captured data was processed using STM32F429 micro-controller. Figure 5.1 shows the hardware circuit:

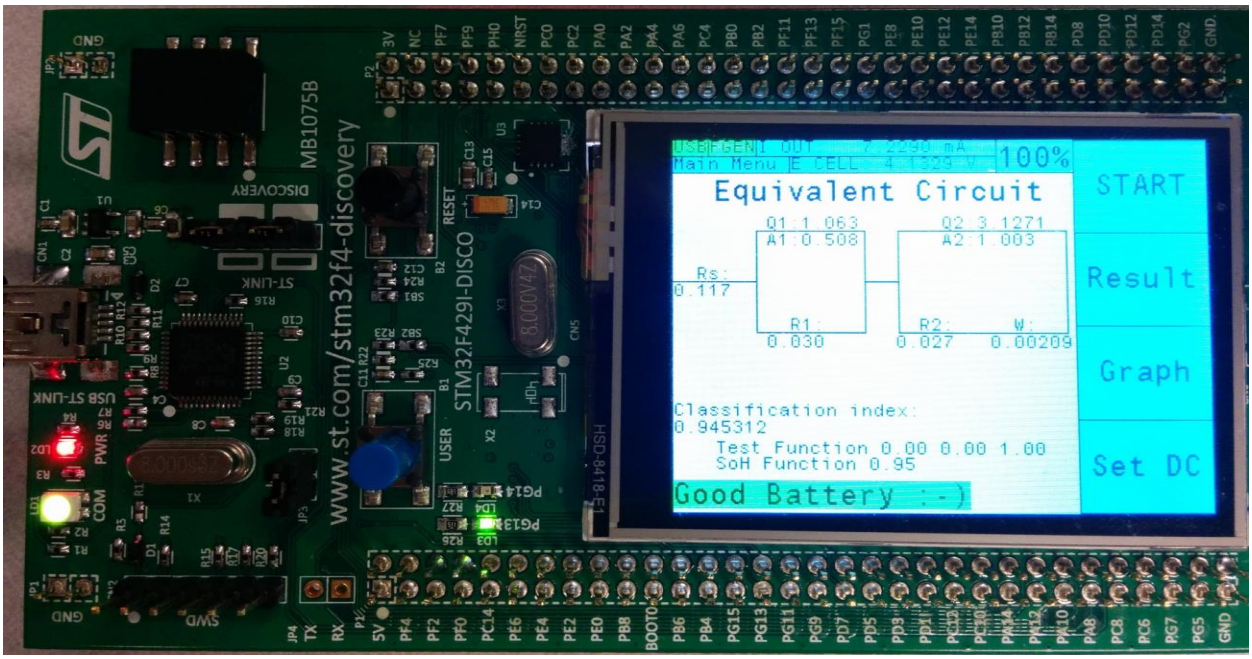

Figure 5.1. Hardware implementation with LCD display

A potentiostat was designed to excite li-ion batteries with a voltage waveform. It included sensors and signal conditioning to measure the voltage and current response of the batteries under test. The basic design was found in [12] and was modified to allow the potentiostat to test batteries ranging from 2.7-4.7V and interface with a 3.3V. Appendix A outlines the potentiostat circuit's main sub circuits. DAC1 is used to generate the waveform. The excitation conditioner is used to generate a low amplitude voltage wave without a DC offset. DAC2 generates a DC reference that allows the output of the potentiostat to be biased anywhere between 2.7-4.7V. The reference is set to match the open circuit voltage of the battery under test. The potentiostatic control sums the waveform and DC reference so it can be passed through the battery. A relay is used to connect the battery to the circuit. The current output is obtained by measuring the voltage across a 0.2 Ω shunt resistor. The voltage output is obtained by subtracting the DC reference from the output using a difference circuit and amplifying in order to measure it with an ADC.

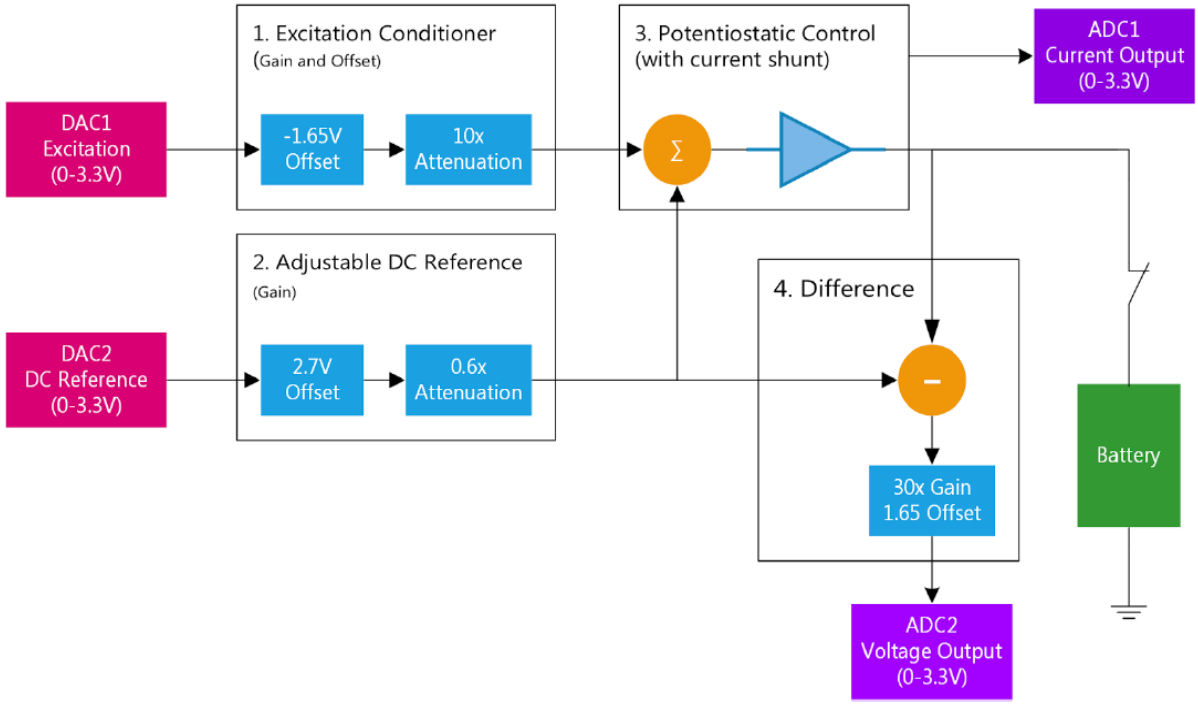

Figure 5.2. Potentiostatic block diagram

5.2 Software

An STM32F429 Discovery development board was used to develop the firmware. The microcontroller interfaces with the potentiostat, relay, LCD touch screen, external SDRAM, and a personal computer. A system level block diagram can be seen below in Figure 5.3.

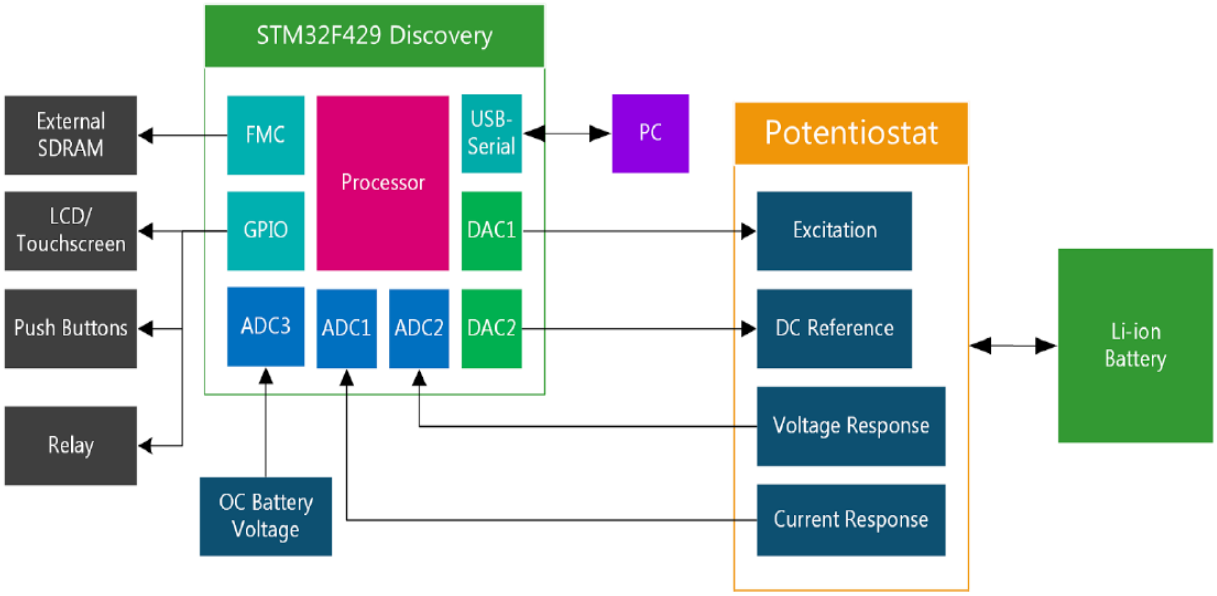

Figure 5.3. EIS test circuit block diagram

The battery tester obtains the impedance spectrum by using a multisine wave and successive sine waves. A multisine wave is used to obtain impedance data from 0.1 Hz to 7 Hz. Successive sine waves are used for 9 Hz to 2 kHz. The higher frequency impedance data was collected using successive sine waves because of sampling constraints and 16 test cycles were used. The EIS measurement consists of setting the DC reference to match the battery voltage, closing the relay, setting the waveform, sampling voltage and current, and computing the complex impedance. A flowchart of this process can be seen in Figure 5.4 below. The waveforms are cycled from multisine to successive sine waves until the complete impedance spectrum from 0.1 Hz to 2 kHz is obtained.

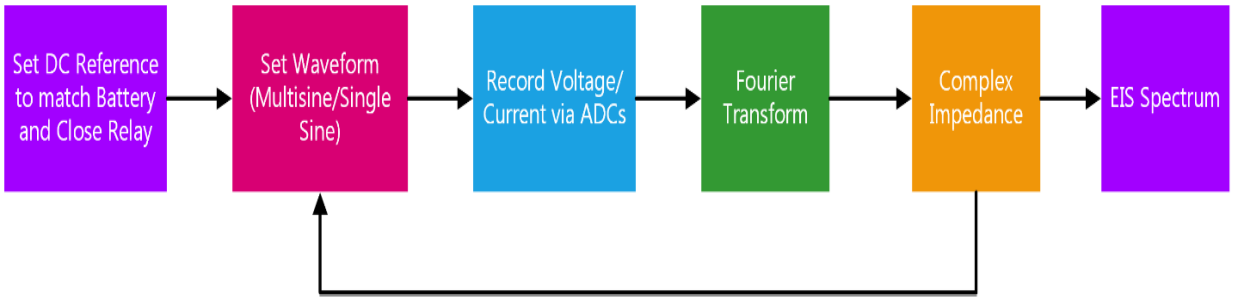

Figure 5.4. Impedance spectrum acquisition diagram

The DC reference is set by first measuring the open circuit (OC) voltage of the battery and then adjusting the second DAC output until the voltage matches the OC voltage. Once the DC reference is set the relay is closed and the battery under test is electrically connected to the potentiostat.

The waveforms are stored in arrays in the microcontroller and a DMA controller is used to control the first DAC to output the excitation wave. The DMA controller makes it possible to output the excitation wave with precise timing and also does not use any processing cycles from the microcontroller. While the waveform is running, ADCs are used to sample the voltage and current response and store the data in external SDRAM.

The data is sampled at 400 kHz, which is possible because of the DMA controller. The voltage and current data are sampled simultaneously, so phase errors are not introduced when computing the impedance.

A Fourier transform is used to obtain the voltage and current spectrum from the time domain data collected by the ADCs. Dividing the voltage and current spectrum yields the complex impedance. A Fourier transform is most commonly computed using a fast Fourier transform (FFT). However, performing an FFT with over 32,000 data points is not feasible on a microcontroller due to memory constraints. A Goertzel algorithm was used because it is able to compute the discrete Fourier transform for specific frequencies in the spectrum, which is

advantageous because when using multisine or successive sine waves only fixed number frequencies need to be computed.

5.3 User interface

The user interface is designed to be user friendly for storefront applications. It utilizes STM32F4 microcontroller's 320x240 touch screen LCD display, and is programmed with touchscreen buttons. The user interface was designed with the help of the STM32F4's online libraries [11]. The main menu has a status bar on the top of the display to indicate the status of the tester. The user is notified whether Serial USB data transfer is connected, whether the waveform is being generated through the DAC channel and current and voltage measurements are also displayed on the top to ensure that no overcurrent has occurred.

In the plot graph menu, on the top left the user have the option to exit the graphing menu and return to the main menu. The grid button allows user to toggle the grid on and off for better visualization of the graph and trace the data points on the plot.

After the result button is pressed it will give a diagnosis of the battery's state of health. The result is shown in the main menu along with the estimate of the SoH of the battery.

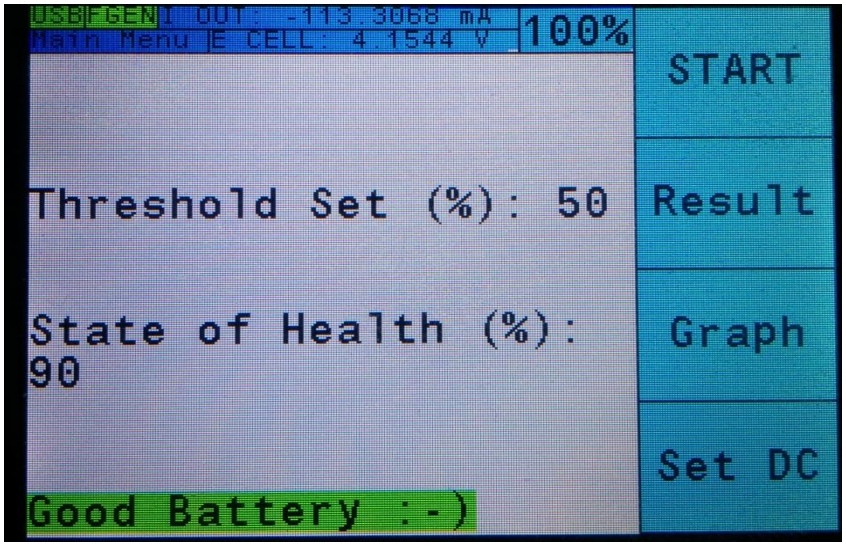

Figure 5.5. User interface with LCD display

5.4 Nyquist plots using the HCC hardware

Using hardware PCB shown in figure 5.1 and the new firmware implemented using STM32F429, EIS scans were performed. The goal was to compare and contrast the output of HCC hardware with research grade VMP2 equipment. The tests performed on the batteries comprised of data arrays of frequency, real impedance and imaginary impedance. The data was sent using USB option on the board to the PC using Hterm interface and baud rate of 9600 was selected. The data array were stored in excel file and later processed in Matlab to draw the comparison. The results of the Nyquist plots captured by the HCC hardware are shown in figure 5.6.

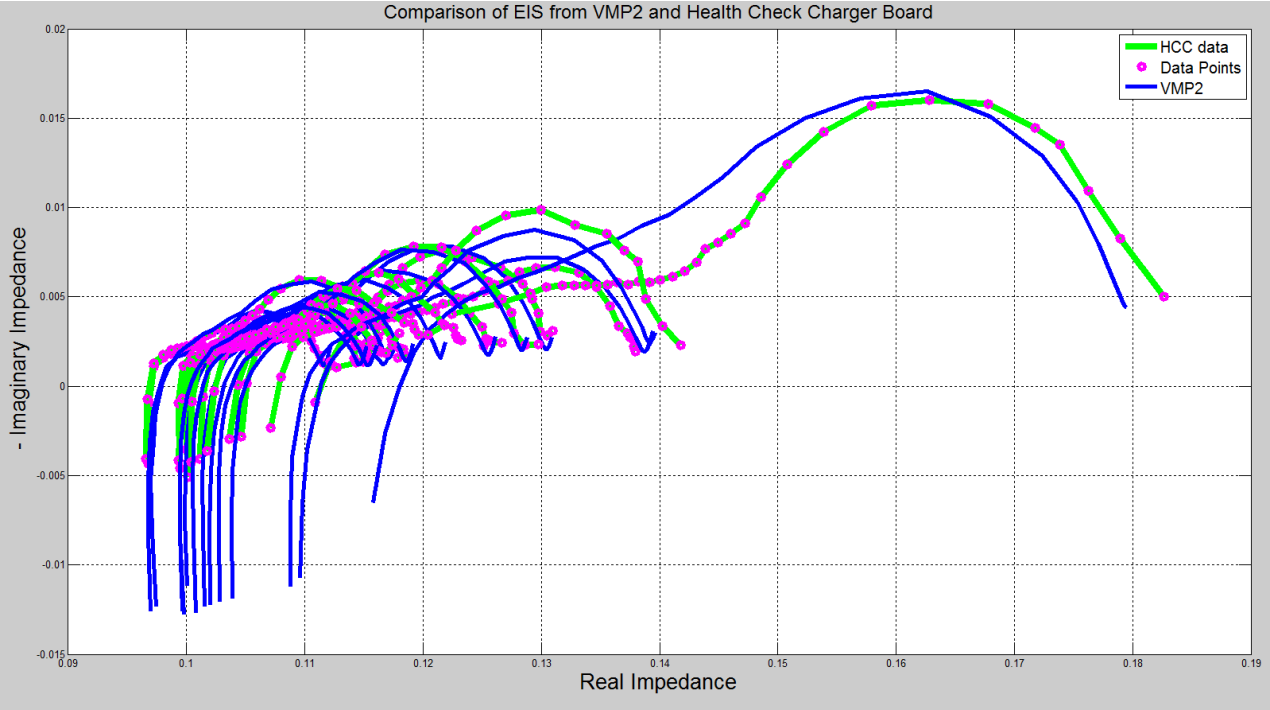

Figure 5.6. HCC nyquist plot comparison with VMP2

The data captured using HCC was identical in shape to VMP2. The circuit had parasitic resistance due to terminal connection that needed to be compensated. However, even after the compensation, slight deviation was observed in the high frequency side. The justification for the deviation stems from the design limitations in the PCB, causing parasitic capacitance.

5.5 SoH algorithm implementation and validation

5.5.1 SoH algorithm implementation

The SoH classification algorithm was coded in C in the firmware for STM32F429 microcontroller. At the end of the operation of the algorithm, the calculated SoH of the battery was displayed on the LCD touch screen.

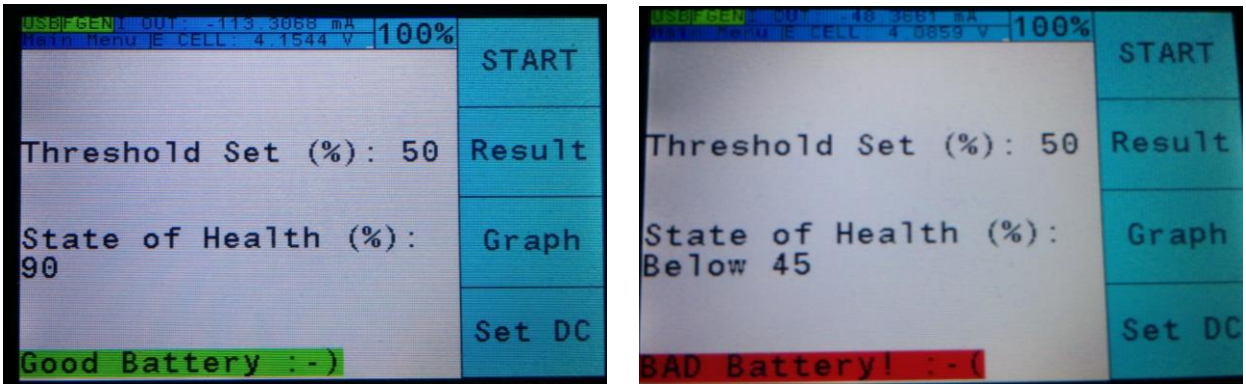

Figure 5.7. SoH algorithm result display on LCD

The user interface panel of firmware was programmed to have a graphing option, where user could view Nyquist plot of the battery. The graphing option comprised of two Nyquist plots, one drawn with the raw data obtained at the end of EIS test and second, having smoothed data after performing moving point average operation (blue line and green line in figure 5.8. respectively).

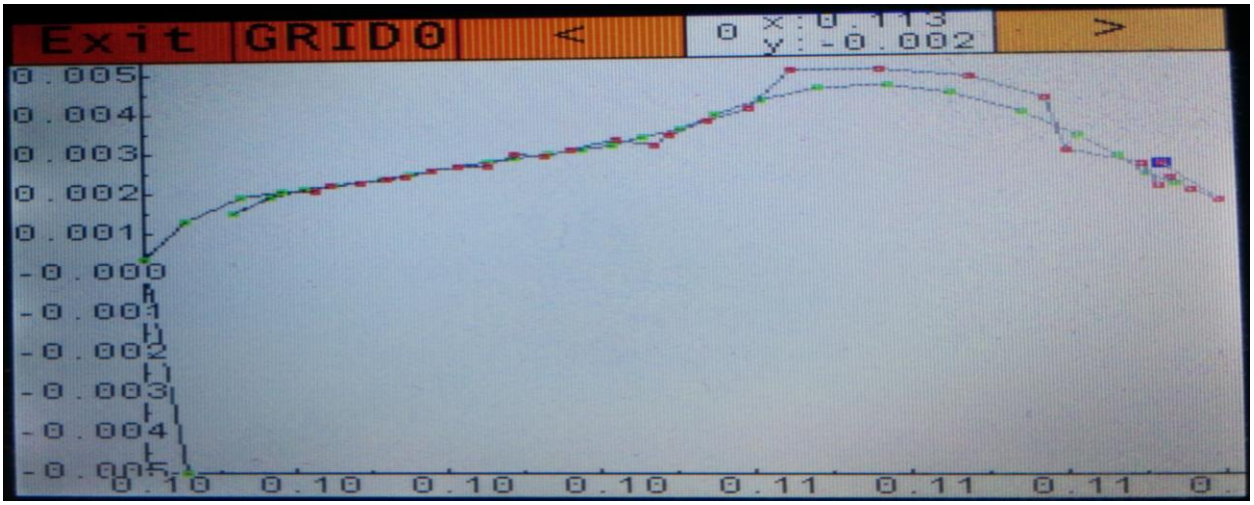

Figure 5.8. Nyquist graph display on LCD

5.5.2 SoH algorithm validation

- *State of Charge factor*

After implementation of the SoH determination algorithm on the firmware, tests were performed to verify the authenticity of the approach. The 14 batteries picked are same as of section 4.2 while other batteries are just used for algorithm verification. SoH of all of them is determined by coulomb counting of full discharge test.

For this test, the batteries were fully charged and 5 consecutive tests were performed to verify if the results were coherent. The average error was calculated for tests that showed that for good batteries the error remained within 10% bracket, whereas, for poor batteries the variation was large and the model showed limited accuracy (T13 and T14). The average time taken to complete the tests was also recorded as shown in figure 5.9.

Battery ID	State of Health in %	Test 1	Test 2	Test 3	Test 4	Test 5	Error Average(%)	Average Test Time(s)
Battery 1	63	61.1	62.55	63.16	62.6	63.02	-0.514	40.57
Battery 2	90	90.65	91.22	91.35	91.75	90.6	1.114	41.23
Battery 3	30	26.83	27.4	23.29	24.28	25.07	-4.626	40.94
Battery 4	65	68.28	69.45	69.73	69.21	70.4	4.414	40.56
Battery 5	2	0	0	0	0	0	-2	42.12
Battery 6	90	83.39	84.14	85.64	83.8	86.42	-5.322	40.68
Battery 7	89	81.64	81.73	83.19	82.42	82.65	-6.674	40.92
Battery 8	84	80.63	80.45	81.64	80.55	79.97	-3.352	40.77
Battery 9	79	80.41	80.27	79.85	79.81	80.7	1.208	41.25
Battery 10	76	75.73	74.01	75.38	74.95	73.31	-1.324	40.87
Battery 11	64	59.72	59.07	57.81	59.37	59.58	-4.89	41.39
Battery 12	13	20.96	23.07	20.48	21.52	23.1	8.826	42.51
Battery 13	86	77.12	77.68	79.27	77.06	77.98	-8.178	41.89
Battery 14	83	82.59	78.92	79.25	76.05	80.32	-3.574	41.05
Battery T1	55	55.59	55.84	55.08	56.83	55.5	0.768	40.74
Battery T3	81	83.22	83.34	82.63	82.5	81.23	1.584	41.28
Battery T2	71	73.74	75.96	75.24	75.7	74.52	4.032	40.84
Battery T9	22	8.79	9.14	13.33	16.75	16.5	-9.098	41.61
Battery T13	43	8.32	7.68	7.12	8.23	10.25	-34.68	41.53
Battery T14	42	23.7	22.65	23.16	23.63	22.49	-18.874	40.98

Figure 5.9. SoH algorithm validation tests

But in order to verify the feasibility of the SoH algorithm, further tests were performed at variable SoC of the batteries. The batteries were discharged by 10% each time and the test was performed to find the SoH using the hardware. The tests were designed to investigate the impact

of SoC on the SoH algorithm, such that as long as the battery in steady state, the algorithm can operate to determine the SoH, independent of battery's SoC. The results are shown in figure 5.10.

Battery ID	SoH in %	SoC: 100 %	SoC: 90 %	SoC: 80 %	SoC: 70 %	SoC: 60 %	SoC: 50 %	SoC: 40 %	SoC: 30 %	SoC: 20 %	SoC: 10 %	SoC: 00 %	Avg. Erro
1	63	60.63	61.38	66.19	63.44	64.26	56.82	55.8	57.62	64.99	56.65	56.65	3.84818
2	92	90.9	95.01	97.18	98.69	98.62	93.97	94.62	92.32	96.7	97.59	94.75	3.68636
3	30	22.34	16.87	21.48	16.61	13.06	9.91	9.34	12.54	32	22.11	21.36	12.3982
4	65	65.89	72.95	71.15	70.05	68.06	64.68	63.52	60.69	74.96	71.66	66.54	4.30636
5	2	0	0	0	0	0	0	0	0	0	0	0	2
6	90	83.93	84.32	90.41	89.5	93.18	85.51	87.86	91.45	80.43	77.87	72.62	5.72727
7	89	80.39	84.16	90.56	87.98	91.9	86.2	84.81	89.46	83.54	84.95	78.89	4.18182
8	84	78.24	83.08	88.88	87.21	90.62	85.62	83.05	88.06	81.72	79.51	83.23	3.23273
9	79	80.02	84.59	85.14	84.57	87.19	81.03	81.66	72.16	82.11	78.63	78.14	3.85273
10	76	73.65	74.92	78.56	81.52	80.25	76.08	71.99	76.61	76.36	75.26	68.59	2.63364
11	64	59.58	67.05	69.39	70.15	71.38	64.42	59.36	59.34	69.59	67.18	64.45	4.12091
12	13	21.84	10.69	11.53	13.35	11.37	12.15	11.29	11.09	24.57	23.85	23.66	4.74091
13	86	76.33	79.63	82.8	79.37	84.31	77.71	79.46	82.07	75.99	73.3	73.47	7.41455
14	83	79.68	81.96	85.03	89.8	87.51	81.07	81.66	79.64	84.64	80.31	77.73	3.08455

Figure 5.10. SoH algorithm validation with varying SoC

The results support the hypothesis that the SoH algorithm is independent of the SoC of the batteries as long as batteries are in steady state. The SoH estimation is highly accurate when battery is fully charged whereas there is small deviation on low SoC. But overall, the average error of the SoH estimation was confined within 10% window bracket.

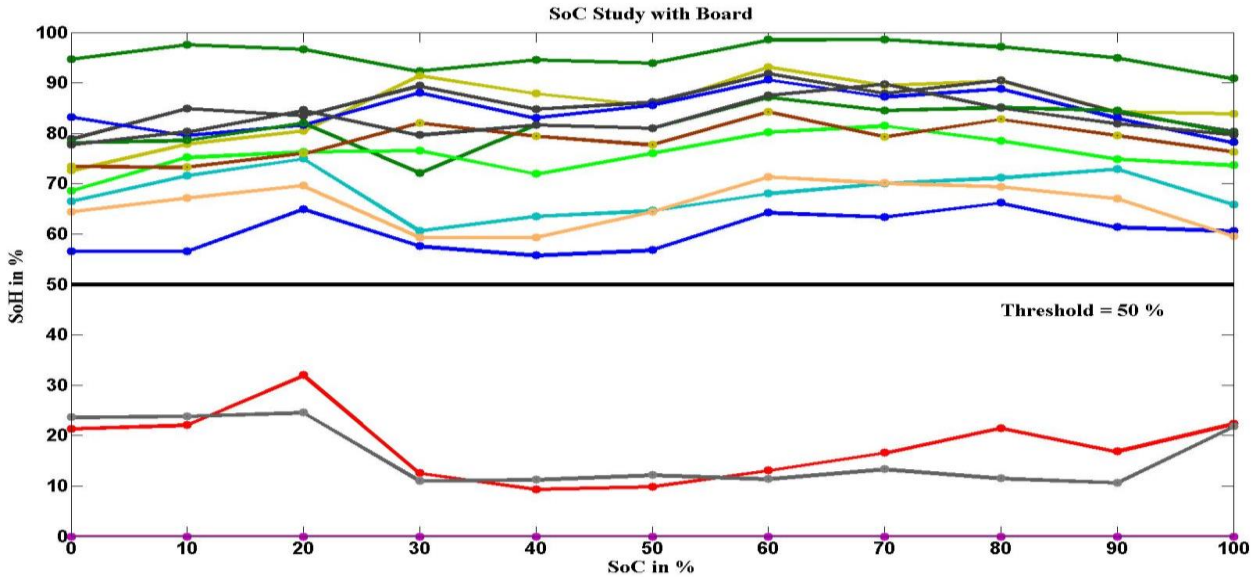

Figure 5.11. SoH Vs SoC readings for algorithm validation

Ideally the lines in the figure 5.11 should have been flat, based on argument that SoH test is independent of the SoC of the battery. However, the lines have small deviation with no particular pattern with variation in the SoC. Therefore, it is not possible to compensate for the slight deviation in the SoH algorithm result as a function of the SoC. Nevertheless, the deviation is small, resulting in accurate estimation of the SoH of the batteries within the 10% bracket.

- *Non steady State condition*

EIS tests were performed on the batteries using the HCC board in non-steady state condition to draw a comparison with the Nyquist plots captured by VMP2. The multi-sine approach used by the HCC board showed slight deviation in the low frequency region because of the drift effect. But overall, the plots captured very highly identical. Three EIS scans were taken at 2.5, 5 and 7 minutes respectively, after batteries were completely charged and results are shown below:

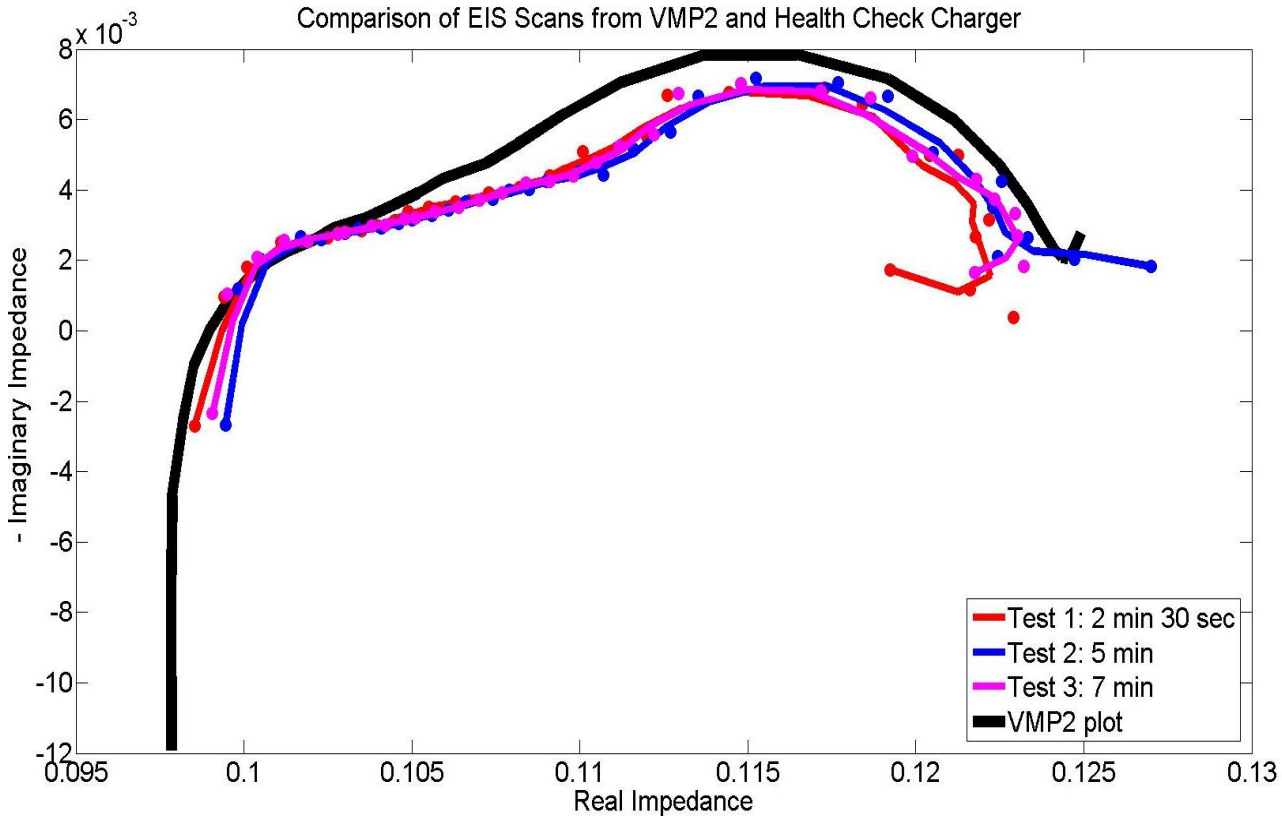

Figure 5.12. HCC comparison with VMP2 battery 1: SoH 64%

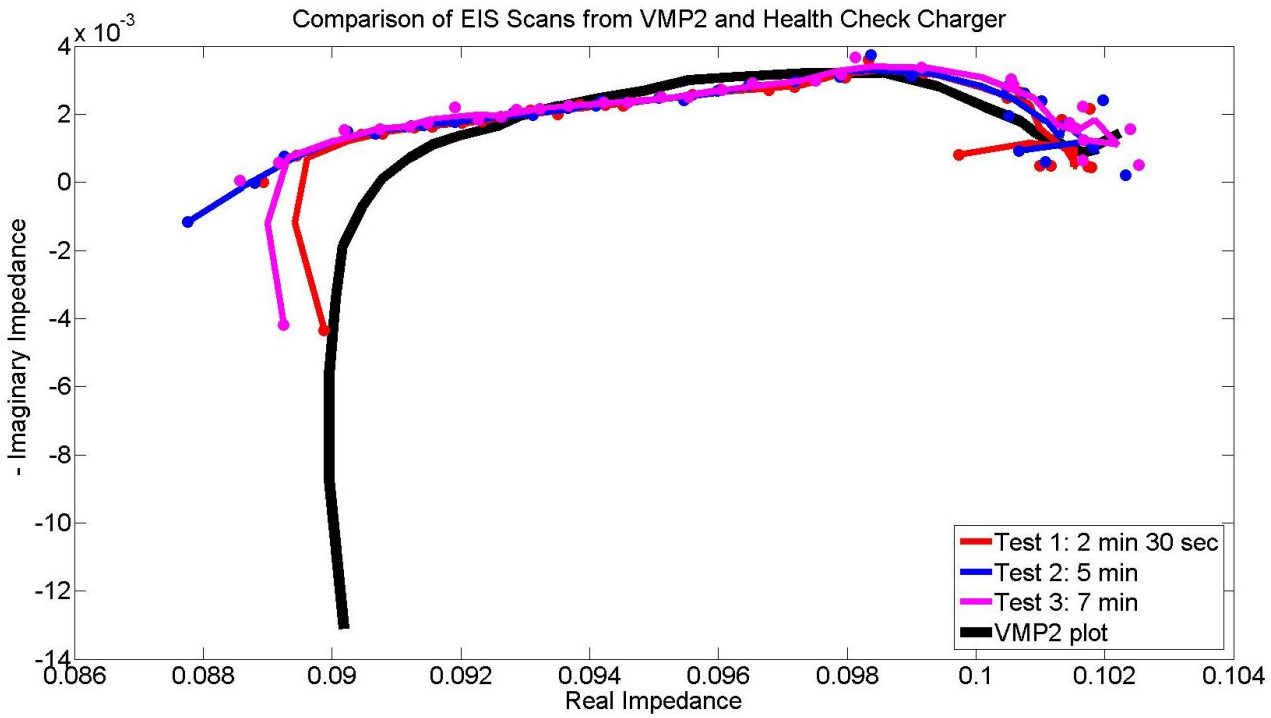

Figure 5.13. HCC comparison with VMP2 battery 2: SoH 90%

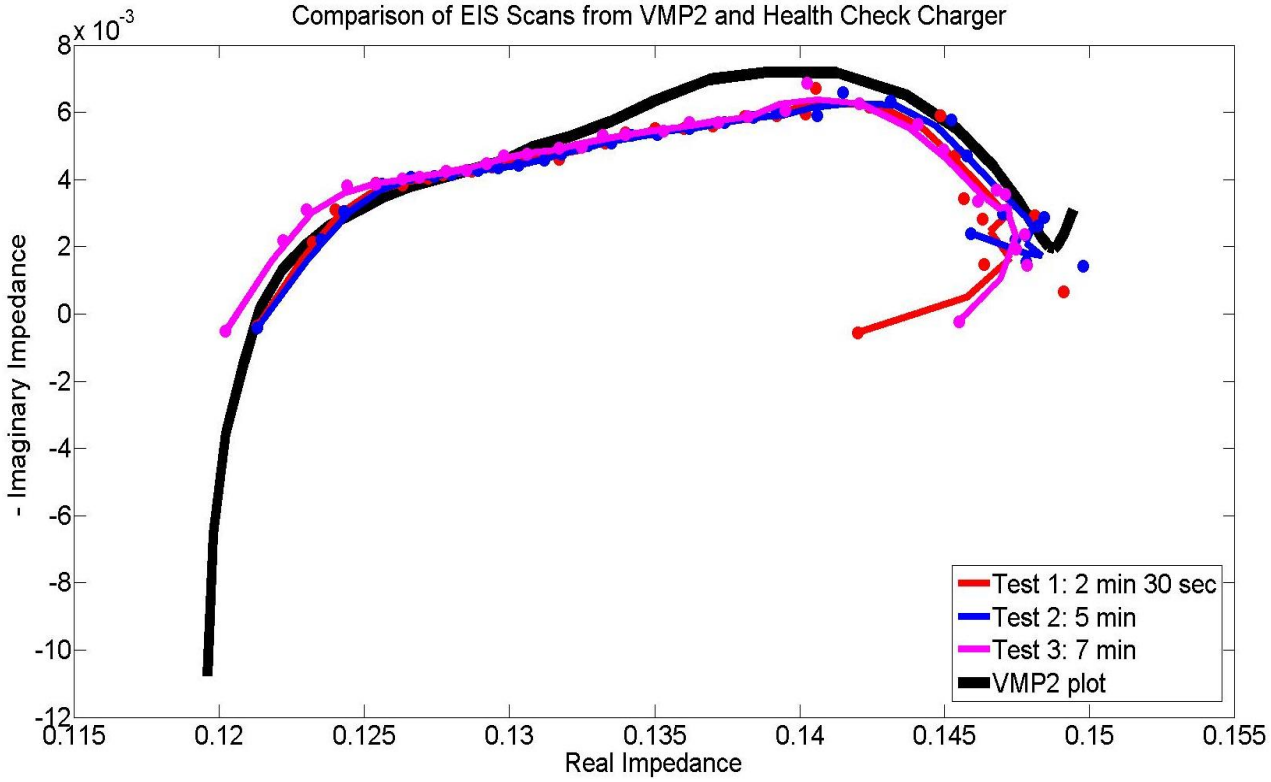

Figure 5.14. HCC comparison with VMP2 battery 3: SoH 30%

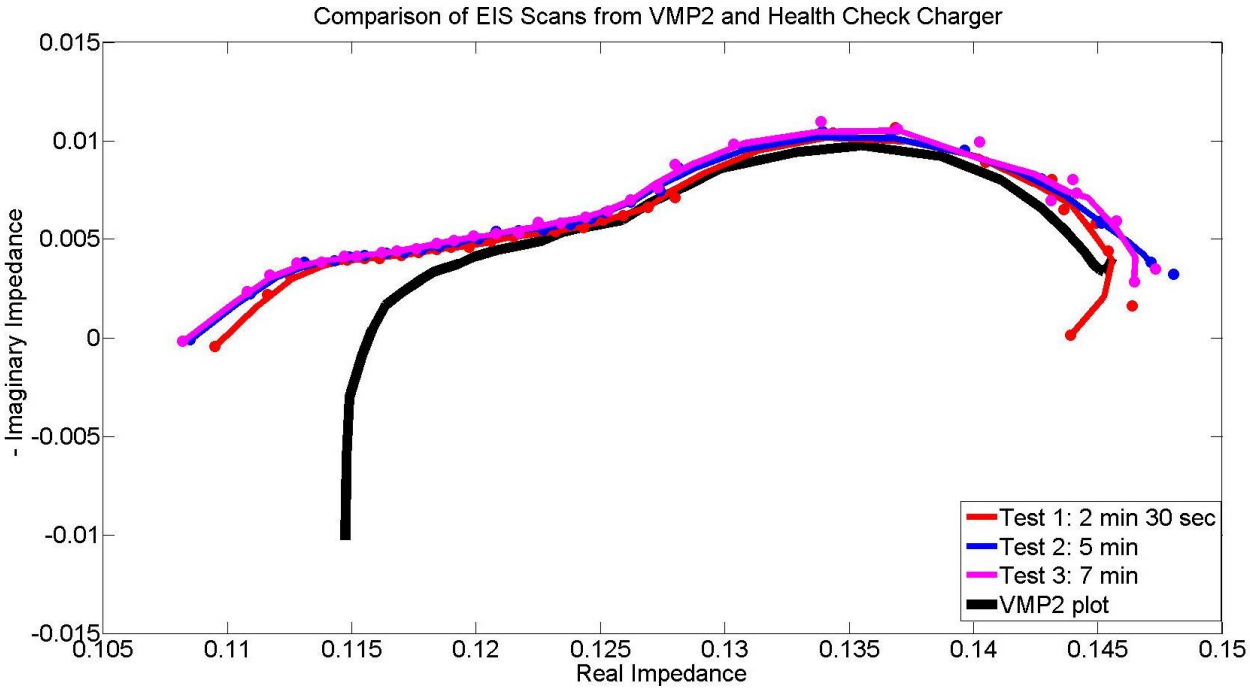

Figure 5.15. HCC comparison with VMP2 battery 4: SoH 12%

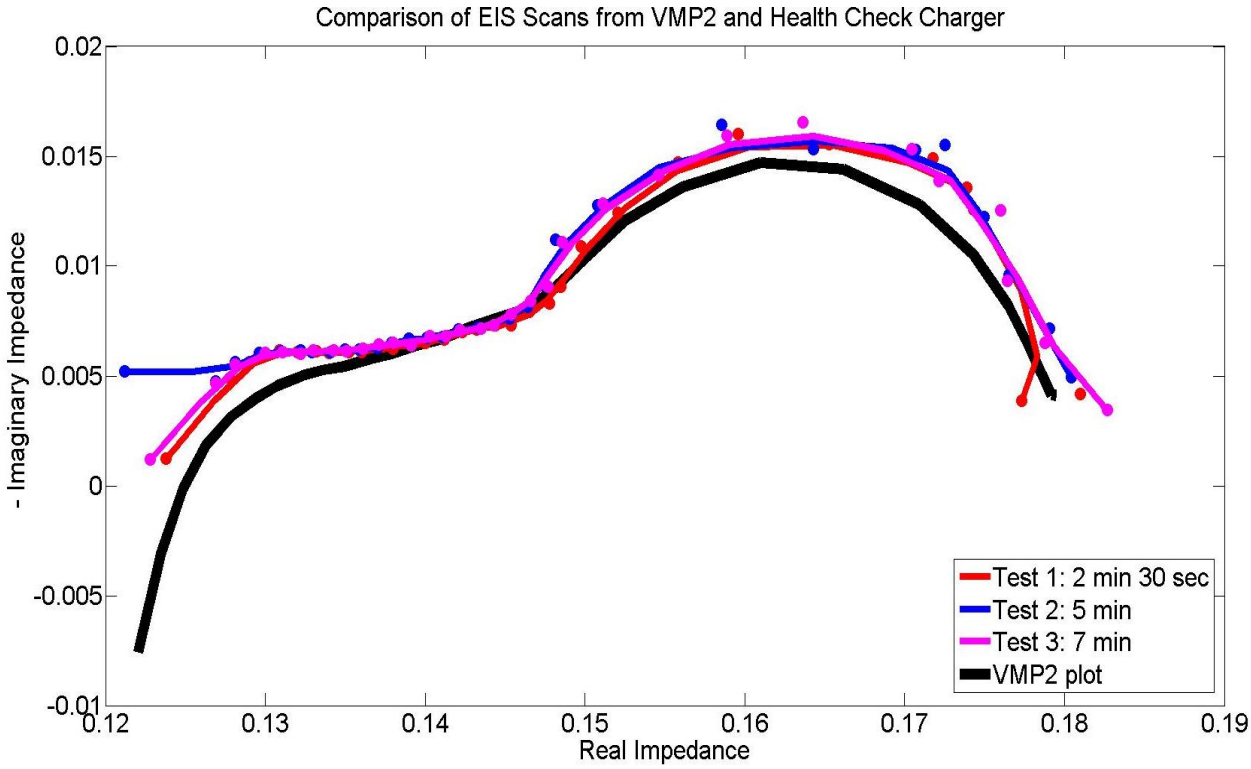

Figure 5.16. HCC comparison with VMP2 battery 5: SoH 02%

The Nyquist plots show that there is small deviation in the Nyquist plot captured by the HCC circuit as compared to the Nyquist plots recorded using VMP2. The reason being, VMP2 has sophisticated self-calibration capability with cutting edge noise removal algorithm. This research grade equipment has very precise instrumentation hardware, whereas, the HCC circuit lacks such sophistication on hardware level. However, the deviation is not detrimental in terms of SoH classification. The algorithm designed for SoH determination is valid even with small deviation since for classification purposes, it's not the absolute comparison with VMP2 that matters, rather the relative difference between the Nyquist plots counts. The comparison of all of the EIS scans captured by HCC circuit is shown in figure 5.17.

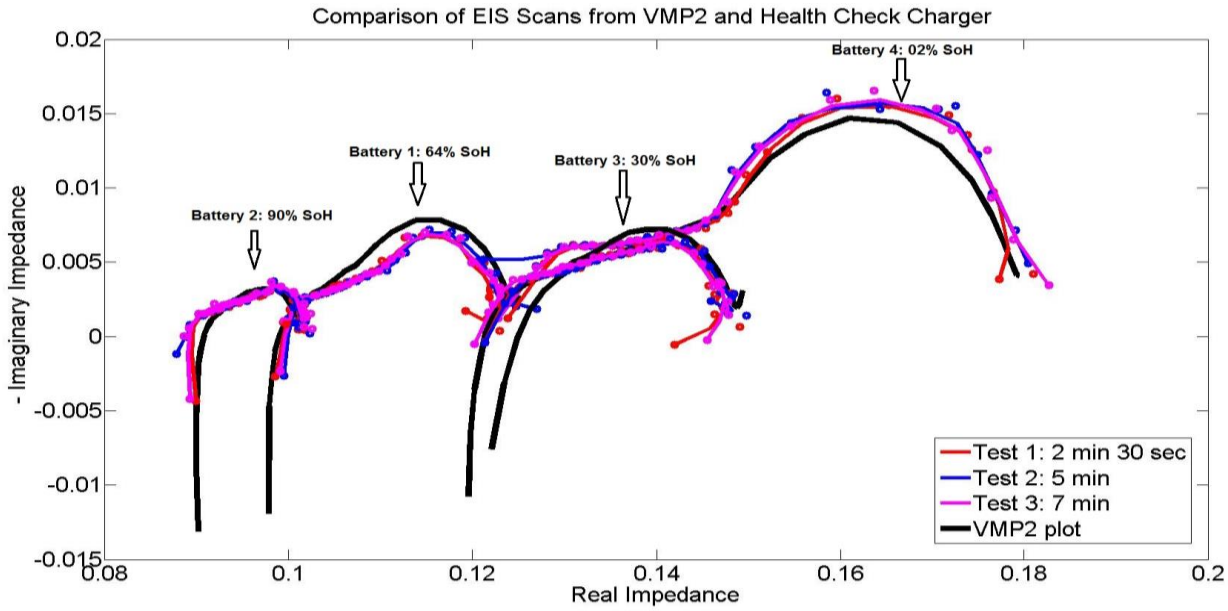

Figure 5.17. Comparison of EIS scans

The figure shows that as battery's SoH goes down, the plot slides towards the right side, which basically implies increase in the resistance of the real component. Also the shape changes, because of the deterioration of surface electrolyte interface and increase in charge transfer resistance. This relative difference is of key interest in deciphering the SoH of the battery using the HCC device.

5.6 Cost estimate and economic analysis

For all industrial or consumer end products, cost is of key concern. It is imperative to keep the fabrication costs low such that ample profit margin exists for the manufacturer. The initial goal for this thesis was to design an HCC such that the overall end of the process cost of the product is less than 500$. Target was successfully achieved with all costs kept way below the set threshold as cumulative material cost turned out to be within 100 $.

Fortunately, as number of units produced increases, the cost per unit goes down. Therefore, in order to come up with a reasonable estimate of the overall cost of the hardware for HCC, bulk purchase price of components and electrical chips was considered (minimum of 1000 number of item ordered for each component). The overall circuit comprised of the EIS potentiostat circuit, power connector, controller board and charger circuit. The breakdown of the overall cost of the device is shown in table 5-1.

Component Type	Component	Cost ($)(Bulk Purchase with at least 1000 pieces)
Potentiostat Circuit	Resistor	2
	Capacitor	2
	Semiconductor Chips	33
Power Connectors	Main DC Adapter	6
	Mini Male-Male Banana Cable	1
	Battery Adapter (Holder)	5
	Micro USB Cable (optional)	3
	Mini USB cable (Power Microcontroller)	3
Charger Circuit	PCB and components	13
Modified STM32F429 Discovery Microcontroller	Controller Board	30
		98

Table 5-1 Cost breakdown of the HCC hardware

Chapter 6: Charge and Discharge Curve Profiling

6.1 Background research

In this chapter a new strategy is proposed to determine the SoH of the battery. The suggested method is an off branch extension of existing method used to classify state of health of battery: Coulomb-counting method. Coulomb counting method has been used extensively in industrial sector to estimate and benchmark the SoH of the battery, but by nature the method is time consuming, as it requires complete information of full discharge/charge cycle of a battery. In some applications the user cannot wait for the battery to be completely charged due to time constraints. As time is of essence, any method that can reduce the overall test time and also provide reliable accuracy is considered valuable.

Basic principle of this method was first identified by Ramadass et al. when he proposed first capacity fade model for Li ion batteries [12]. The existence of side reaction that consumes the available capacity of the battery was further investigated by Branko [13]. The study concluded the presence of a side chemical reaction that consumes the available Li ions present in electrolyte increase the overall charge transfer impedance. The dissolution of Solid Electrolyte Interface layer and reduction in active surface area for redox reaction added up to the capacity fading causes. The study concluded that, as batteries cycle, the overall charge storing capacity of the battery reduces which can be predicted from the charge profile of the battery. The main impact of the capacity fade was observed in the constant current charging region of the charge profile as shown in figure 6.1. It is also important to notice the charge pumped in during constant current charging comprises of the major chunk of the overall charge storing capability of the battery and the charge stored in constant voltage region is very small.

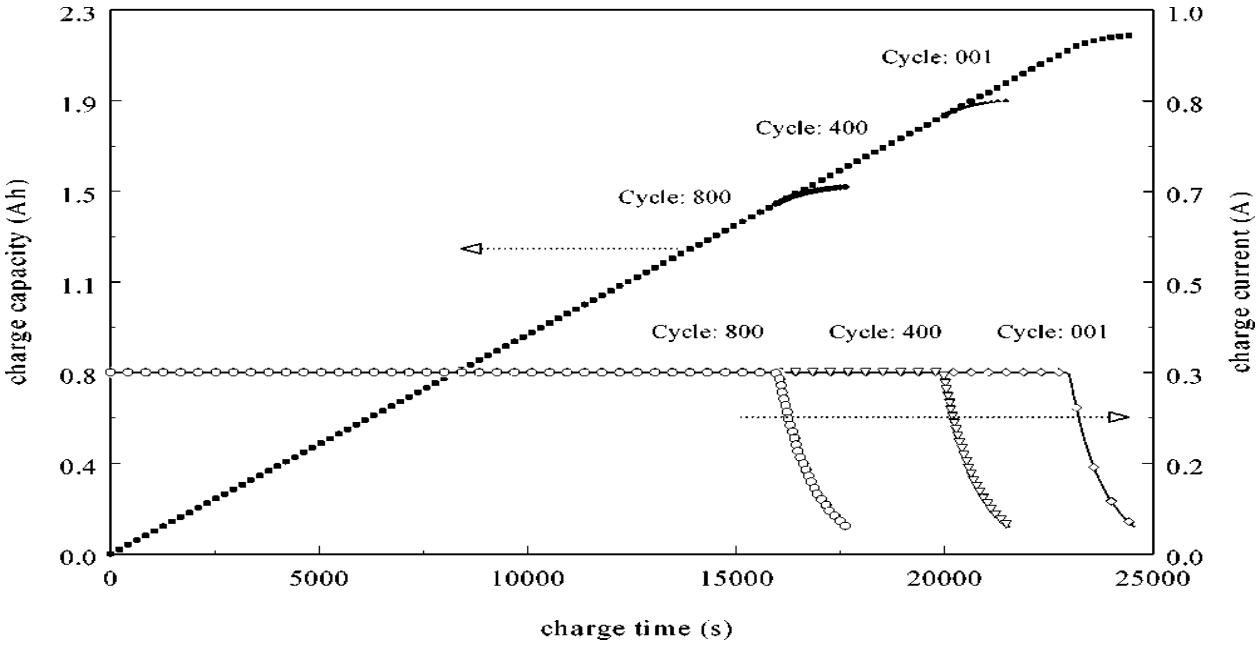

Figure 6.1. Charge profile variation with number of cycles

Similarly work was done to decipher the state of health of the battery using charging characteristics in [14]. Three characteristics were considered for this application, constant current time, constant voltage time and the resistance of the battery.

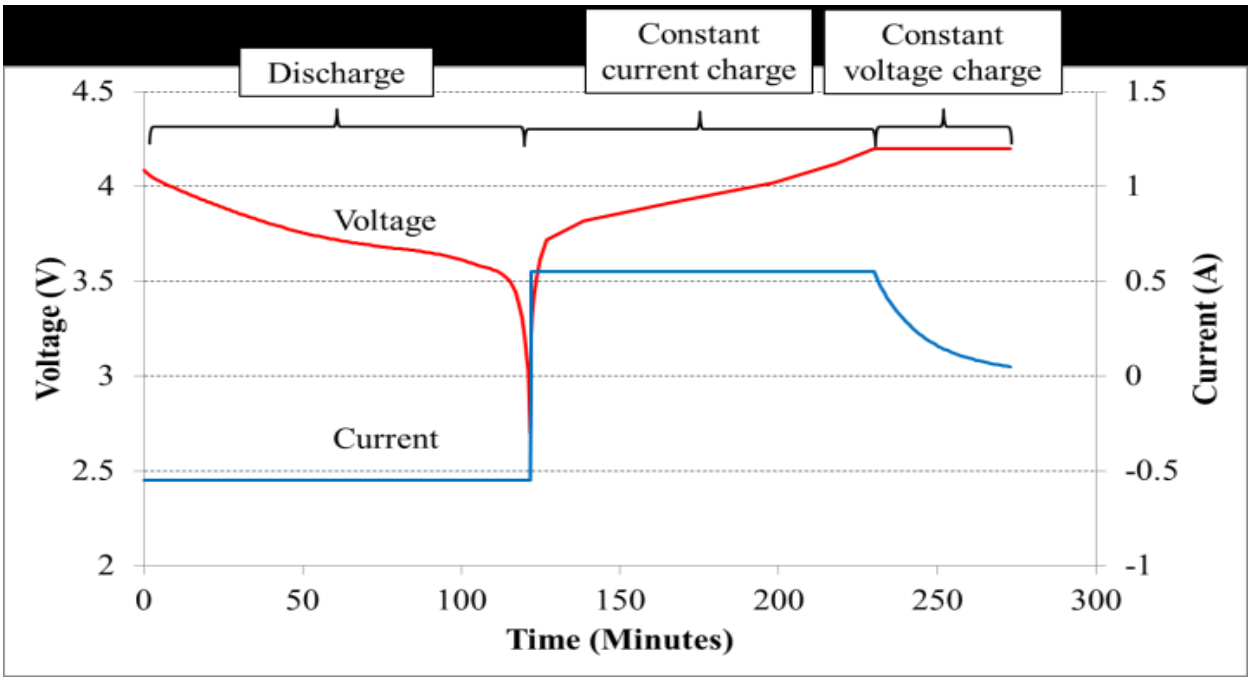

Figure 6.2. Charge profile characteristics for a battery [14]

The study concluded that constant current timing method turned out to be the most reliable characteristic of the charging curve. The shape of capacity plot, fig 6.3 is identical to constant current charge time (CCCT) plot, figure 6.5. There is not pattern in capacity plot 6.3 and resistance plot or constant voltage charge time (CVCT) plot, fig 6.4 and 6.6 respectively. [14]

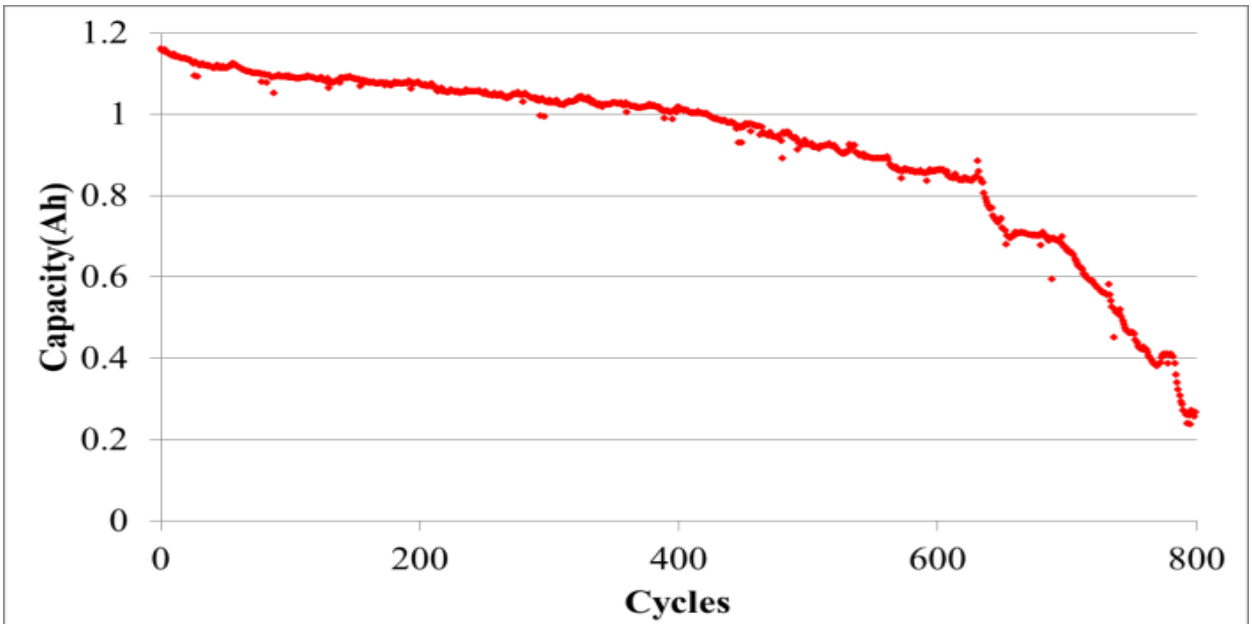

Figure 6.3. Number of cycles Vs battery capacity

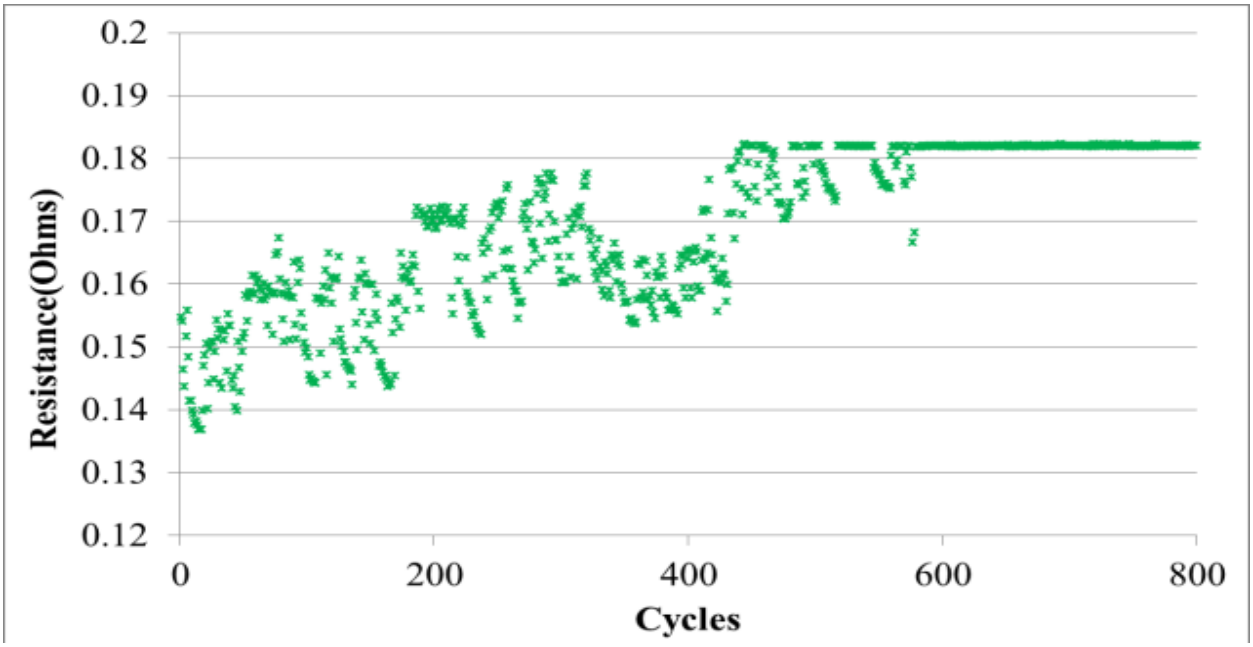

Figure 6.4. Number of cycles Vs battery resistance

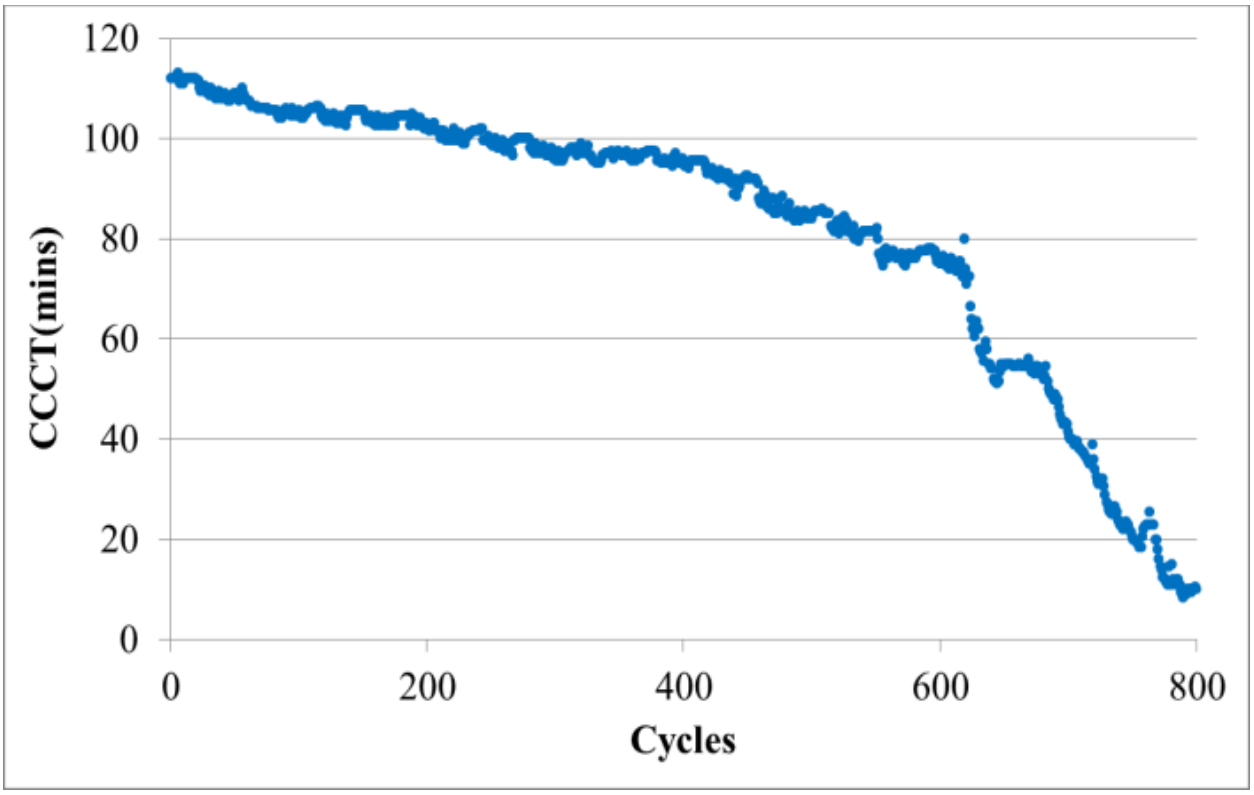

Figure 6.5. Number of cycles Vs constant charge current time

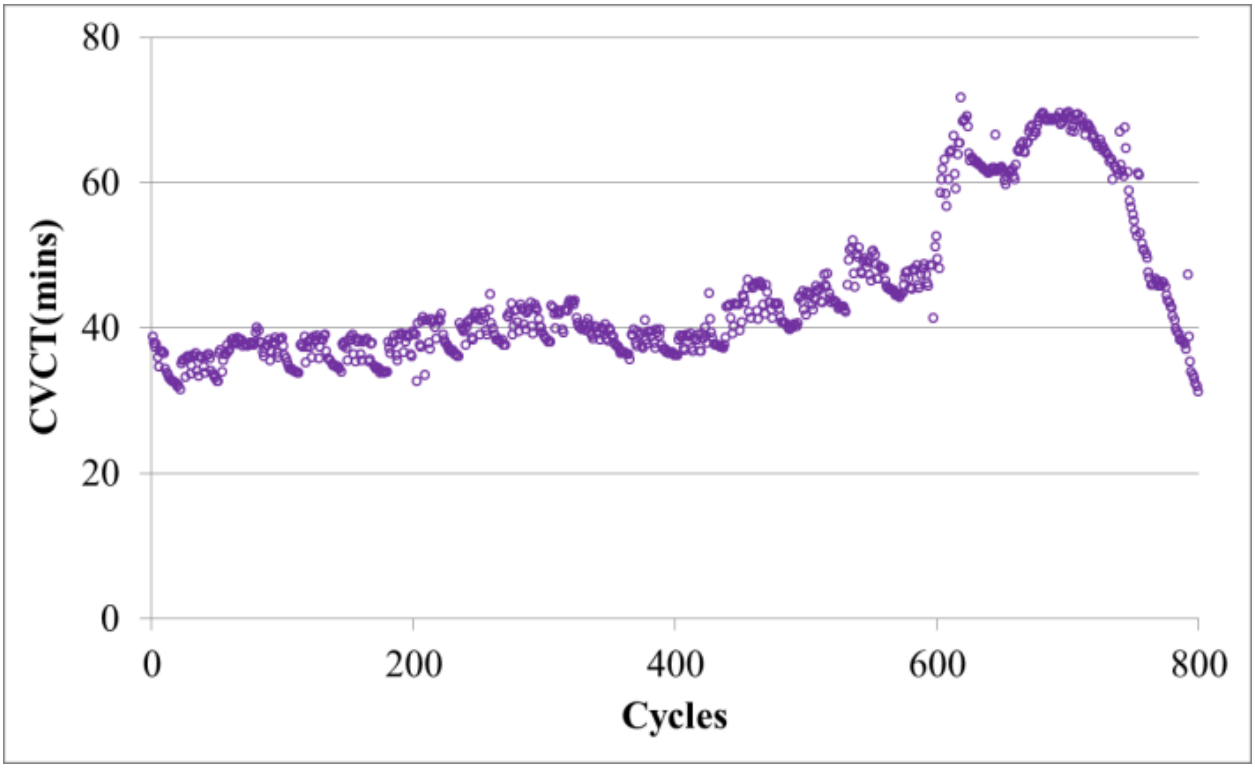

Figure 6.6. Number of cycles Vs constant voltage charging time

The underlying principle for this method is that the charge storing capacity of the battery reduces as the battery ages and the effect of the reduced capacity is evident on the charging profile of a battery. The change is the shape of the charge profile can be evaluated to determine SoH of the battery. Major advantages of using this method are the decrease in the overall testing time and the elimination of an additional hardware on the existing BMS and battery chargers. This is a low cost inclusion on the existing infrastructure to provide battery health monitoring capability.

However, coulombic efficiency of the battery is not 1. This means that the charge stored in the battery might not necessarily be equal to the charge taken out of the battery [15]. For new batteries the efficiency is high, however, for poor batteries, the difference in charge pumped in and taken out can differ by a large amount. Therefore, constant current charge timing method needed further investigation to come up with a generic relation between state of health and constant current timing method that can compensate for the difference in charge stored and taken out.

6.2 Proposed strategy

The charging process of a lithium ion battery depends on various factors such as battery cut of voltage, charging current (C-rate) and overall capacity of the battery. Usually the manufacturer specifies these parameters. It is pertinent to ensure that battery charger operates with in the operational range defined by the manufacturer because overcharging of lithium ion batteries can result in serious safety concerns. However, irrespective of the exact cut of thresholds and values, the overall charging process can be segregated into two main categories: constant current and constant voltage charging. There is no trickle charging stage for lithium ion batteries as observed in the case of lead acid batteries due to low self-discharge rate.

For this study, 5 different battery models were considered as shown in table 6-1. The charging rate was selected to be C/4 for all battery models. The charge profiles were for these models using Cadex 7400 battery analyzer to record time, voltage, current and temperature simultaneously. All tests were performed on room temperature and pressure.

Battery Manufacturer	No of Batteries	Application	Capacity (mAhr)
Li Air Canada	28	Radio Handsets	4800
Samsung Galaxy S4	54	Cell Phone	2600
Samsung Galaxy Note 1	40	Cell Phone	2500
LG	10	Cell Phone	1700
Samsung S3	50	Cell Phone	2100

Table 6-1 Type of battery models used for data acquisition and analysis

6.3 Data acquisition and analysis

For the models listed in Table 6-1, prime tests were performed on all the batteries. The prime test comprised three full charge and discharge cycles for each battery. The data was logged in an Excel file for each battery and the entire data bank was imported to Matlab for data processing. A generic function was written in Matlab that can take excel files as input. The format of the excel file was programmed in Cadex battery shop software. Matlab script was written to import raw data and process the information to plot the following graphs and make desirable comparisons of the parameters in investigation. Same script was used for all battery models.

This Figure 6.7 shows the charge current characteristics of 54 Samsung galaxy S4 batteries sorted in order of their SoH. Similarly figure 6.8 shows charge current plotted on the same scale for all Samsung galaxy S4 batteries. Only single charge cycle is shown to present a direct correlation between the SoH of the battery with constant current charging time. The good batteries (shown with blue color) have longer constant current charging region as compared to the poor batteries (shown with red color).

The same tests were repeated for other battery models such as Samsung galaxy S3 and Samsung galaxy note 1. The plots for these battery models are shown on the in the following figures 6.7-6.12. Regardless of the overall capacity of the battery of the constant charging current value, there is a very obvious trend observed in the plots. The duration for which the battery stayed in the constant charging current region replicated the SoH profile of the battery. However, these plots only show partial information. The exact correlation between SoH of these batteries and constant current charge time is presented in next section.

Samsung Galaxy S4 plots:

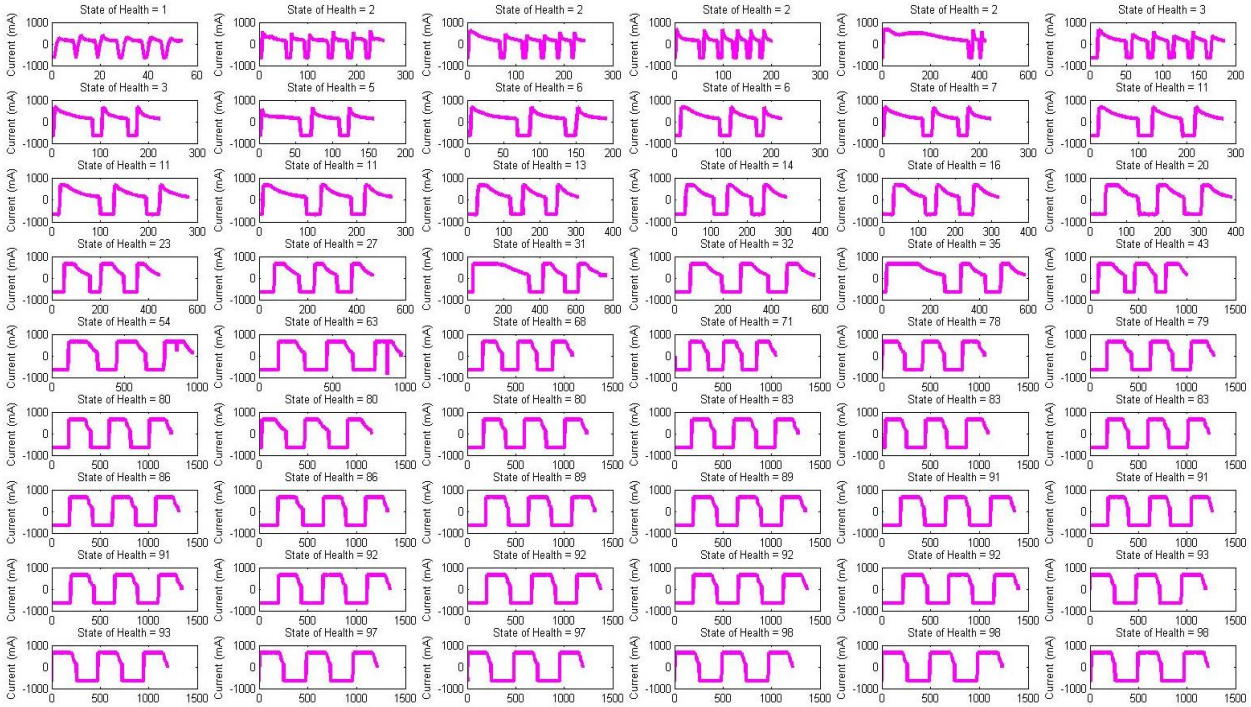

Figure 6.7. Charge current characteristics of Samsung Galaxy S4 batteries

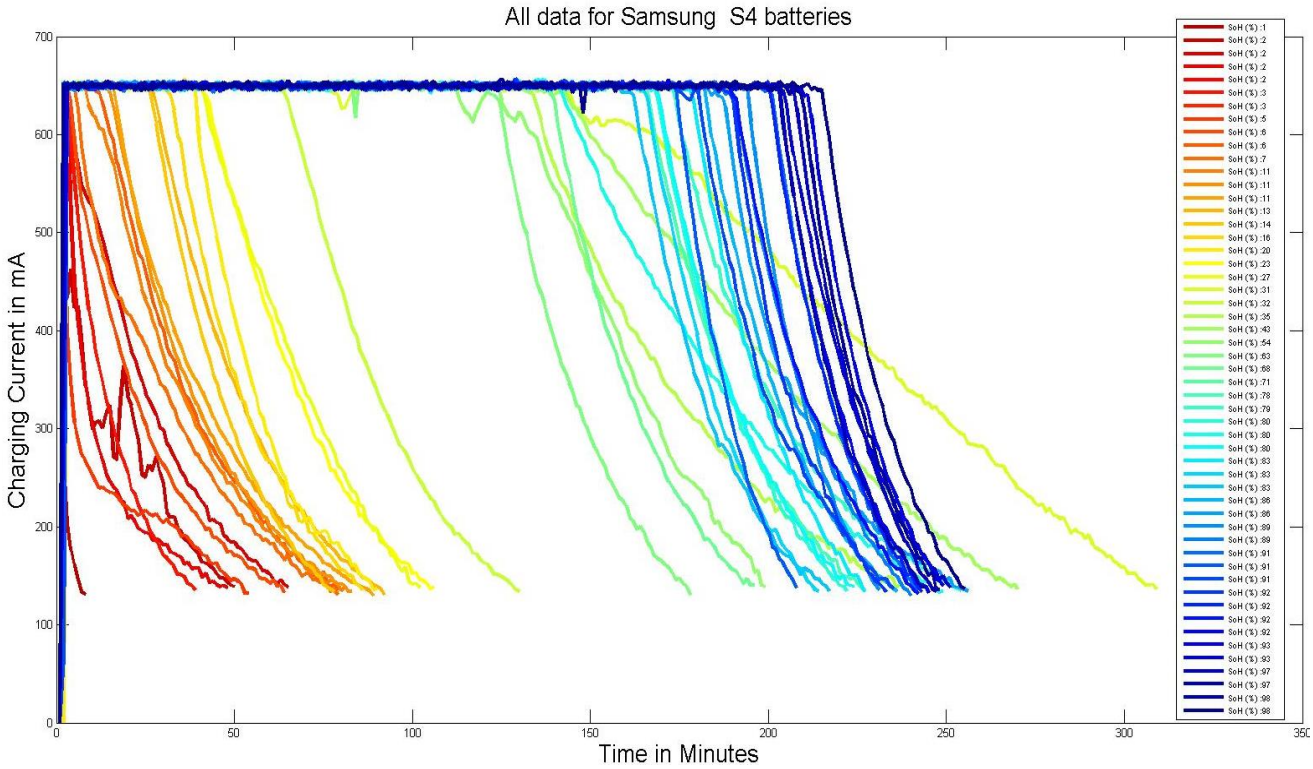

Figure 6.8. Overlap of single charging current cycle for Samsung Galaxy S4 batteries

Samsung Note 1 plots:

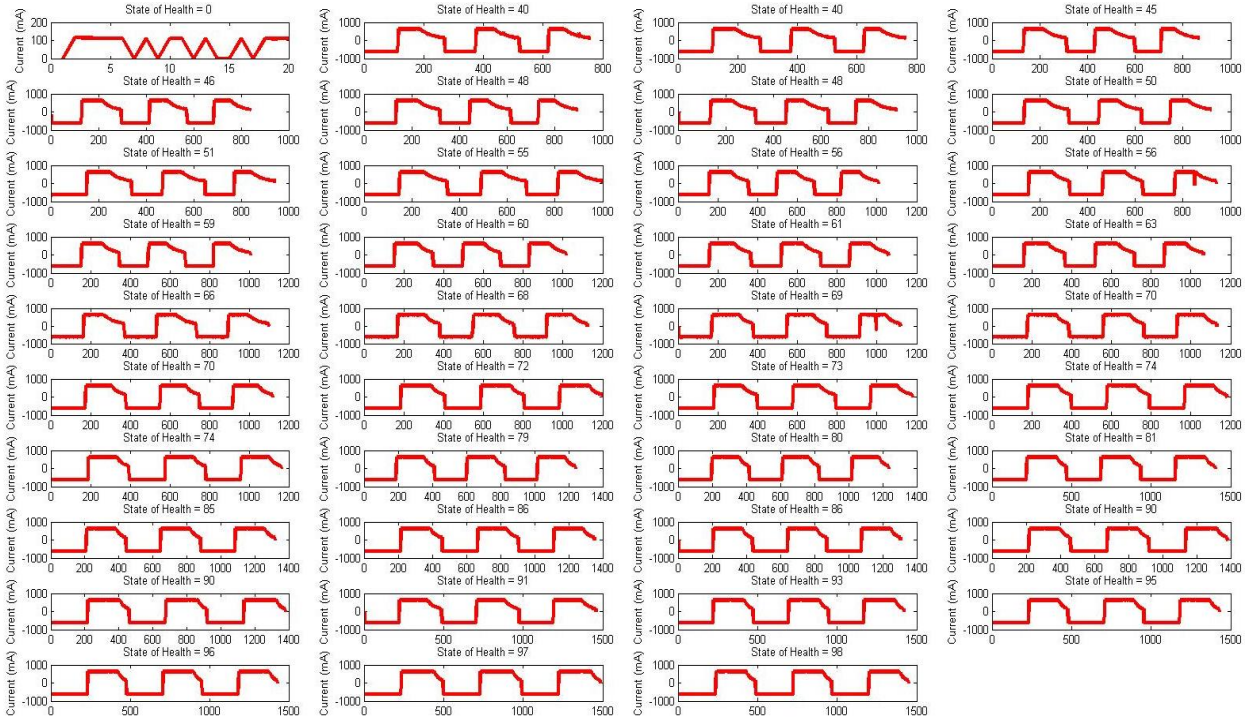

Figure 6.9. Samsung Galaxy Note 1 charge current profiles

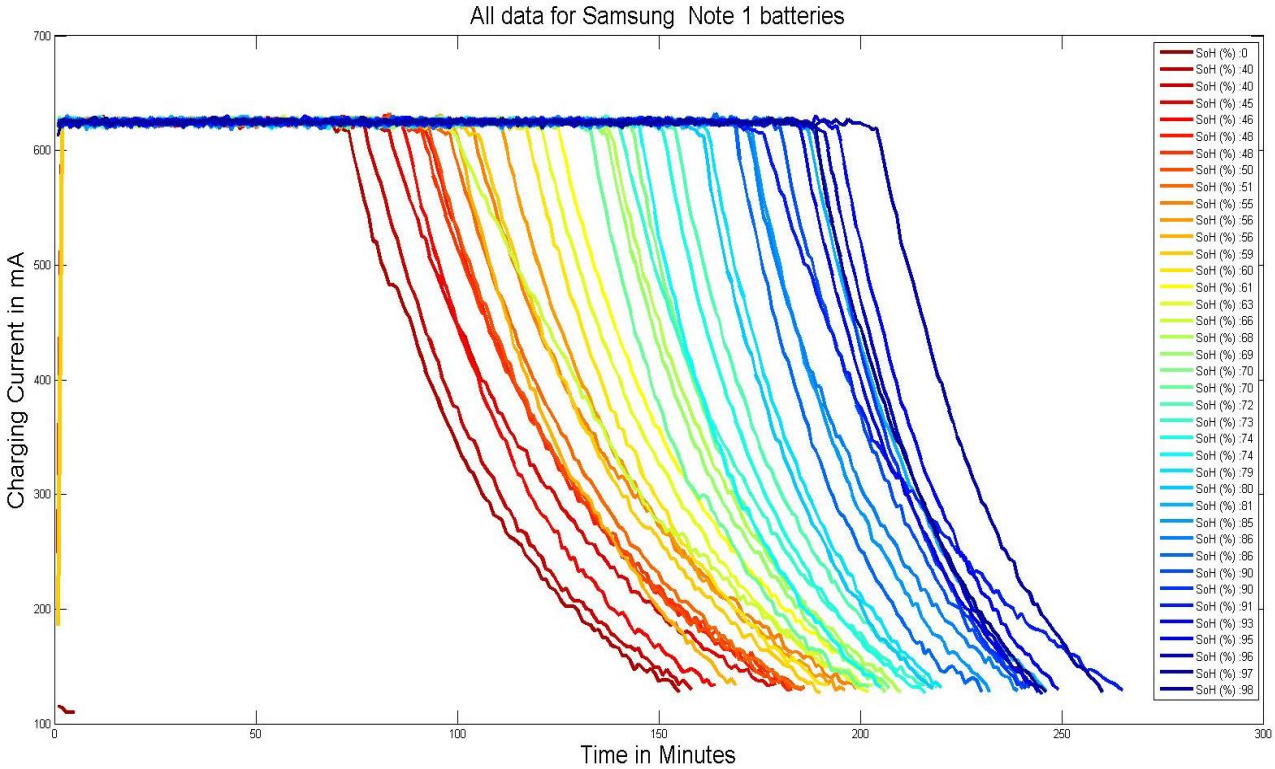

Figure 6.10. Overlap of single charging current cycle for Samsung Galaxy Note 1 batteries

Samsung Galaxy S3 plots:

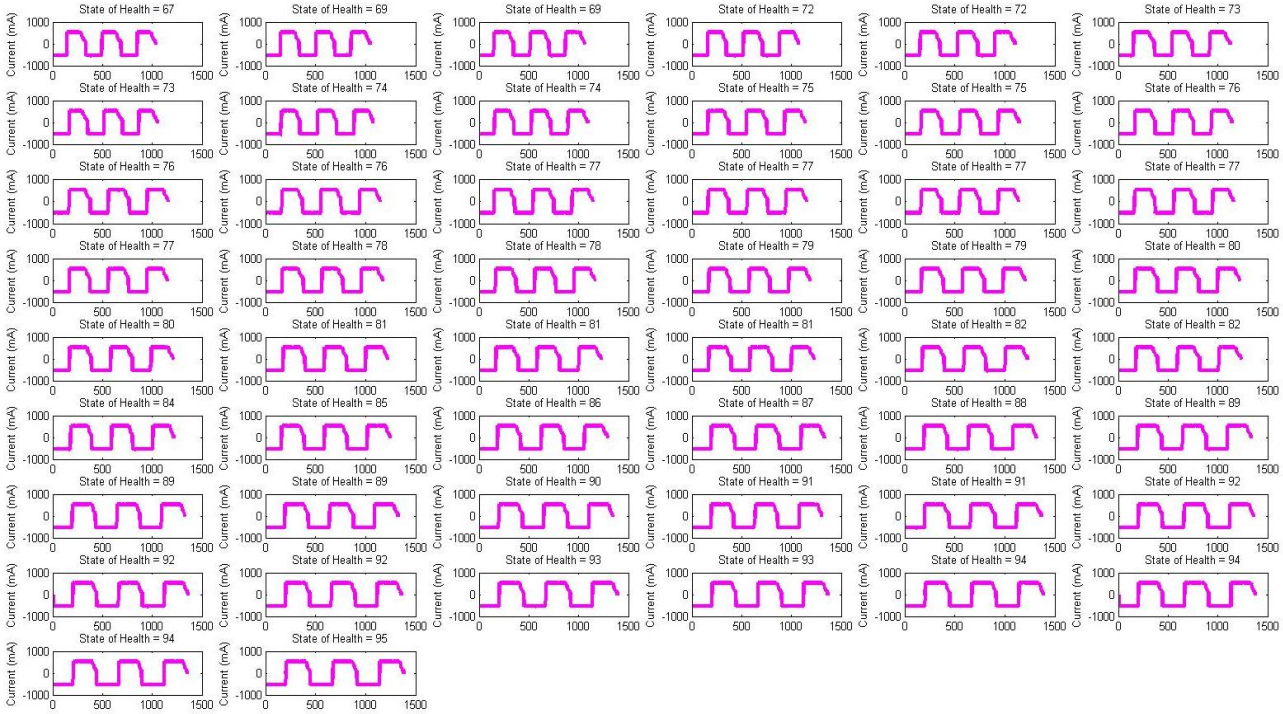

Figure 6.11. Samsung Galaxy S3 charge current profiles

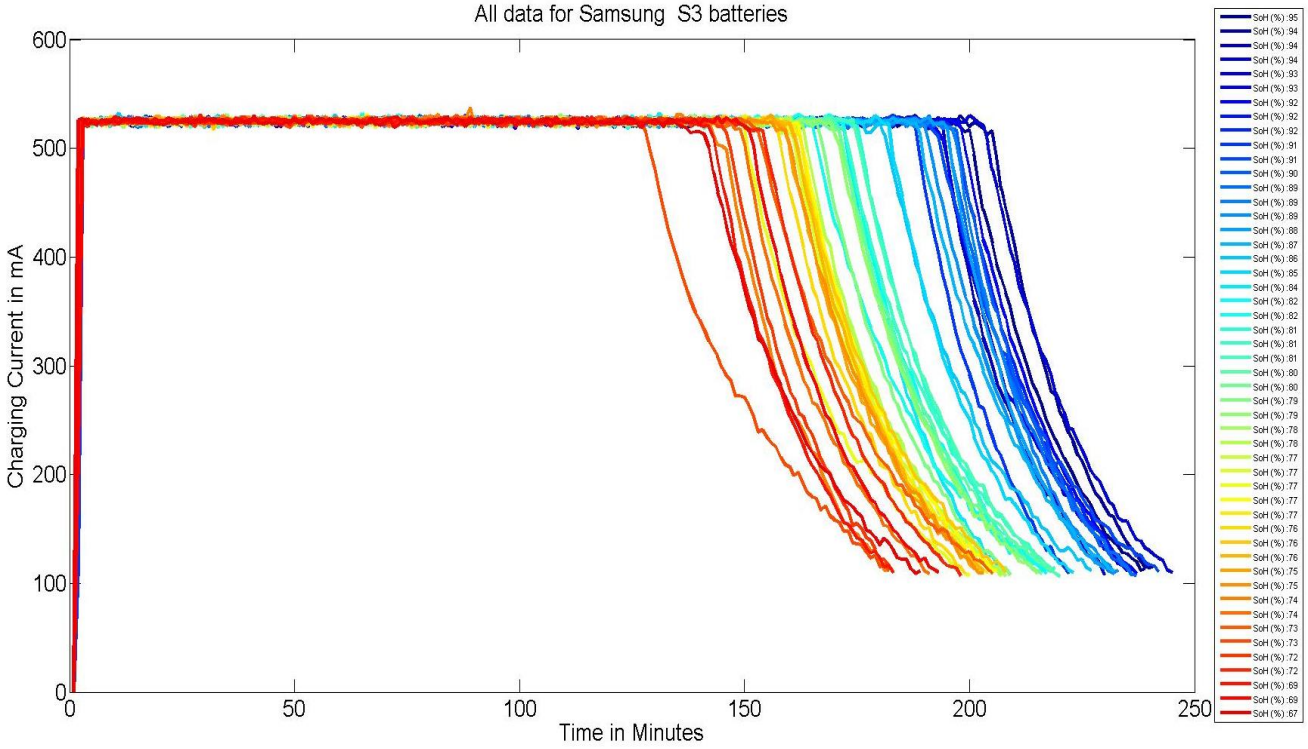

Figure 6.12. Overlap of single charging current cycle for Samsung Galaxy S3 batteries

6.4 Charge vs. discharge capacity analysis

Charge and Discharge Capacities of the batteries are two different ways of determining the SoH of battery. The former refers to the amount of charge stored in the battery during charging, whereas the later corresponds to the amount of the charge taken out of the battery during discharge. It is very important to note that the charge capacity of the battery might not be exactly same as the discharge capacity i.e. batteries don't have 100% coulombic efficiency. This implies that some of the charge pumped into the battery is not stored as chemical energy rather it is wasted in loss mechanisms resulting in hysteresis effect. The hysteresis effect can be observed by running prime tests on the batteries of different models and using coulomb counting method to compare the charge and discharge capacities.

In order to provide numerical data and supportive results, we have carried out tests on 4 different battery models of batteries. The exact model, capacity, number of batteries tested and battery vendors are specified in figure 1.

Different battery models had different nominal voltages and different end of charge cut off voltages.

Battery Manufacturer	No of Batteries	Application	Capacity (mAhr)
Li Air Canada	28	Radio Handsets	4800
Samsung Galaxy S4	54	Cell Phone	2600
Samsung Galaxy Note 1	40	Cell Phone	2500
LG	10	Cell Phone	1700
Samsung S3	50	Cell Phone	2100

Figure 6.13. List of battery models used for the study

The results shown in the image are extracted from the prime tests performed on the batteries. The excel data of the C7000 prime tests was imported to Matlab where computation was performed. Since C7000 records one sample per minute, the precision of the charge and discharge capacities calculated can vary by a small amount (i.e. within 5% window) of the original value. The charge and discharge rate of all test results presented to support the arguments are carried out with C/4 charge and discharge current rate.

The plot shows State of Health of the batteries (referenced to the discharge capacity) versus the capacity estimated through coulomb counting during charge and discharge profile. The plot shows that the coulombic efficiency is not exactly 100% and there is slight deviation between the charge and discharge capacity.

Charging Capacity $Q_c = \int_{t=0}^{t_\circ} i_c(t)dt$

Where $i_c(t)$ is charge current

$t_\circ$ is the final charging time

Discharge Capacity $Q_d = \int_{t=0}^{t_\circ} i_d(t)dt$

where $i_d(t)$ is discharge current

$t_\circ$ is the final discharging time

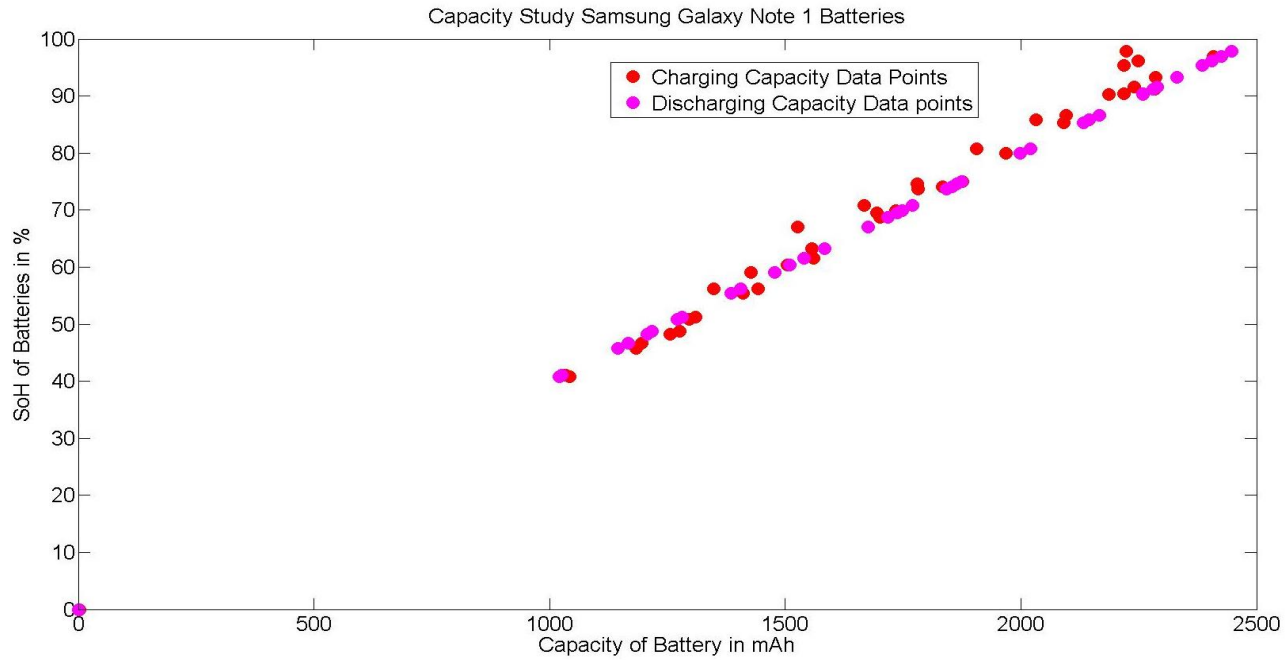

Figure 6.14. Comparison of measured capacity for Samsung Note 1 during charge and discharge operation

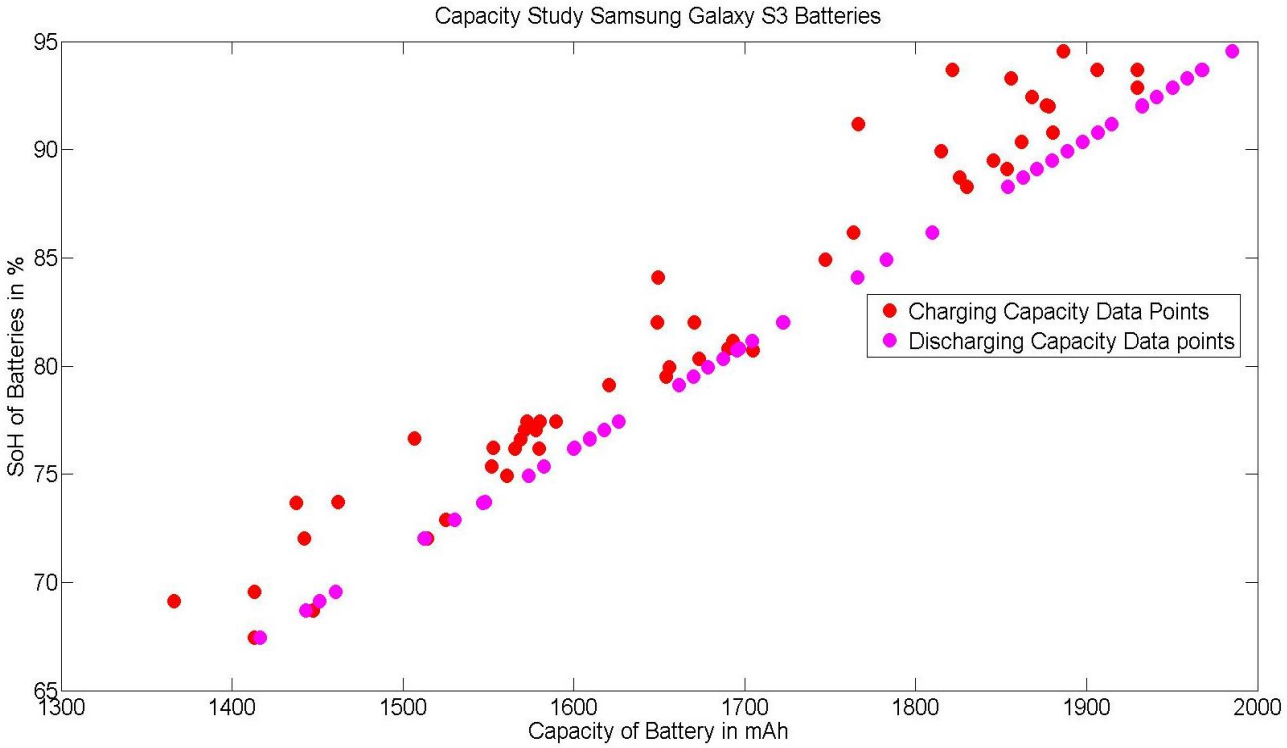

Figure 6.15. Comparison of measured capacity for Samsung Galaxy S3 during charge and discharge operation

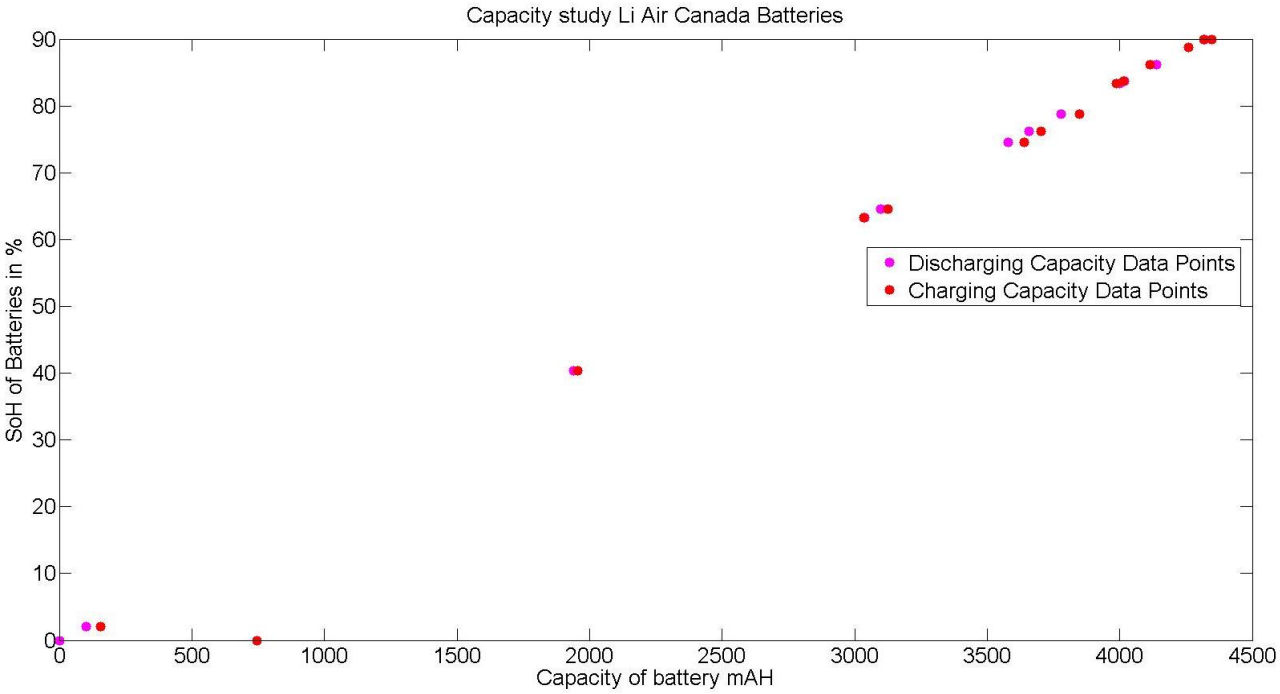

Figure 6.16. Comparison of measured capacity for Li Air Canada during charge and discharge operation

As observed from the plots, the coulombic efficiency of the batteries decreases as SoH battery degrades. For good batteries, the charge stored in the battery is almost the same as charge taken out of the battery. This observation is logical as good batteries have less series impedance and loss mechanisms are slow. However as batteries ages, the side reactions increase, causing the battery to heat up while charging. This causes loss of charge and therefore low coulombic efficiency. The heating effect was observed to amplify the hysteresis loss, however, the compensation for this is possible as one can ignore the charging duration for which temperature of battery is higher than a threshold. The maximum mismatch between the charge and discharge capacity was observed to be 31%. The thermal loss of energy while charging partially explains the difference between the charge and discharge capacity. For some models hysteresis compensation is necessary for implementation of this method.

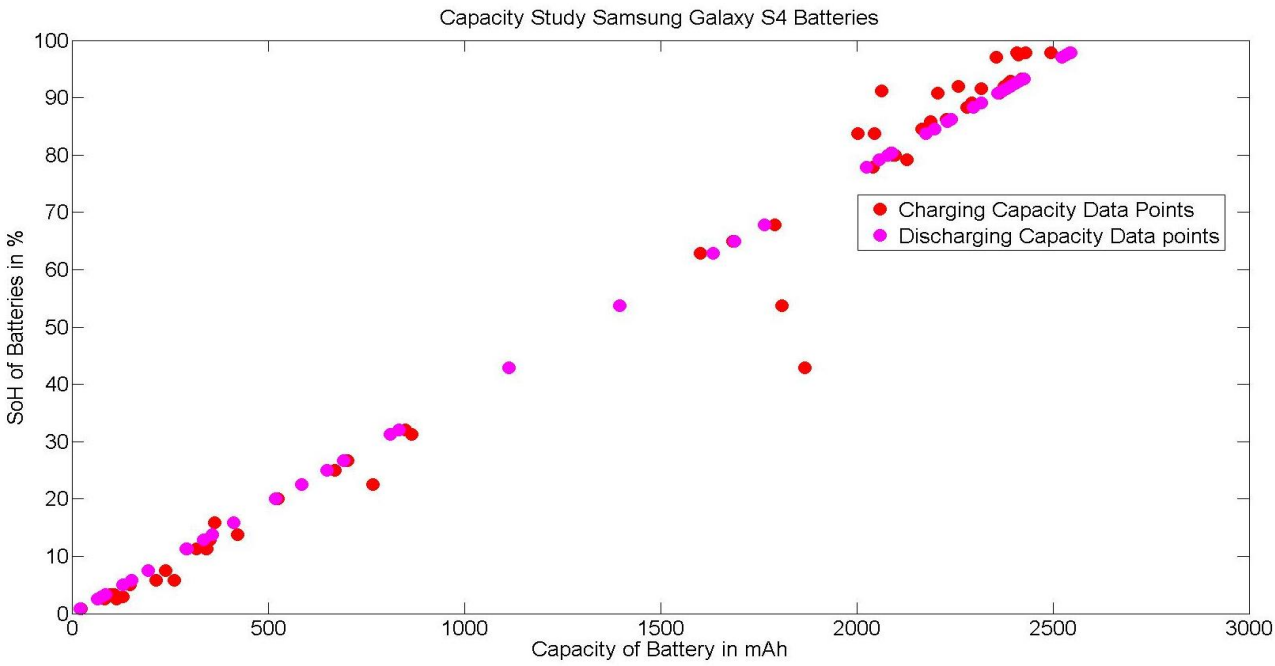

Figure 6.17. Comparison of measured capacity for Samsung Galaxy S4 during charge and discharge operation without temperature compensation

There were some outliers for samsung galaxy S4 batteries. However, when compensated for thermal losses, a good trend was observed, reinforcing the argument that charge profile is good indicator of SoH of the battery if the battery parameters are taken care of in runtime.

The temperature compensation method used for this analysis was model specific to this battery model. The amount of charge pumped in the battery during the time for which the battery temperature was higher than specified threshold, was ignored. The justification for ignoring that amount of charge comes from heat loss as electrical energy is dissipated as thermal energy and not stored as chemical energy inside the battery. The figure 6.18 shows the compensated charge and discharge capacity calculated for Samsung S4 batteries.

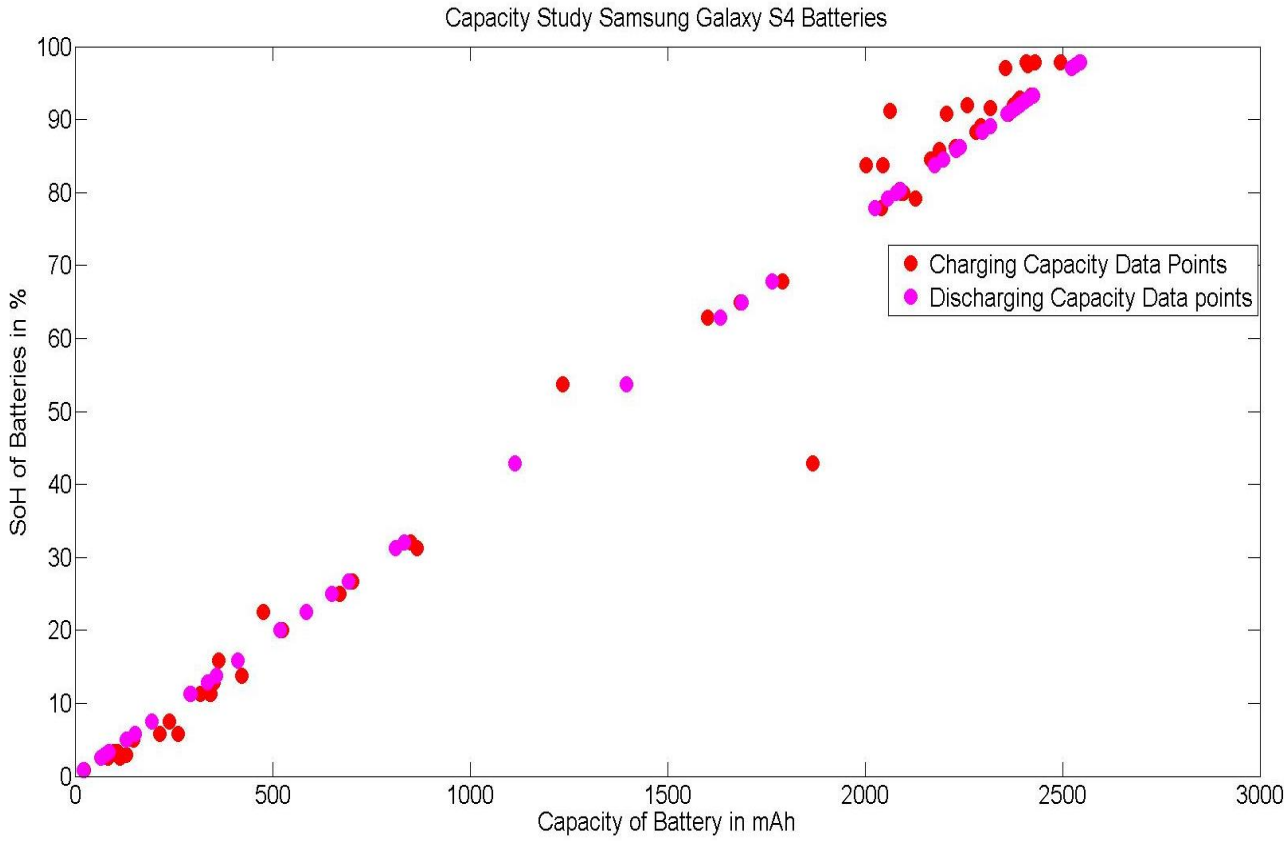

Figure 6.18. Comparison of measured capacity for Samsung Galaxy S4 during charge and discharge operation with temperature compensation

This study shows that there is hysteresis loss, which increases as the battery ages as degradation processes accelerate. The main indicator of the mismatch between the charge and discharge capacity is temperature. Although thermal loss of energy during the charging process contributes to large deviation in charge and discharge capacities, this loss mechanism can be easily detected and compensated.

Energy lost $= I^2 R_s t$ where I is charge/discharge current, R_s is series resistance and t is time. Once suggested compensation method is to ignore the time period for which the charge was pumped into the battery if the battery's temperature is higher than a predetermined value. However, this aspect needs to be further explored as threshold value of temperature might very across battery models and chemistries.

6.5 Comparison across different battery models

Data of 5 different battery models was used for analysis. These models have different charge profiles. The rated capacity of these battery models and charge voltage thresholds are different as summarized in the Figure below.

Battery Manufacturer	No of Batteries	Charge Voltage Threshold	Capacity (mAhr)
Li Air Canada	28	4.2	4800
Samsung Galaxy S4	54	4.3	2600
Samsung Galaxy Note 1	40	4.2	2500
Samsung S3	50	4.3	2100
LG	10	4.35	1700

Figure 6.19. Battery models with varying charge voltage threshold and capacities

The charge profile of good batteries (above 90% SoH) of all these models was compared to observe the effect of having different charge voltage on the current and voltage charge profile. The key parameter of interest in this test is the time duration at which the battery goes from constant current region to constant voltage region. The first cycle of the following plot presents a precise comparison of current and voltage profiles for different battery models during charging:

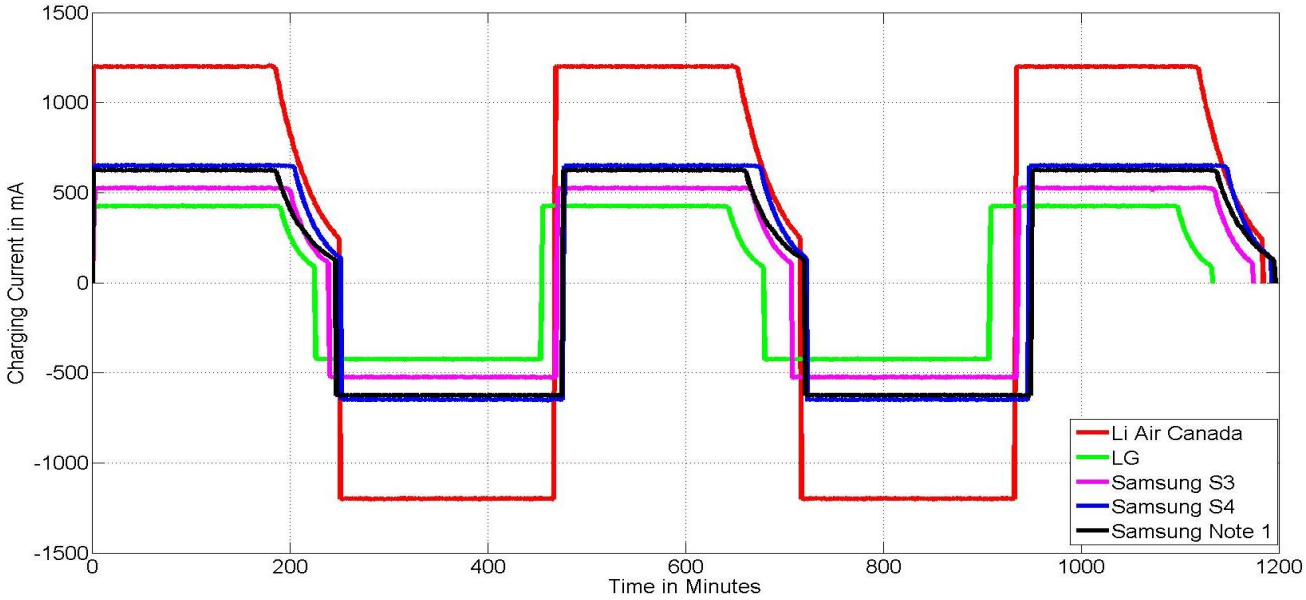

Figure 6.20. Current profile comparison of different battery models

Time to charge/discharge a battery completely = $\frac{Rated\ Capacity\ of\ battery}{charge\ or\ discharge\ current}$

Charging current = $\frac{C}{4} = \frac{Rated\ Capacity\ of\ battery}{4\ hours}$

Therefore time taken to charge/discharge = $\frac{Rated\ Capacity\ of\ battery}{Rated\ capacity\ of\ battery\ /4}$ = 4 hours = 240 minutes.

This the normalized time to charge/ discharge a battery and it remains constant for batteries with different rated capacities. The change in charging current compensates for the change in capacity such that the normalized charging time becomes independent of the battery model and rated capacity.

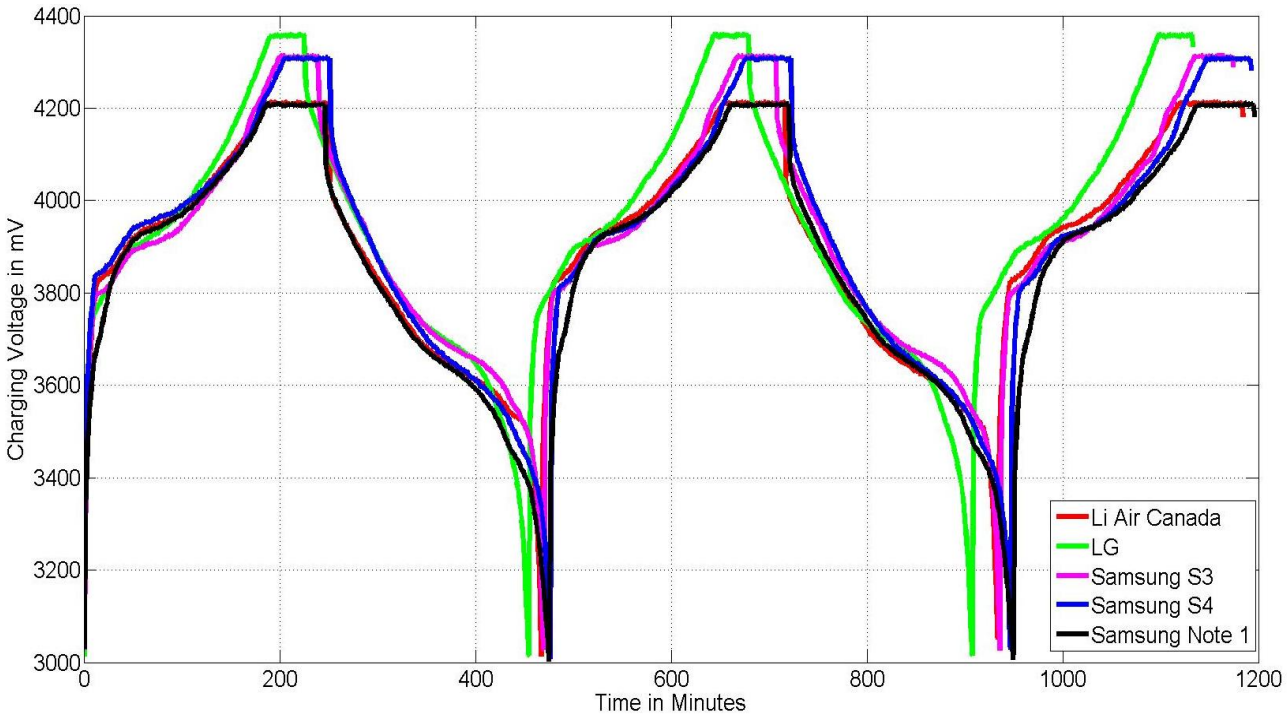

Figure 6.21. Voltage profile comparison of different battery models

The figure 6.21shows that even though the charging voltage was different for these batteries, the time instant at which they switch from constant current mode to constant voltage mode, is approximately same. This reinforces the point that the proposed method is independent of battery model and hence, varying capacity or cut off charging voltage has no impact on the results.

The results in this section are derived from the use of following mathematical equations:

Efficiency of a cell = $\eta = \frac{Q_d}{Q_c}$

$$= \frac{\int_{t=0}^{t_\circ} i_d(t)dt}{\int_{t=0}^{t_\circ} i_c(t)dt}$$

Where Q_d is the discharge capacity and Q_c is the charge capacity and η is coulombic efficiency

Energy lost as heat = Q_c - Q_d = (1- η) × Q_c= $I^2 R_s t$

Chapter 7: Results and Conclusions

7.1 Results and accomplishments of EIS technique

For EIS technique, experiments were performed to investigate three different parameters affecting this approach, State of Charge impact, Non-steady state condition and State of Health algorithm design. The proposed SoH estimation algorithm (design discussed in section 4.6) exhibits accuracy with in 10% bracket for the SoH estimation as shown in figure 7.1. The tests were performed when the batteries were sitting at 100% SoC for this analysis.

$$Function\ Input = 30*Max_x + 20*Max_y + 40*Min_x + 10*Zero$$

Where x is function input for the state of health function.

$$\text{State of Health}(x) = \begin{cases} -16.3 * x + 107.6, & 0 < x < 5.5 \\ -1.77 * x + 27.7 & 5.5 < x < 14.5 \end{cases}$$

Battery ID	State of Health in %	Test 1	Test 2	Test 3	Test 4	Test 5	Error Average(%)	Average Test Time(s)
Battery 1	63	61.1	62.55	63.16	62.6	63.02	-0.514	40.57
Battery 2	90	90.65	91.22	91.35	91.75	90.6	1.114	41.23
Battery 3	30	26.83	27.4	23.29	24.28	25.07	-4.626	40.94
Battery 4	65	68.28	69.45	69.73	69.21	70.4	4.414	40.56
Battery 5	2	0	0	0	0	0	-2	42.12
Battery 6	90	83.39	84.14	85.64	83.8	86.42	-5.322	40.68
Battery 7	89	81.64	81.73	83.19	82.42	82.65	-6.674	40.92
Battery 8	84	80.63	80.45	81.64	80.55	79.97	-3.352	40.77
Battery 9	79	80.41	80.27	79.85	79.81	80.7	1.208	41.25
Battery 10	76	75.73	74.01	75.38	74.95	73.31	-1.324	40.87
Battery 11	64	59.72	59.07	57.81	59.37	59.58	-4.89	41.39
Battery 12	13	20.96	23.07	20.48	21.52	23.1	8.826	42.51
Battery 13	86	77.12	77.68	79.27	77.06	77.98	-8.178	41.89
Battery 14	83	82.59	78.92	79.25	76.05	80.32	-3.574	41.05

Figure 7.1. State of Health algorithm average error analysis

The validation tests show that the algorithm can relate the EIS scan to the SoH of the battery without the need of equivalent circuit modeling and parameter extraction. The method

successfully differentiates between good and poor SoH batteries and even provides an estimate of SoH with in 10% window of the original value. The test comprises of less than a minute and without the need of complex computation (modeling and optimization method) a fairly accurate of estimate of SoH can be extracted. Although the algorithm proposed for SoH evaluation is model specific, the approach can be extended to different battery models by obtaining a data bank of their EIS scans and using similar technique to obtain a mathematical expression for SoH.

The analysis for the evaluation of State of Charge parameter comprised of a series of tests as explained in section 4.2. The motivation of this analysis was to investigate how the EIS scans varied along with the SoC of the batteries and how that will impact the SoH estimation algorithm. The results for this analysis are presented in figure 7.2.

Battery ID	SoH in %	SoC: 100 %	SoC: 90 %	SoC: 80 %	SoC: 70 %	SoC: 60 %	SoC: 50 %	SoC: 40 %	SoC: 30 %	SoC: 20 %	SoC: 10 %	SoC: 00 %	Avg. Erro
1	63	60.63	61.38	66.19	63.44	64.26	56.82	55.8	57.62	64.99	56.65	56.65	3.84818
2	92	90.9	95.01	97.18	98.69	98.62	93.97	94.62	92.32	96.7	97.59	94.75	3.68636
3	30	22.34	16.87	21.48	16.61	13.06	9.91	9.34	12.54	32	22.11	21.36	12.3982
4	65	65.89	72.95	71.15	70.05	68.06	64.68	63.52	60.69	74.96	71.66	66.54	4.30636
5	2	0	0	0	0	0	0	0	0	0	0	0	2
6	90	83.93	84.32	90.41	89.5	93.18	85.51	87.86	91.45	80.43	77.87	72.62	5.72727
7	89	80.39	84.16	90.56	87.98	91.9	86.2	84.81	89.46	83.54	84.95	78.89	4.18182
8	84	78.24	83.08	88.88	87.21	90.62	85.62	83.05	88.06	81.72	79.51	83.23	3.23273
9	79	80.02	84.59	85.14	84.57	87.19	81.03	81.66	72.16	82.11	78.63	78.14	3.85273
10	76	73.65	74.92	78.56	81.52	80.25	76.08	71.99	76.61	76.36	75.26	68.59	2.63364
11	64	59.58	67.05	69.39	70.15	71.38	64.42	59.36	59.34	69.59	67.18	64.45	4.12091
12	13	21.84	10.69	11.53	13.35	11.37	12.15	11.29	11.09	24.57	23.85	23.66	4.74091
13	86	76.33	79.63	82.8	79.37	84.31	77.71	79.46	82.07	75.99	73.3	73.47	7.41455
14	83	79.68	81.96	85.03	89.8	87.51	81.07	81.66	79.64	84.64	80.31	77.73	3.08455

Figure 7.2. SoH algorithm evaluation with varying SoC

Figure 7.2 shows that the SoH evaluation algorithm provides accurate estimate of the SoH at varying SoC level for all the batteries. The algorithm provides accuracy of within the window of 10% of the original SoH. One reason for this small error is the slight deviation in the EIS scans of the battery as SoC varies from 0% to 100%. However, overall the result endorses that a battery can be tested at any SoC for EIS techniques to obtain a reasonable estimate.

Last parameter investigated for EIS technique is non-steady state condition. Conventionally EIS technique has always been investigated under the limitation of the steady state condition, however, meeting this requirement is more conducive in laboratory setting rather than field operation. Therefore, the tests were designed to predict how non-steady state condition would impact EIS scans of the battery. The experimental details of the tests are provided in section 4.5. Figure 7.3 shows EIS scans after 30 seconds of rest time, while figure 7.4 shows EIS scans after 10.5 minutes of rest time. The rest time started when batteries were removed from charging.

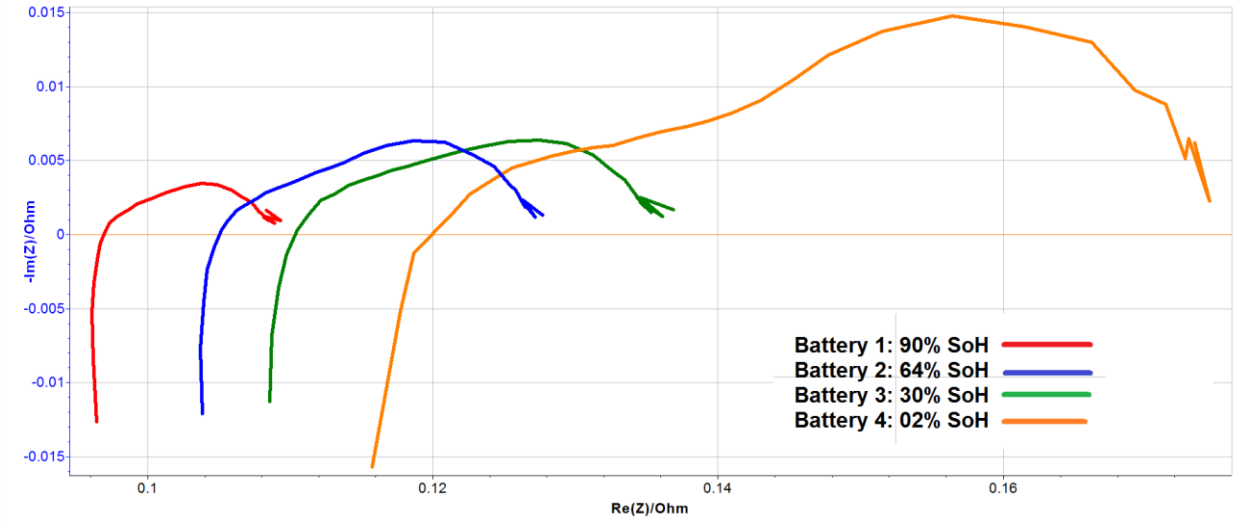

Figure 7.3. EIS scans of batteries after 30 seconds of rest time

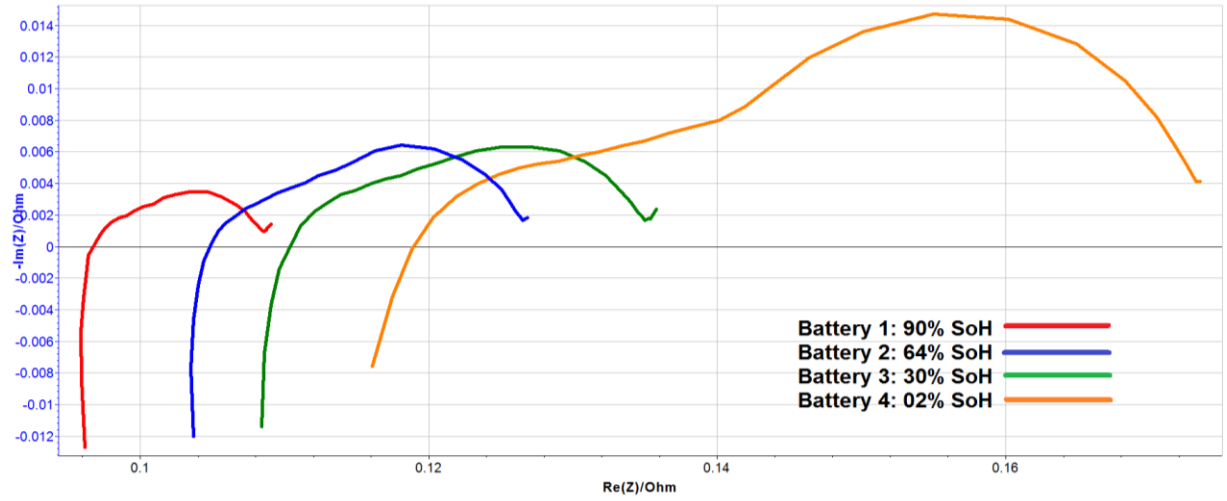

Figure 7.4. EIS scans after 10.5 minutes of the rest time

The comparison show that non steady state condition mostly impacts the low frequency region of the EIS scans. For low frequencies, a larger time window is required to acquire samples, and drifting OCV can therefore have a greater impact on this region of the Nyquist plot.

However, in order to overcome the steady condition limitation it is proposed that OCV of the battery is logged before taking the EIS scan and the gradient of the voltage time graphs is sampled. Once the OCV gradient is small enough such that the steady state condition can be assumed, an EIS scan should be captured. Figure 7.4 shows the OCV gradient profile used for one of the batteries used for this study.

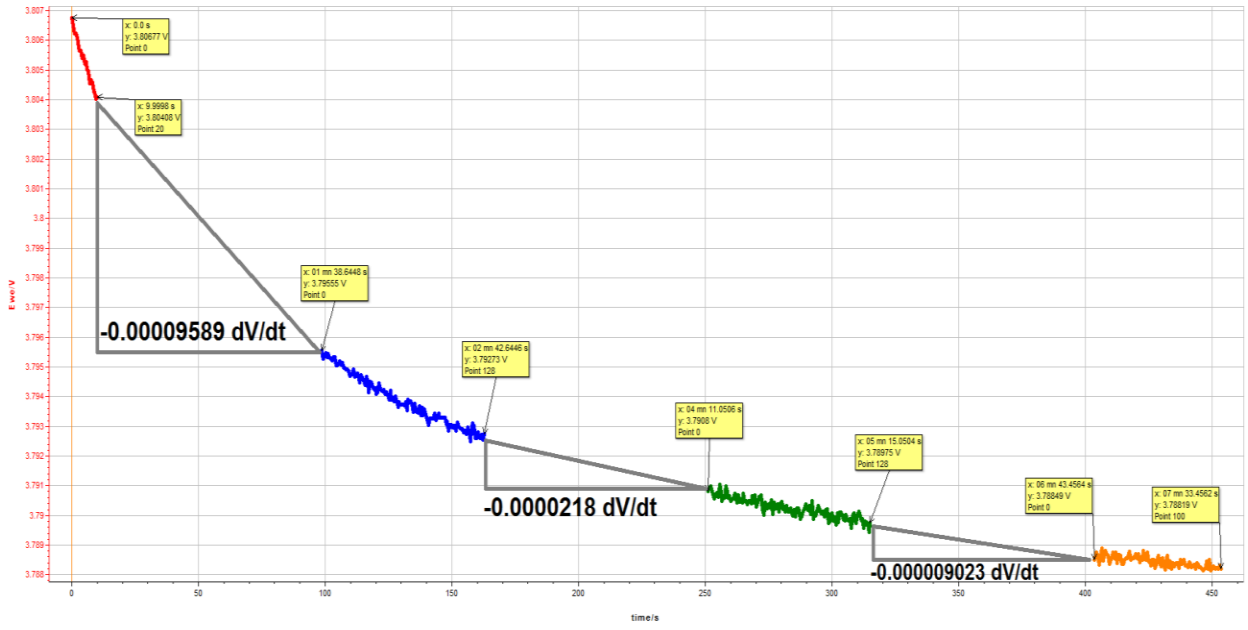

Figure 7.5. OVC gradient for Battery 2

Therefore, the study extends the previous work done on EIS approach and its application to real world contingencies. The limiting factors of EIS method were explored with respect to three different parameters, SoH algorithm design, impact of SoC variation and non-steady state analysis. The experimental results endorse the findings presented in the study to ease these limitations such that the EIS approach can used more effectively for field operations.

7.2 Results and accomplishments of charge profiling method

For the charge profiling method, the battery bank comprises of around 200 different batteries, coming from five different vendors and having different capacities, with their complete charge and discharge cycles recorded using Cadex c7000 battery analyzer. Different battery models have different nominal voltages and different end of charge cut off voltages. The data obtained is at C/4 charging rate and therefore, the charge time is independent of the capacity of the battery.

Figure 7.1 highlights the results of this method to relate the normalized constant current time variable to the SoH of the batteries. The graph shows that the approach seems to be consistent across all battery models and relation is independent of battery condition. The average error that can stem out of this estimation is expected to be precise to 8% of window of the original value.

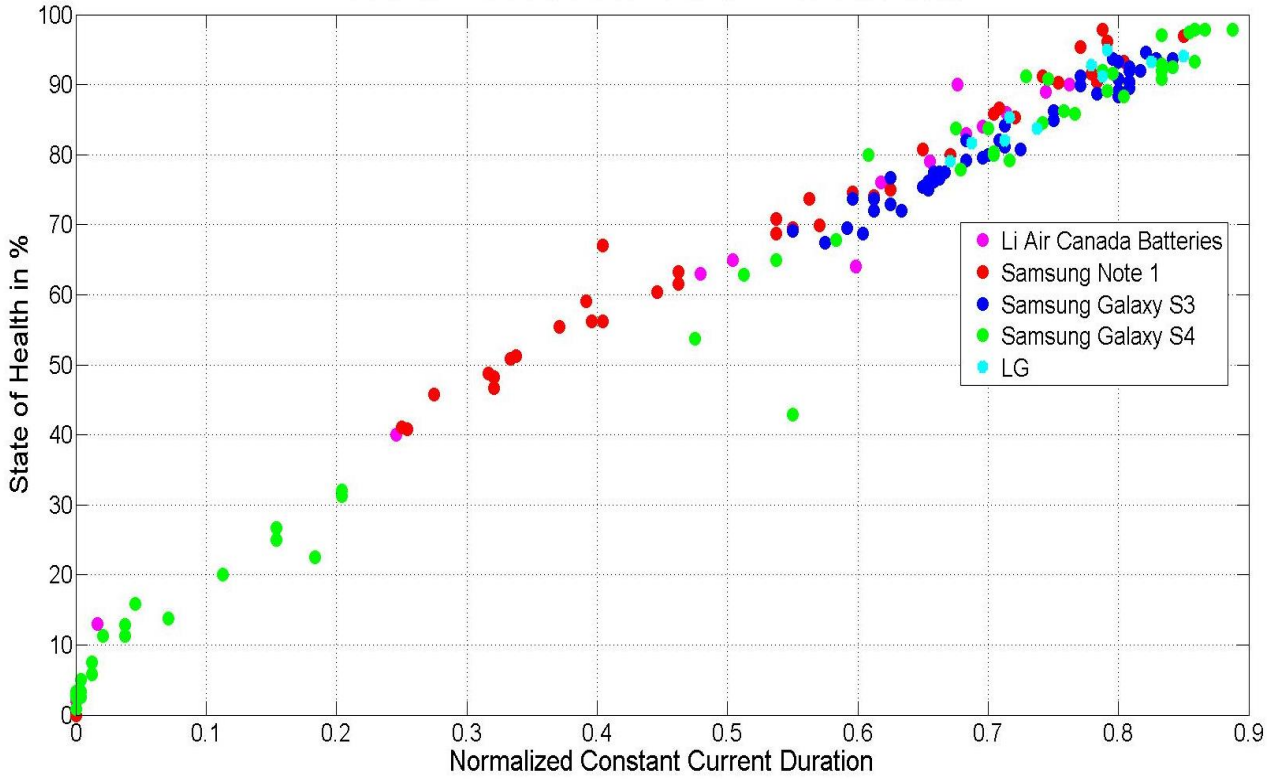

Figure 7.6. Relation between SoH of the batteries and normalized constant current duration

There are several advantages of using just constant charge region versus the entire charge profile. First of them is that it takes less amount of the time for the algorithm to provide the result. Since time is of essence in real world application, reducing the overall test is critical for state of the art devices. The overall test time saved for all these batteries if constant current method is used and not the entire profile of the battery is presented in the following figure:

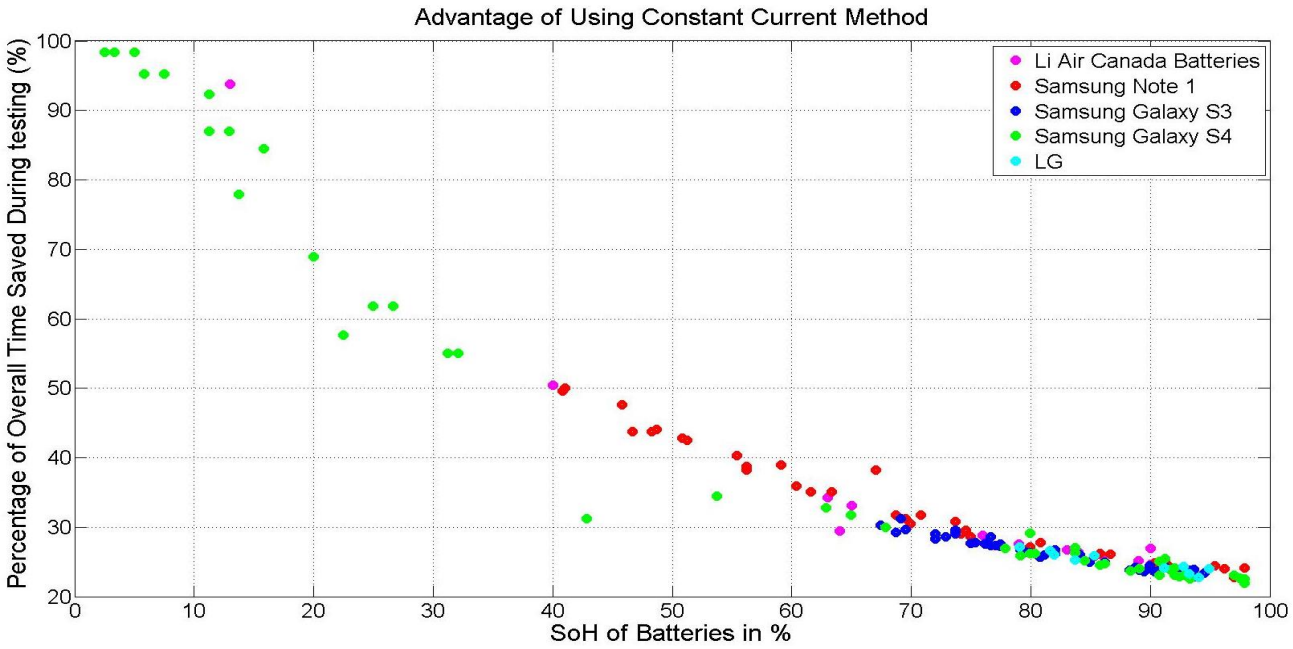

Figure 7.7. Percentage of overall test time saved Vs. SoH of the batteries

As shown the poor batteries show large time saving as compared to the good batteries. This is because good batteries stay in constant current region for longer period of time.

The second advantage of having just constant current method and not the complete profile is that it suits the daily routine applications in a better way. This approach allows the user to remove the battery from the charging dock, even if the battery is not completely charged. Since user doesn't have to wait for the full charge time to get an accurate estimate of the overall SoH of the battery, this method has a concrete advantage as compared to the overall charge cycle profiling of the battery.

7.3 Comparison of EIS with charge/discharge profiling

This section provides the summary of comparison of two different approaches presented for the SoH estimation of Li-Ion batteries. The following characteristics of the proposed techniques should be considered, however, the exact suitability of the method depends on the user application.

	EIS Technique	Charge curve profiling
Testing Time	Quick Test: 30 sec – 3 minutes depending on battery condition	Long Test: Usually take long time (few hours)
SoC dependency	No dependence	Needs to be in specific state(constant current region)
Test strategy	Needs steady state or quasi Steady state	No Steady State required, charging profile is required
Model Specific	SoH algorithm is model specific	Not model specific
External hardware	Requires a circuit to perform test and implement SoH algorithm	No external hardware required, charging circuit is sufficient
Cost Comparison	Expensive: addition hardware	Cheap: no hardware needed
SoH Accuracy in %	10% margin of error	8% margin of error
Repeatability	Accurate	Highly Accurate

Figure 7.8. Comparison of EIS technique with charge curve profiling

Since cost and time are key factors of interest in industrial sector, both these methods provide a flexible solution as per demand. The charge curve method provides cheaper solution, as it requires no external hardware. However, the method is time consuming. For time sensitive application, EIS technique seems to be a suitable method. The hardware circuit required for performing EIS scan has to be very precise therefore; it increases the overall cost of the BMS.

7.4 Future work

So far, the results presented in the thesis are based on some assumptions regarding the operating conditions of the battery. There assumptions might not be valid which real life operation of the batteries in field and therefore extensive analysis is required to mature this technology for industrial applications. The assumptions range from room temperature and pressure condition for the operation of the battery to recommended charge/discharge operating conditions.

A significant change in the ambient temperature of a battery might result in abnormal operation. Similarly, charging or discharging a battery beyond its recommended ratings and limits can cause damage to the electrochemical properties of the battery. Therefore, these contingencies have to be taken into consideration before a user end device is introduced as a commercial product in the market.

Further tests are recommended on various battery models of varying capacity, chemical configuration and cut-off voltages to validate the results across a range of models. This will amplify the accuracy of the algorithms proposed and also highlight the limitation of the proposed solutions to decipher the state of health of the batteries.

As far as the EIS scan technology is concerned, improving the safety measures for the proposed design and circuit for HCC is essential. Since Li Ion cells have large energy density, a small failure can trigger catastrophic reaction that can damage the device under use completely. A small short circuit of the battery terminals can cause a high short circuit current resulting in thermal runway where flaming gases are ejected. Therefore, this area needs further improvement.

Bibliography

[1] Zu, Chen-Xi, and Hong Li. "Thermodynamic analysis on energy densities of batteries." Energy & Environmental Science 4.8 (2011): 2614-2624.

[2] A Comparison of Lead Acid to Lithium-ion in Stationary Storage Applications, Published by AllCell Technologies LLC. March; 2012

[3] Tröltzsch, Uwe, Olfa Kanoun, and Hans-Rolf Tränkler. "Characterizing aging effects of lithium ion batteries by impedance spectroscopy." Electrochimica Acta51.8 (2006): 1664-1672.

[4] Piller, Sabine, Marion Perrin, and Andreas Jossen. "Methods for state-of-charge determination and their applications." Journal of power sources 96.1 (2001): 113-120.

[5] R. Grois, 10. Entwicklerforum Batterien, Ladekonzepte und Stromversorgungsdesign, M¨unchen, 19 March, 2003.

[6]Andre, D., et al. "Characterization of high-power lithium-ion batteries by electrochemical impedance spectroscopy. I. Experimental investigation."Journal of Power Sources 196.12 (2011): 5334-5341.

[7] Bose, C.S.C.; Laman, F.C., "Battery state of health estimation through coup de fouet," Telecommunications Energy Conference, 2000. INTELEC. Twenty-second International , vol., no., pp.597,601, 2000

[8] Jossen, Andreas. "Fundamentals of battery dynamics." *Journal of Power Sources* 154.2 (2006): 530-538.

[9]Stroe, D.I.; Swierczynski, M.; Stan, A.I.; Knap, V.; Teodorescu, R.; Andreasen, S.J., "Diagnosis of lithium-ion batteries state-of-health based on electrochemical impedance

spectroscopy technique," in *Energy Conversion Congress and Exposition (ECCE), 2014 IEEE* , vol., no., pp.4576-4582, 14-18 Sept. 2014

[10] Thanh-Tuan Nguyen; Van-Long Tran; Woojin Choi, "Development of the intelligent charger with battery State-Of-Health estimation using online impedance spectroscopy," in *Industrial Electronics (ISIE), 2014 IEEE 23rd International Symposium on* , vol., no., pp.454-458, 1-4 June 2014

[11] STM32F4 Discovery, " Libraries and tutorials for STM32F4 series MCUs" Tilen Majerle,[Online]. Available: http://http://stm32f4-discovery.com/.[Accessed: Apr 6, 2014]

[12] Ramadass, P., et al. "Development of first principles capacity fade model for Li-ion cells." *Journal of the Electrochemical Society* 151.2 (2004): A196-A203.

[13] Ning, Gang, and Branko N. Popov. "Cycle life modeling of lithium-ion batteries." *Journal of The Electrochemical Society* 151.10 (2004): A1584-A1591.

[14] Williard, Nick, et al. "Comparative analysis of features for determining state of health in lithium-ion batteries." *Int. J. Progn. Health Manag* 4 (2013): 1-7.

[15] K. Li and K. J. Tseng, "Energy efficiency of lithium-ion battery used as energy storage devices in micro-grid," *Industrial Electronics Society, IECON 2015 - 41st Annual Conference of the IEEE*, Yokohama, 2015, pp. 005235-005240.

Appendix A

The circuit level schematics and mathematical relations for the sub-sections of the potentiostatic circuit fig 5.1 are presented here. UBC capstone group 76 designed these hardware schematics.

1) *Excitation Condition*

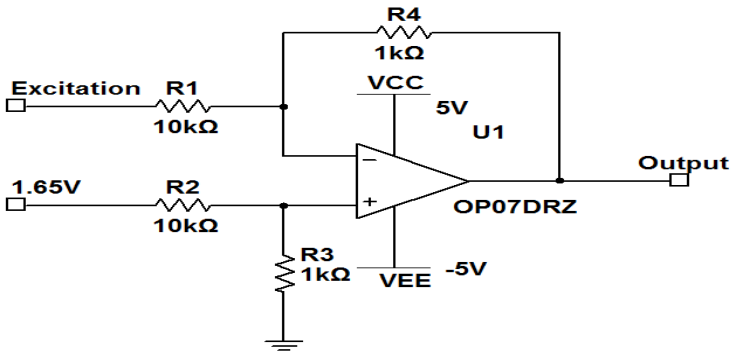

Excitation Conditioner Circuit

$$\text{DAC 1 swing output} = 250 \times \frac{3.3\text{V}}{2^{12}} = 201\text{mV}_{\text{pp}}$$

$$\text{Output} = \frac{\text{R}_4}{\text{R}_1}(\text{Excitation -1.65 V})$$

2) *Adjustable DC Reference*

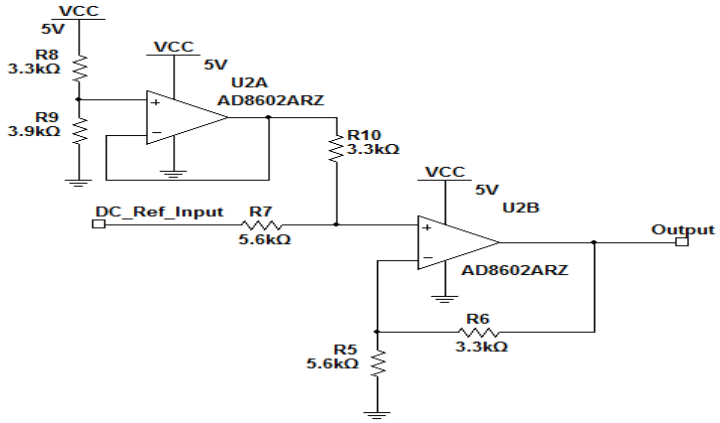

DC Reference Circuit

$$DC\ reference\ resolution = \frac{4.7V - 2.7V}{2^{12}} = 488\ \frac{\mu V}{LSB}$$

$$Output\ Voltage = DC_Ref_Input \times \frac{3.3\ k\Omega}{5.6\ k\Omega} + 2.7V$$

3) Potentiostatic Control (with shunt resistor)

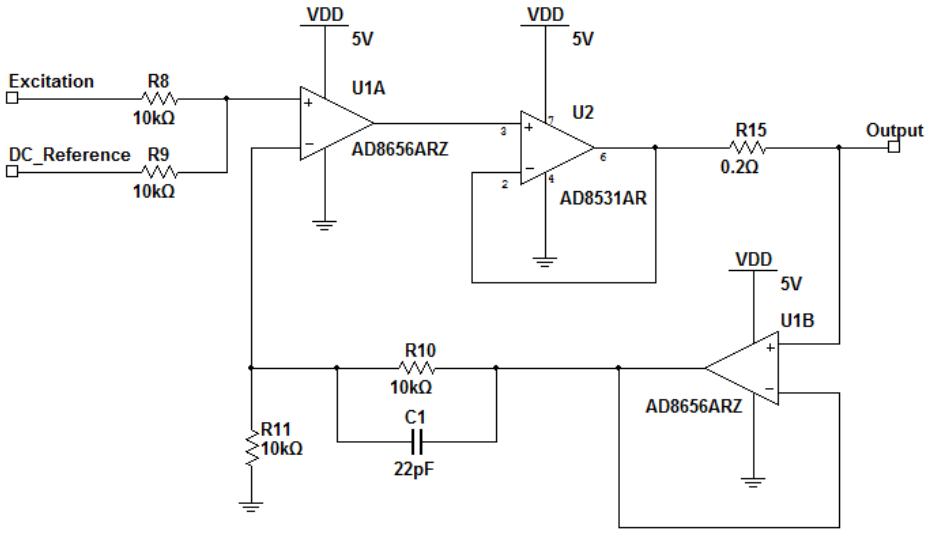

Potentiostatic controller circuit

$$Current\ measurement\ swing = (200mA*0.2\Omega).\frac{50V}{V} = 2\ V$$

AD8531 Buffer current source/ sink ability = 250mA

4) Difference (voltage response measurement)

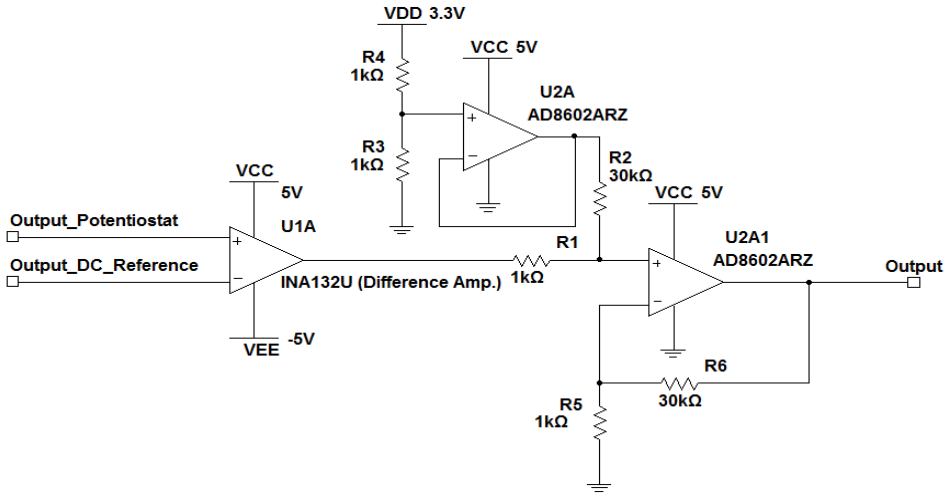

Voltage Measurement circuit

Output = ((Output_potentiostat – Output_DC-Reference) × 30) + 1.65V